INVESTIGATION OF NITROGEN LASERS FOR

DYE LASER PUMPING

Submitted for the degree of

DOCTOR OF PHILOSOPHY by

STEWART WYNN WILLIAMS

in 1984 whilst registered at

ROYAL HOLLOWAY COLLEGE

R.H.C. LIBRARY
CLASS No. T BF Wil
ACC. No. 617,019
Date ACQ. Jun. '85

ProQuest Number: 10097556

All rights reserved

INFORMATION TO ALL USERS
The quality of this reproduction is dependent upon the quality of the copy submitted.

In the unlikely event that the author did not send a complete manuscript
and there are missing pages, these will be noted. Also, if material had to be removed,
a note will indicate the deletion.

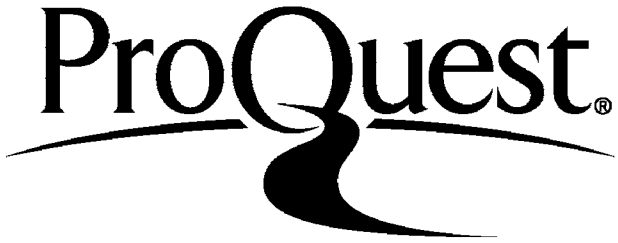

ProQuest 10097556

Published by ProQuest LLC(2016). Copyright of the Dissertation is held by the Author.

All rights reserved.
This work is protected against unauthorized copying under Title 17, United States Code.
Microform Edition © ProQuest LLC.

ProQuest LLC
789 East Eisenhower Parkway
P.O. Box 1346
Ann Arbor, MI 48106-1346

ABSTRACT

The dependence of certain properties of nitrogen lasers on various parameters have been examined and the design of two original nitrogen lasers is presented. The output characteristics of these lasers have been studied as a function of gas pressure, gas flow rate and direction, applied potential, repetition rate, electrode geometry, drive circuitry including the effects of preionization, and the effect of optical feedback by the addition of an optical cavity. The operation of these two lasers in a master oscillator/power amplifier configuration is described and the optimization of this system by varying the drive circuit parameters has been achieved. In the optimized state this configuration produced as much energy per pulse as did the amplifier when operating separately as an oscillator. However, the oscillator/amplifier system produces an output with some additional useful characteristics, such as lower beam divergence and a high degree of polarization.

The design of a dye laser which uses a grating at grazing incidence and three mirrors is desribed. This laser utilizes the polarized output from the oscillator/amplifier system to generate simultaneously two independently tunable wavelengths. A novel pumping arrangement is used which ensures that there is no mode competition between the two wavelengths, that they can have any polarization ratio, that the linewidth of each wavelength can be independently varied and allows the two wavelengths to be generated in different dyes.

R.H.L.
LIBRARY

C O N T E N T S

ILLUSTRATIVE MATERIAL

LIST OF FIGURE CAPTIONS

LIST OF TABLES

LIST OF PHOTOGRAPHS

INTRODUCTION

The original aim of this work was to build and develop a nitrogen laser pumped dye laser system for use on an experiment to produce spin polarized monochromatic electrons by selective two photon ionization of sodium. The first (MkI) nitrogen laser that was built was not an original design and proved unsatisfactory. A second (MkII) laser was then designed and built as a replacement for the MkI version. Having designed this laser it was realised that the requirements of the experiments (wavelength less than 400nm and a linewidth less than 1 nm) could be fulfilled by the nitrogen laser itself. The order of magnitude increase in available pulse energy by omitting the dye laser would lead to a substantial increase in the yield of polarized electrons. There were two major drawbacks to this scheme. The closest position an optical component could be placed to the interaction region was 1m, a significant distance given the large and unequal beam divergence of the nitrogen laser. Also the shape of the interaction region was determined by the shape of the colinear exciting argon ion laser pumped dye laser and since this shape was circular, with a diameter of about 5mm, efficient coupling of the radiation from the nitrogen laser to the interaction region would be difficult. The other drawback was that the incident radiation needed to be circularly polarized and the output from the nitrogen laser is completely unpolarized. To overcome these problems it was decided to operate the MkII laser as the amplifier part of an oscillator - amplifier (MOPA) system. Hence a third (MkIII) laser was designed and built as a low power oscillator and coupled with the MkII laser as an integrated system.

When the concept for the two wavelength dye laser was devised it was decided to use the polarized output of the MOPA system for pumping this laser. As such the aim of the development of the MOPA system was to produce at least as much energy in a fully polarized beam as could be achieved by operating the MkII laser as a single oscillator with an external polarizer.

The operating principles and design criteria upon which the MkII and MkIII lasers were designed are discussed in Chapter I. Chapter II describes the MkI laser and why it was unsuitable. Chapters III and IV describe the design and operation of the MkII and III lasers respectively. The coupling together and sychronization of these lasers are presented in Chapter V. Chapter VI outlines the principles of operation and cavity designs for nitrogen laser pumped dye lasers, and also reviews previous reports of two wavelength nitrogen laser pumped dye lasers. Chapter VII describes the design and operation of an original two wavelength dye laser.

CHAPTER I

PRINCIPLES OF OPERATION, THEORETICAL AND DESIGN CONSIDERATIONS FOR NITROGEN LASERS

1.1 PRINCIPLES OF OPERATION

The nitrogen laser produces radiation in the near ultraviolet with a wavelength of 337.1 nm. This radiation is generated in the triplet second positive system, ie. between levels $C^3\pi_u$ and $B^3\pi_g$. The relevant potential energy curves for the nitrogen molecule are shown in figure 1.1. The radiation corresponds to the transition between the levels with the lowest vibrational energy ($V'=0$ and $V''=0$) and because of the presence of several rotational transitions has an overall bandwidth of 0.1 nm (Parks et al. (1.1)). The lifetime of the upper laser level ($C^3\pi_u$) is pressure dependent due to the effect of deexcitation via molecular collisions and this lifetime is related to the pressure by the following formula (1.2):

$$T = \frac{36}{1 + (\rho/_{68})} \quad \text{ns} \qquad (1.1)$$

where ρ is the pressure in torr. Table 1.1 shows various values of the lifetime for different pressures.

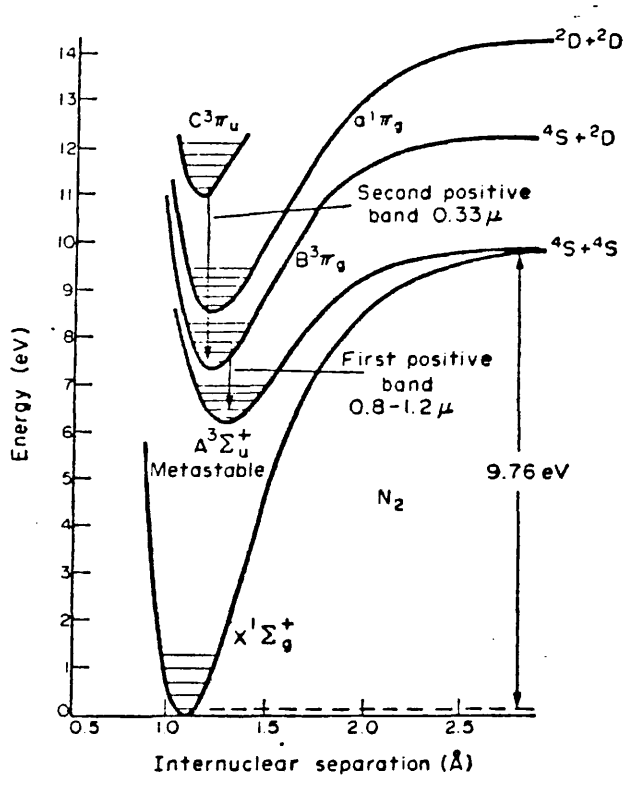

FIGURE 1.1 Relevant potential energy curves for the nitrogen molecule.

Table 1.1

Pressure dependence of the lifetime of the $C^3\pi_u$ level.

Pressure (Torr).	Lifetime (nanoseconds).
1	35.4
10	30.7
20	26.8
40	21.3
60	17.7
100	13.2
200	8.1
400	4.6
760	2.6
1520	1.3

The lifetime decreases with pressure from the radiative lifetime of 40ns at very low pressures to 2.6ns at atmospheric pressure. Considering that the lifetime of the lower laser level ($B^3\pi_g$) is 5 μs and is therefore much longer than that of the upper laser level one would not anticipate laser action in the nitrogen molecule. The method whereby laser action is achieved is to preferentially excite the $C^3\pi_u$ level in a time much shorter than the natural lifetime of that level. Preferential excitation is possible due to favourable differences in the Frank-Condon factors for the different transitions. For a diatomic molecule the Frank-Condon principle is most simply stated by saying that an electronic transition will have a higher probability of

taking place if the separation of the nucleii remains constant. The probability of a transition taking place based upon this principle is related to the Frank-Condon factors and these are shown in Table 1.2 for some relevant transitions for the nitrogen laser (from McCallum et al. (1.3)).

Table 1.2

Some Frank-Condon factors for the nitrogen molecule.

Transition	Upper Level Vibrational Level	Frank-Condon Factor
$X^1\Sigma_g^+ - C^3\pi_u$	0	5.46×10^{-1}
	1	3.06×10^{-1}
	2	1.07×10^{-1}
$X^1\Sigma_g^+ - B^3\pi_g$	0	6.06×10^{-2}
	1	1.46×10^{-1}
	2	1.95×10^{-1}
	3	1.90×10^{-1}
	4	1.52×10^{-1}

From this table it is seen that when the nitrogen molecule is excited the vibrational level most readily populated in the $C^3\pi_u$ level is the one with V = 0; whilst for the $B^3\pi_g$ level the molecules are excited to higher vibrational levels. Hence a population inversion is readily achieved on the $C^3\pi_u$ ($V'=0$) to the $B^3\pi_g$ ($V''=0$) transition. In addition, because of the larger Frank-Condon factors high energy electrons (>12 eV) are more

likely to excite the nitrogen molecule to the $C^3\pi_u$ state than the $B^3\pi_g$ state. Cartwright (1.4) calculated the total electron cross-sections for the excitation of the seven lowest triplet electronic states of nitrogen as a function of the electron energy from the V =0 of the ground state and the results are shown in figure 1.2. The maximum cross section ratio occurs with electrons with an energy of 14ev as confirmed experimentally by Burns et al. (1.5). The energy of the electrons in a discharge is determined primarily by the electric field to pressure ratio (E/p); hence for one particlar value of applied voltage the output of a nitrogen laser should peak at a particular value of gas pressure. Fitzsimmons et al. (1.6) calculate that the best E/p value is about 80 V/cm torr. Therefore to obtain laser action in nitrogen one must excite the molecules in a very short time with a high density of electrons with energies around 14eV.

As laser action proceeds the number of molecules in the $B^3\pi_g$ state increases because of the relatively long lifetime of that state. Eventually the population inversion will be destroyed and laser action will cease, hence the nitrogen laser is termed a self terminating laser. The larger the current produced at the beginning of the pulse (i.e. a faster rising pulse) the greater will be the peak power produced. However this will lead to a more rapid population of the $B^3\pi_g$ level and consequently a shorter pulse width.

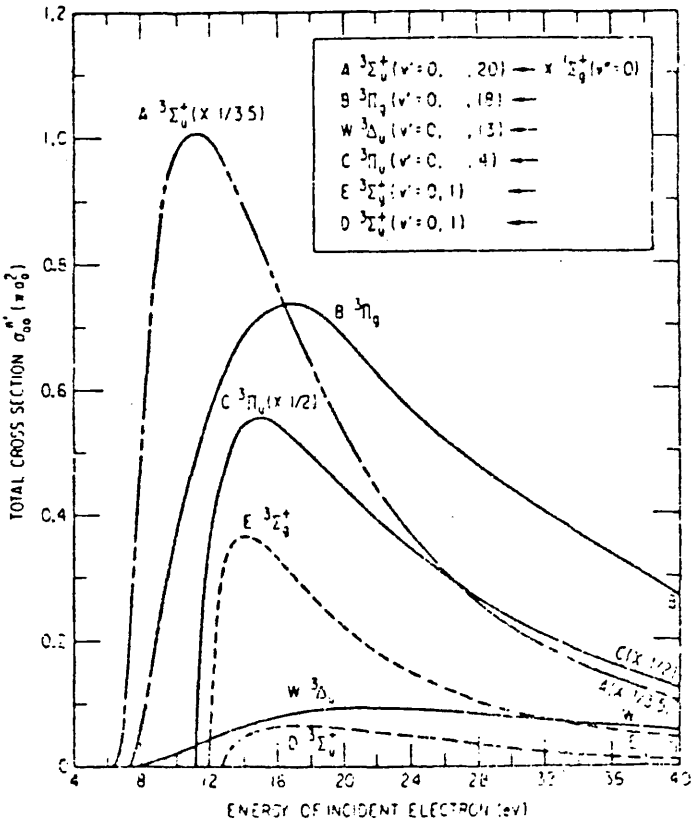

FIGURE 1.2 Calculated total electron cross-sections for the excitation of the seven lowest triplet electronic states of nitrogen as a function of electron energy.
(From Cartwright (1.4)).

1.2 THEORETICAL CONSIDERATIONS

The criterion for population inversion in the nitrogen laser was first developed by Ali et al. (1.7). The general rate equations for a three level collision dominated laser are as follows:-

$$\frac{dN_3}{dt} = X_{13} N_1 + X_{23} N_2 - (Y_{31} + Y_{32} + T_{31}^{-1} + T_{32}^{-1}) N_3 - R_{32}^{i} \left[N_3 - \frac{g_3}{g_2} N_2 \right], \quad (1.2)$$

$$\frac{dN_2}{dt} = X_{12} N_1 + (T_{32}^{-1} + Y_{32}) N_3 - (T_{21}^{-1} + Y_{21} + X_{23}) N_2 + R_{32}^{i} \left[N_3 - \frac{g_3}{g_2} N_2 \right], \quad (1.3)$$

$$\frac{dN_1}{dt} = - (X_{12} + X_{13}) N_1 + (T_{21}^{-1} + Y_{21}) N_2 + (T_{31}^{-1} + Y_{31}) N_3, \quad (1.4)$$

where N_1, N_2 and N_3 denote the population densities of the ground level ($X^1 \Sigma_g^+$) the lower ($B^3 \pi_g$) and upper ($C^3 \pi_u$) laser levels respectively. X_{ij} denotes the rate of collisional excitation by electron impacts from level i to level j, where $i \neq j$;

also Y_{ji} is the rate of collisional deexcitation from j to i and $(T_{ji})^{-1}$ is the rate of radiative decay from j to i. R^i_{ji} denotes the rate of induced emission, which includes the linewidth, Einstein's B coefficient and the energy density. g_3 and g_2 are the statistical weights of the upper and lower laser levels respectively. The induced emission and absorption rates and the deexcitation through collision from the laser levels to the ground state can be neglected. Using the fact that $T_{31} >> T_{32}$ (since the C state is metastable), $X_{13} > X_{12}$ in accordance with the Frank-Condon principle and $T_{21} >> T_{32}$ (T_{32}= 40ns whilst T_{21} = 5μs) the sum of equations (1.2) and (1.3) can be written as:

$$\frac{d}{dt} (N_3 + N_2) = X_{13} N_1 \qquad (1.5)$$

which on integration yields:

$$N_3 + N_2 = X_{13} N_1 t. \qquad (1.6)$$

Modifying equation (1.2) according to the above and substituting equation (1.6) yields:

$$\frac{dN_3}{dt} = X_{13}N_1 + X_{23} \left[X_{13}N_1 t - N_3\right] - \beta N_3 \qquad (1.7)$$

where

$$\beta = (T_{32}^{-1} + Y_{32})$$

Solving (1.7) results in:

$$N_3 = \frac{N_1X_{13}}{\alpha^2} \beta - \frac{N_1X_{13}}{\alpha^2} \beta e^{-\alpha t} + \frac{N_1X_{13}X_{23}t}{\alpha} \qquad (1.8)$$

where $\alpha = \beta + X_{23}$

For small times equation (1.8) can be written by expanding $e^{-\alpha t}$ up to terms in t^2 as

$$N_3 = N_1 X_{13} t - N_1 X_{13} (Y_{32} + T_{32}^{-1}) \frac{t^2}{2} \qquad (1.9)$$

Substituting for N_3 from equation (1.6) in (1.9) yields:

$$N_2 = \frac{1}{2} N_1 X_{13} (Y_{32} + T_{32}^{-1}) t^2 \qquad (1.10)$$

Dividing (1.9) by (1.10) produces

$$\frac{N_3}{N_2} = \frac{2}{(Y_{32} + T_{32}^{-1}) t} - 1 \qquad (1.11)$$

Thus, for $N_3 > N_2$ one must have

$$\frac{1}{Y_{32} + T_{32}^{-1}} > t \qquad (1.12)$$

which implies that inversion takes place in a time small compared to $(Y_{32} + T_{32}^{-1})^{-1}$

Neglecting the collisional mixing effect, ie $T_{32}^{-1} > Y_{32}$ one sees that population inversion can only take place during the order of, but less than, the radiative lifetime (40ns) of the $C^3\pi u$ state. For high electron densities ($> 6 \times 10^{14} cm^3$) the collisional mixing effect cannot be neglected ($Y_{32} > T_{32}^{-1}$) and the inversion duration is further shortened. Therefore it is necessary to have a very fast excitation of the nitrogen.

Ali et al. (1.7) proceeded to couple the rate equations to the circuit, ionization rate and the electron energy equations. They did this by considering the case of a nitrogen molecule, as a

lasing system, coupled to an electric circuit consisting of a capacitance C, charged originally to some voltage V_o, a fixed external resistance R_e, an inductance L and the variable resistance R(t) of the lasing medium all connected in series. The circuit equation is

$$L\left(\frac{di}{dt}\right) + R_t I = V_o - \int_o^t \left(I\frac{dt'}{C}\right) \qquad (1.13)$$

where $R = R_e + R(t)$. The rate of ionization is

$$\frac{dNe}{dt} = N_e N_1 s \qquad (1.14)$$

where s is the ionization rate coefficient. The rate at which the electrons are heated is given by (1.7)

$$\frac{d}{dt}\ \frac{3}{2}\ N_e T_e = \gamma I^2 (R(t) - N_1 (X_{13} E_{31} + X_{12} E_{21})$$
$$-N_e N_1 S E_\infty - N_e N_1 X_v E_v - E_{32}(N_2 X_{23} - N_3 Y_{32}) \qquad (1.15)$$

where E_{ji} are the energies of the transition $j \rightarrow i$, E_∞ is the ionization energy of the molecule, T_e the electron temperature, all expressed in units of eV. I is the total current, γ a conversion factor to eV per unit volume. Ali et al. (1.7) solved (numerically) these equations (1.13 - 1.15) and the rate equations to find the power density variation with time. Initially they used the saturation approximation first developed by Gerry (1.8), this assumes that saturation takes place very rapidly, ie. $N_3 - N_2 \ll N_3$ and $N_3 \simeq N_2 = N$. They also solved the equations without the saturation approximation and the result of both methods are shown in figure 1.3. The two methods produce very similar results apart from the early

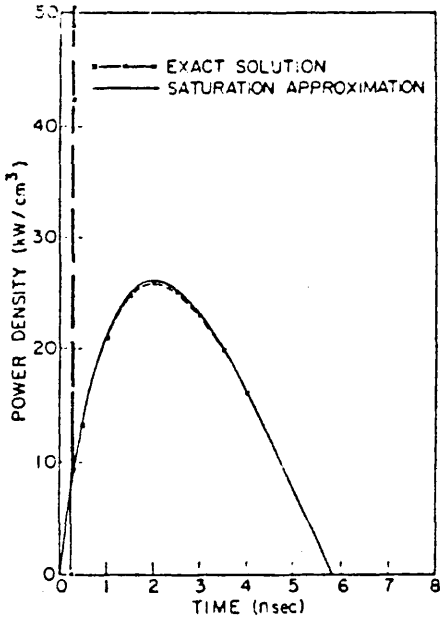

FIGURE 1.3 Calculated variation of laser power density with time. (from Ali et al. (1.7)).

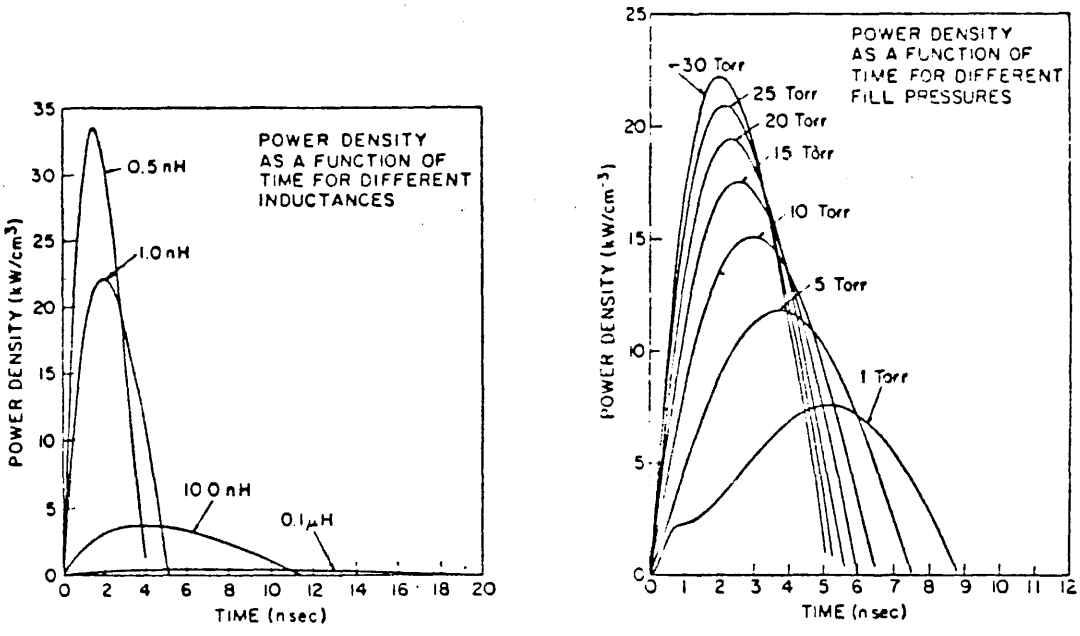

FIGURE 1.4 Calculated effect of the circuit parameters on the laser power density variation with time.
(from Ali (1.9)).

oscillation predicted by the exact solution, this has not been observed experimentally. Ali (1.9) then used these equations and the saturation approximation to evaluate the effect of the circuit parameters on the laser power density and his results are presented in figures 1.4 (a) and (b). The main conclusions are that decreasing the inductance (hence decreasing the current risetime) produces pulses with higher peak powers and shorter pulse widths, and that operating with a higher pressure produces the same effect.

Richter et al. (1.10) derived the threshold conditions and the peak power as a function of the discharge length and the initial inversion density. They assume that the excitation occurs during a very short time which they justify by refering to a paper by Ali (1.7) which states that the electron temperature falls below a value sufficient for excitation to either laser level less than 1ns after the discharge. They also neglect deexcitation from the lower laser level and spontaneous emission from the upper laser level due to the long lifetimes compared with the pulse duration. They found that the initial inversion density and the discharge length are related by the equation

$$L = \frac{6}{5} \frac{1}{\alpha_o n(t_i)} \qquad (1.16)$$

where $n(t_i)$ is the initial inversion density, L is the length of the discharge and α_o is the gain coefficient of the laser transition. This equation shows that for a particular inversion density there will be a threshold length L_T. They also derive an equation relating the output peak power to the inversion density

and discharge length. This equation is

(1.17)

$$\phi_+ (L, t_p) = \frac{3}{5} \left\{ n(t_1) - \frac{6}{5\alpha_o L} \left[1 + \log \frac{5}{6} \alpha_o n(t_i) L \right] \right\}$$

where $\phi_+(L, t_p)$ is the output peak power. Taking no account of the frequency dependence of the amplification factor and not considering line broadening effects (the linewidth is only 0.1nm) they plotted the output peak power as a function of both discharge length and initial inversion density. Their results are presented in figure 1.5 (a) and (b) and the peak power is seen to increase with both increasing discharge length and initial inversion density. Higher inversion densities are produced by faster rising current discharges. For moderate inversion densities the threshold length is about 20cm. In a later paper (1.11) they showed that the increase of peak power with length saturates when the length is much greater than the threshold length. Rewriting equation 1.17 in terms of the threshold length L_T given by equation 1.16 gives

$$\phi_+ (L, t_p) \alpha 1 - \frac{L_T}{L} \left(1 + \log \frac{L}{L_T}\right) = f\left(\frac{L}{L_T}\right) \quad (1.18)$$

where $f(L/L_T)$ is the normalized output peak power. Fig. 1.6(a) is a plot of $f(L/L_T)$ against L/L_T and shows that initially, up to about 5 times the threshold length (i.e. ≃ 100cm), the peak power increases with length as a saturated linear amplifier, but with further increases in length the peak power reaches a maximum value. In their first paper (1.10) they also calculated the pulse width (full width at half maximum (FWHM)) as a function of discharge length at various initial inversion densities. Their result is shown in figure 1.6 (b) and it shows two interesting

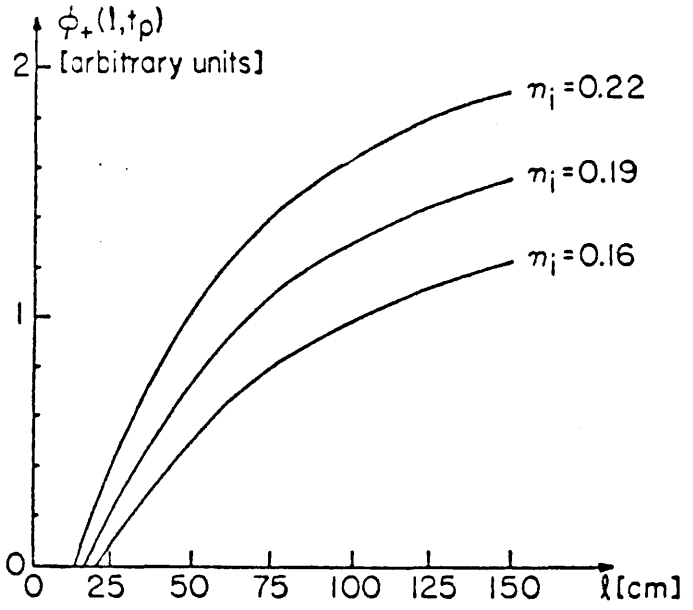

The dependence of the output peak power on the length of the laser.

(a)

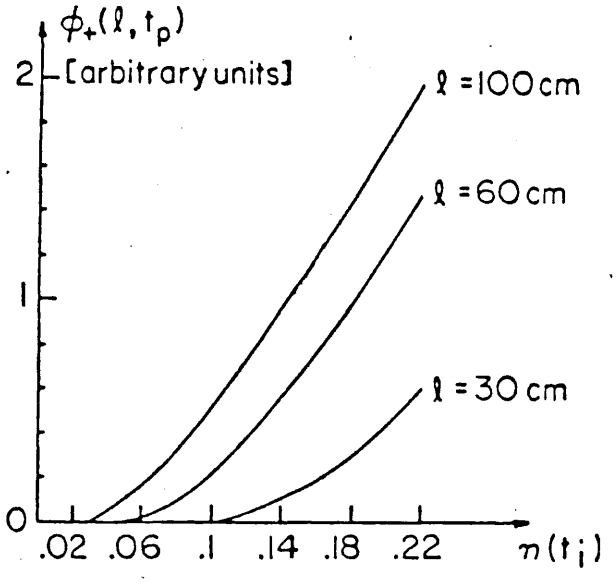

The dependence of the output peak power on the initial inversion density.

(b)

FIGURE 1.5 Variation of the output peak power as a function of discharge length (a) and initial inversion density (b). (from Richter et al. [1.10]).

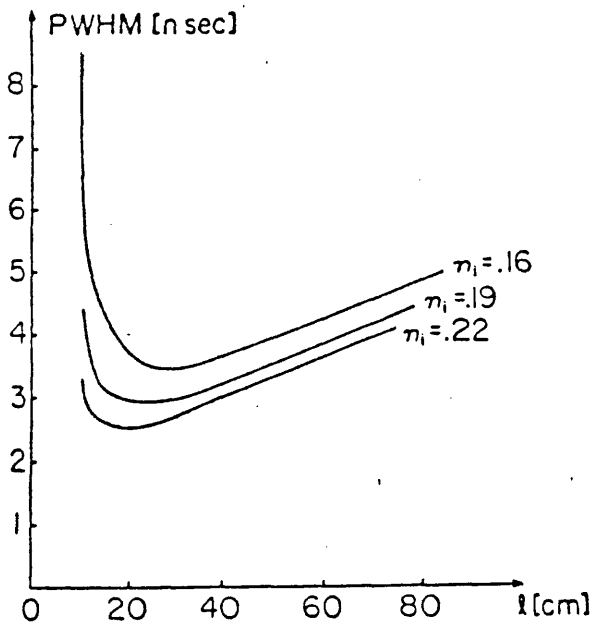

Pulse width at half-maximum (PWHM) as a function of length of the laser for different initial inversion densities.

(b)

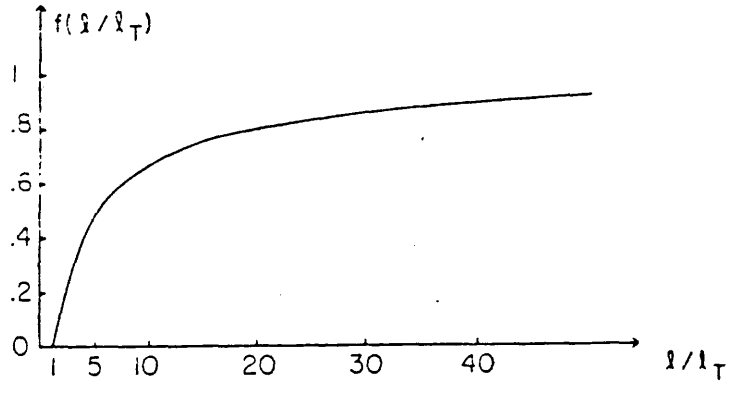

(a) The length dependence of the output peak power.

FIGURE 1.6 Saturation of the output peak power with length (a) and variation of pulse width as a function of discharge length and initial inversion density (b) (from Richter et al. (1.10 and 1.11)).

features. Firstly the pulse width increases with length from a minimum at a length of about 20cm (ie. near the threshold length). Secondly higher initial inversion densities produce pulses with narrower widths. These results are consistent with both the work of Ali (1.9) and experimental observations in general.

1.3 DESIGN CONSIDERATIONS

Since Heard's (1.12) discovery of the nitrogen laser there have been a large number of papers describing various designs (1.15-1.62). In this section design alternatives and their effect on the operation and output characteristics of the nitrogen laser are discussed.

1.3.1 Electrical Aspects

As mentioned previously the nitrogen molecules are excited by direct electron impact. If F_e is the electron flux (electrons cm^{-2} sec^{-1}) a total nitrogen molecule electron collision cross section σ_e can be defined as follows

$$dF_e = -\sigma_e N_g F_e \, dz \qquad (1.19)$$

Here dF_e is the change of flux which takes place when the beam propagates a distance dz through the ground state nitrogen molecules of density N_g. Collisions which produce

electronic excitation account for some fraction of the total cross section σ_e. If σ_{e2} is the cross section for electronic excitation from the ground level to the upper laser level, then the rate of population of the upper state due to the pumping process is

$$\left(\frac{dN_2}{dt}\right)_p = \sigma_{e2} \; N_g F_e = N_g N_e v_e \sigma_{e2} \tag{1.20}$$

Where N_e is the electron density and v_e is the electron velocity. The above applies to a monoenergetic beam of electrons. In a gas discharge however the electrons will not be monoenergetic but will have some particular energy distribution f(E) where f(E)dE is the probability of an electron having its energy between E and E + dE. In this case the rate of population of the upper state is obtained from (1.20) by averaging over the distribution, i.e.,

$$\left(\frac{dN_2}{dt}\right)_p = N_g \; N_e \; \langle v_e \sigma_{e2} \rangle \tag{1.21}$$

where

$$\langle v_e \sigma_{e2} \rangle = \int_0^\infty v_e \sigma_{e2} \; (E) f(E) \; dE \tag{1.22}$$

It has been shown (1.13) that the electron distribution function for a nitrogen discharge can be closely approximated by a Maxwellian function when the electric field to pressure ratio E/p exceeds $30 Vcm^{-1}\ torr^{-1}$. This is the case for nitrogen lasers during the time of interest. For a Maxwellian distribution

$$f(E) \propto E^{-1/2} \exp\left[-(E/kT_e)\right] \qquad (1.23)$$

so that knowing the effective electron temperature T_e is sufficient to characterise the distribution (k is Boltzmann's constant). Assuming that at each collision some fraction δ of the kinetic energy of the electron is lost then T_e can be related to the applied electric field. The power delivered by the electric field to the electrons is given by

$$P_D = eEv_d \qquad (1.24)$$

where e = electronic charge, E = applied electric field and v_d is the drift velocity given by

$$v_d = \frac{e\,lE}{mv_{th}} \qquad (1.25)$$

l is the mean free path, m is the mass and v_{th} is the average thermal electron velocity. The average kinetic energy of the electrons is given by

$$k_e = \frac{mv_{th}^2}{2} \qquad (1.26)$$

and the collision rate by v_{th}/l so the power lost by the electrons (which equals the power delivered by the electric field) is given by

$$P_L = \delta \frac{v_{th}}{l} \frac{mv_{th}^2}{2} \qquad (1.27)$$

By equating (1.27) and (1.24) and using the fact that

$$T_e = \frac{mv_{th}^2}{2k} \qquad (1.28)$$

the following expression is obtained:-

$$T_e = \frac{e}{(2\delta)^{1/2}k} El \qquad (1.29)$$

Since the mean free path l is inversely proportional to the pressure p then

$$T_e \propto \frac{E}{p} \qquad (1.30)$$

As the cross sections for the various processes (X → C, X → B, ionisation etc.) vary with electron energy there will be some value of T_e and hence E/p which maximises the differential rate of excitation to the laser levels. Newman and Detemple (1.14) calculated the excitation rates to the various levels as a function of E/N (≡E/p) and their results are shown in figure 1.7. The solid lines correspond to an 'exact' solution of the Boltzmann transport equation whereas the dashed lines refer to a Maxwellian distribution. Although it appears that the excitation to the B state is always greater than that of the C state it should be noted that these rates are summed over all the vibrational levels. For excitation rates to the laser levels the excitation rate shown here should be multiplied by the Frank-Condon factor (shown in Table 2.2) appropriate to the particular vibrational level.

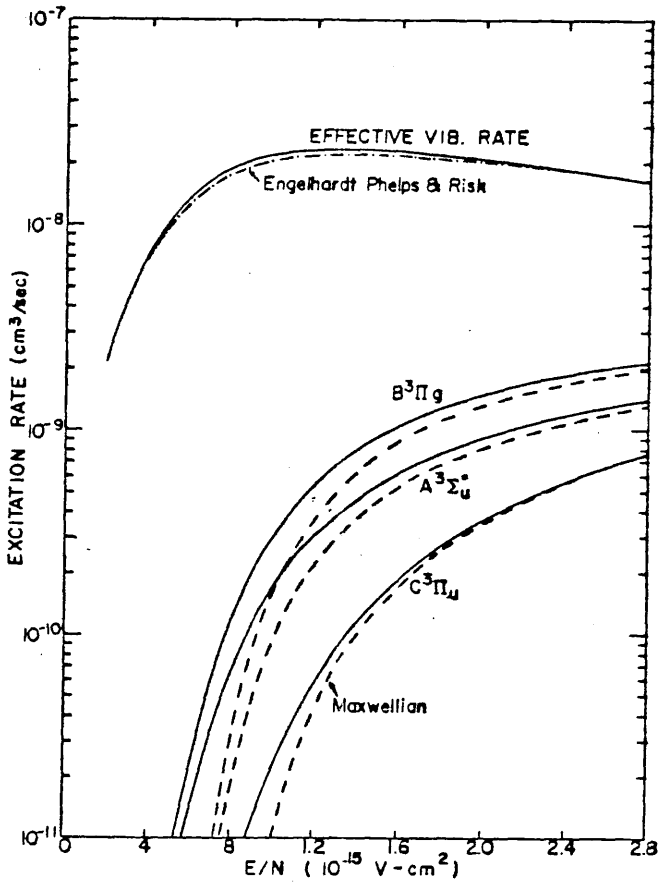

FIGURE 1.7 Excitation rates for electron impact of nitrogen (from Newman and DeTemple (1.14)).

If the E/N value is too low then the C state is not pumped effectively, whereas if it is too high losses due to other processes occur (eg. excitation to higher levels and particularly excessive ionisation which may cause discharge instability). Hence there is an optimum value for T_e. The value for nitrogen lasers is about 4ev (1.6) which corresponds to an E/p of 80V cm^{-1} $torr^{-1}$ (or an E/N of 2.4×10^{-15} Vcm^{-2}) (1.14). The rate of population of the upper laser level is given by

$$\left(\frac{dN_2}{dt}\right)_p = W_p N_g \qquad (1.31)$$

Hence using (1.21), the pump rate Wp is given by

$$W_p = N_e \langle v_e \sigma_{e2} \rangle \qquad (1.32)$$

The electron density N_e can be expressed as a function of the current density J and the drift velocity v_d thus

$$N_e = \frac{J}{ev_d} \qquad (1.33)$$

Using (1.28) and (1.29) to eliminate v_{th} from (1.25) one obtains

$$v_d = \left(\frac{\delta}{2}\right)^{1/4} \left(\frac{elE}{m}\right)^{1/2} \qquad (1.34)$$

Substituting (1.34) and (1.33) into (1.32) produces

$$W_p = \frac{J}{e} \left[\langle v_e \sigma_{e2} \rangle \left(\frac{2}{\delta}\right)^{1/4} \left(\frac{m}{elE}\right)^{1/2}\right] \qquad (1.35)$$

The expression in the square brackets depends only on the E/p value which as discussed previously is already optimised for efficient pumping of the laser levels. Hence the only way to increase the rate of pumping is to increase the current density J. The two practical parameters that determine the size of the population inversion in a nitrogen laser are the E/p ratio and the current density.

The rate of pumping into the two laser levels are given by

$$\frac{dN_2}{dt} = N_g \frac{J}{ev_d} \langle v_e \sigma_{e2} \rangle \qquad (1.36)$$

$$\frac{dN_1}{dt} = N_g \frac{J}{ev_d} \langle v_e \sigma_{e1} \rangle \qquad (1.37)$$

The population inversion ΔN can be found by integrating and combining these equations to give

$$\Delta N = N_g J \left[\langle v_e \sigma_{e2} \rangle - \langle v_e \sigma_{e1} \rangle\right] t \qquad (1.38)$$

Practical values for a nitrogen laser with a gas pressure of 50 torr and an optimum T_e of 4ev are $N_g = 1.77 \times 10^{18} cm^3$, e = $1.602 \times 10^{-19} C$ and $v_d = 2.18 \times 10^7$ (1.14). Using (1.14) and (1.3) $\langle v_e \sigma_{e2} \rangle$ and $\langle v_e \sigma_{e1} \rangle$ are found to be 3.10 and $1.13 \times 10^{-10} cm^3 s^{-1}$ respectively so that equation (1.38) reduces to

$$\Delta N = 10^{20} \quad Jt \quad cm^{-3} \qquad (1.39)$$

Hence for a pumping duration of 2ns (1.7) and a typical average current density of 50A cm^{-2} ΔN has a typical value of 10^{13} cm^{-3}.

Successful pumping of nitrogen molecules can be achieved with either a longitudinal or transverse discharge. The longitudinal discharge does produce a beam with circular geometry and low divergence but it suffers from two major drawbacks. Firstly because the optimum E/p ratio is quite high in nitrogen lasers ($80 V cm^{-1} torr^{-1}$ (1.6)) the applied voltage has to be high and the pressure low. Secondly the combination of low pressure (small N_g) and small active volume means that the total number of nitrogen molecules is low resulting in lower output energies and peak powers. Typically the number of ground state nitrogen molecules in a longitudinal device is 10^{18} (length 20cm, discharge diameter 0.3cm, pressure 20 torr) compared to 1.5×10^{20} in a transverse device (discharge

cross-section 0.5 x 2.5cm^2, length 75cm, pressure 50 torr). Due to these limitations there have been relatively few reports of longitudinal discharge nitrogen lasers (Borgstrom (1.15), Wladimiroff et. al. (1.16)) since the first report of a transverse discharge device by Leonard (1.20).

The two types of discharge circuit most commonly used for the excitation of the nitrogen laser are the Blumlein and capacitor transfer (C - C) circuits. Schematic lumped parameter and equivalent circuits are shown in figure 1.8. In the equivalent circuits (figures 1.8 (b) and (d)) S_1 represents the high voltage switch with L_s and R_s being its series inductance and resistance respectively. S_2 represents the switching of the tube by breakdown of the laser gas with L_T and R_T being the tube series inductance and resistance (R_T includes the time varying resistance of the laser gas). In both cases R can be neglected during the time of the discharge. For the Blumlein equivalent circuit (figure 1.8 (b)) the following circuit equations apply:-

$$I_1 = I_2 + I_3 \tag{1.40}$$

$$\frac{dq_1}{dt} = -I_2, \quad \frac{dq_2}{dt} = -I_3 \tag{1.41}$$

$$I_1 = -\left(\frac{dq_1}{dt} + \frac{dq_2}{dt}\right) \tag{1.42}$$

With S_1 only closed

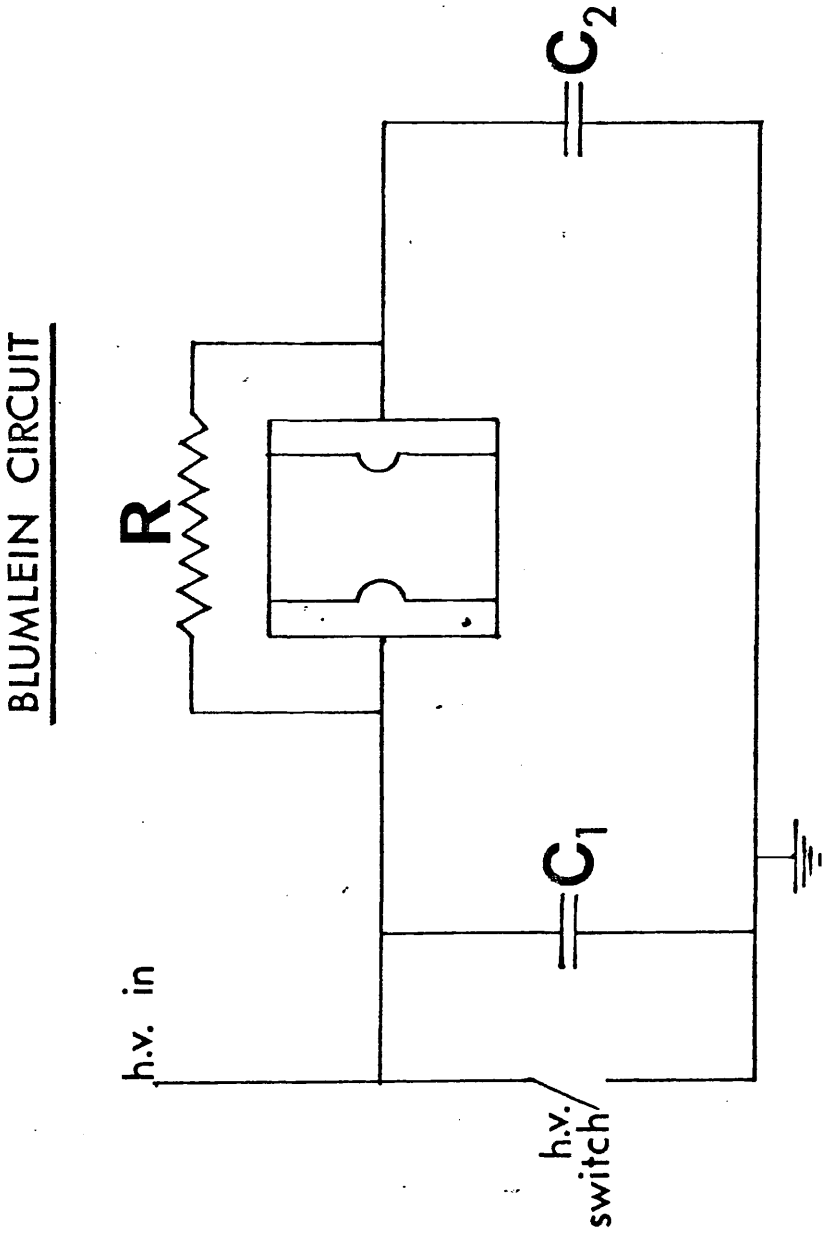

Figure 1.8(a).Schematic Blumlein circuit.

FIGURE 1.8. Electrical circuits used for excitation of nitrogen lasers.

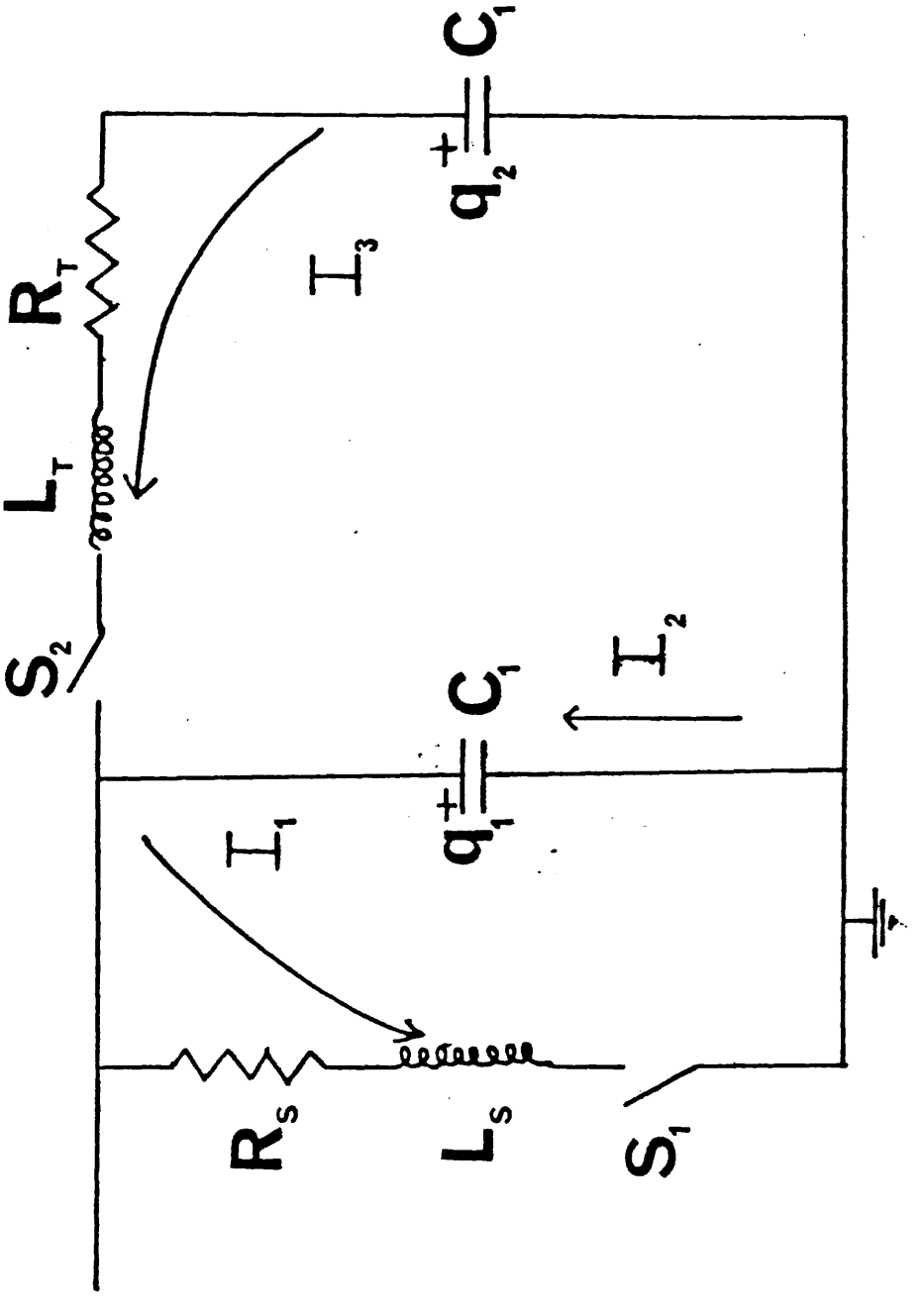

Figure 1.8(b).Equivalent Blumlein circuit.

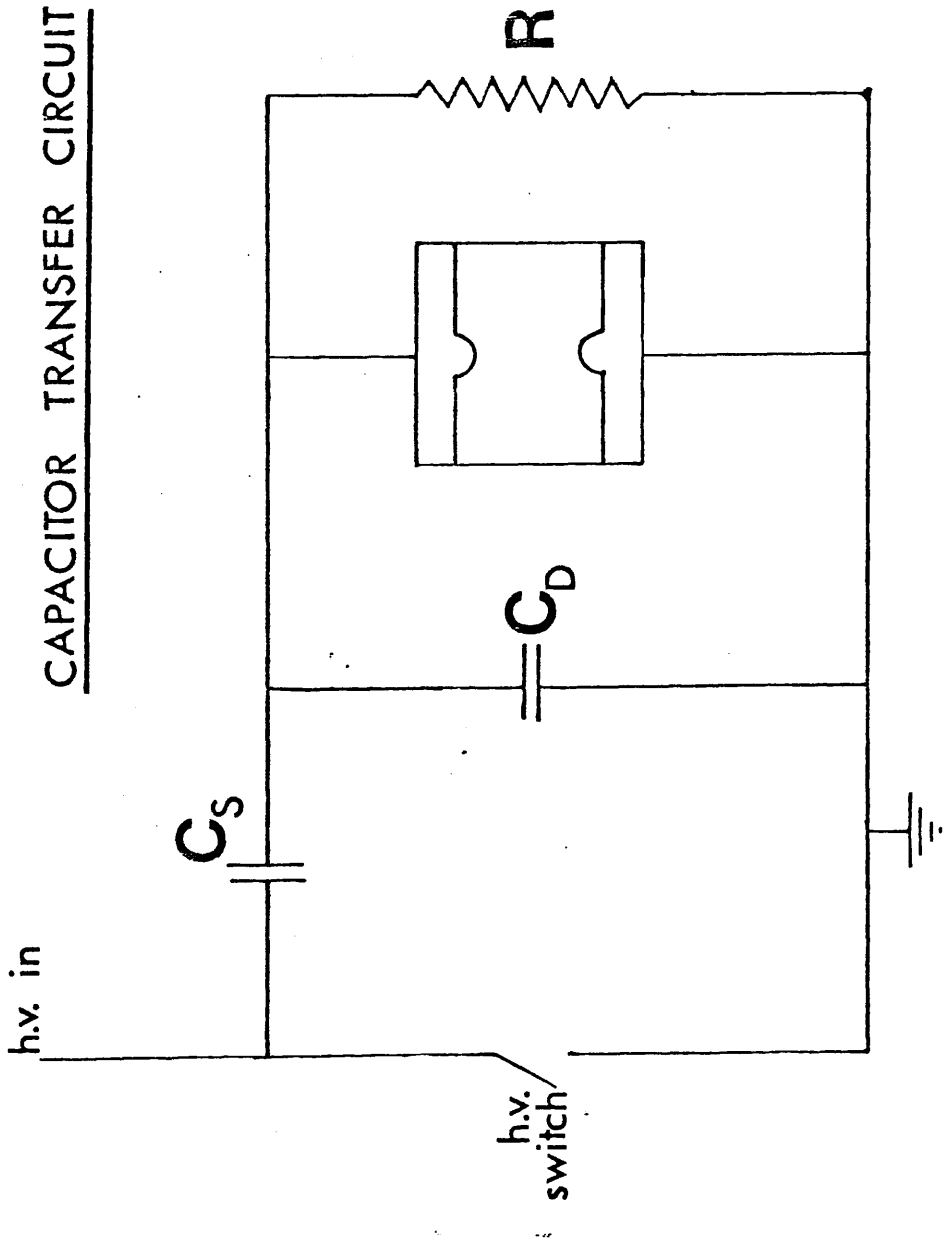

Figure 1.8(c).Schematic capacitor transfer circuit

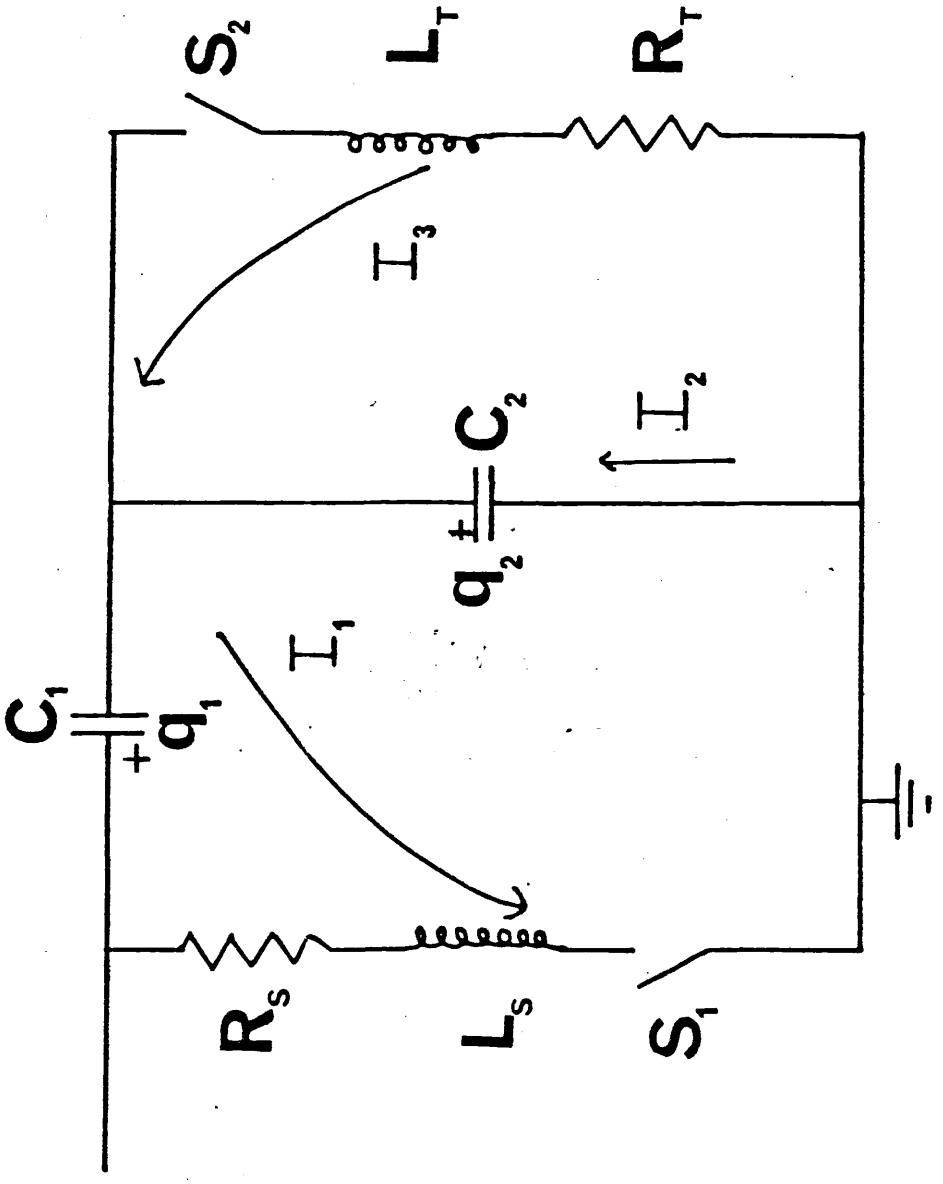

Figure 1.8(d).Equivalent capacitor transfer circuit.

$$L_s\left(\frac{d^2q_1}{dt^2} + \frac{d^2q_2}{dt^2}\right) + R_s\left(\frac{dq_1}{dt} + \frac{dq_2}{dt}\right) + \frac{q_1}{C_1} = 0 \qquad (1.43)$$

and with S_2 closed

$$L_T \frac{d^2q_2}{dt} + R_T \frac{dq_2}{dt} + \frac{q_2}{C_2} - \frac{q_1}{C_1} = 0 \qquad (1.44)$$

Initially S_2 is open and upon closure of the switch S_1, the voltage V_1, can be calculated using the facts that

$$\frac{d^2q_2}{dt^2} = \frac{dq_2}{dt} = 0 \qquad (1.45)$$

Equation (1.43) therefore reduces to

$$L_s \frac{d^2q_1}{dt^2} + R_s \frac{dq_1}{dt} + \frac{q_1}{C_1} = 0 \qquad (1.46)$$

The particular solution of this equation applicable to the nitrogen laser is

$$q_1 = \exp(-t/T)\,[a \sin \omega t + b \cos \omega t] \qquad (1.47)$$

$$\text{with } \omega = \left(\frac{1}{L_sC_1} - \frac{R_s^2}{4L_s}\right)^{1/2} \qquad (1.48)$$

and $T = \frac{2L_s}{R_s}$

At $t = 0$ $I_1 = 0$ due to L_s, hence $\frac{dq_1}{dt} = 0$,

also $\frac{d^2q_2}{dt^2} = 0$ so that $\frac{dI_1}{dt} = \frac{-V_o}{L_s}$.

Using these and assuming $\omega >> \frac{1}{T}$ (i.e. small damping) gives

$$q_1 = \frac{Vo}{L_s \omega^2} \exp(-t/T) \cos \omega t \qquad (1.50)$$

so that

$$V_1 = \frac{q_1}{C_1} = \frac{Vo}{L_s \omega^2 C_1} \exp(-t/T) \cos \omega t \qquad (1.51)$$

The voltage across the laser tube (i.e. S_2 because it is open) is given by $V_T = V_o - V_1$ (due to the slow effect of R shown in figure 1.8 (a)). So that

$$V_T = V_o \left(1 - \frac{\exp(-t/T) \cos \omega t}{C_1 L_s \left(\frac{1}{L_s C_1} - \frac{R_s^2}{4L_s^2} \right)} \right) \qquad (1.52)$$

Using the assumption that $\omega >> \frac{1}{T}$ gives

$$V_T \simeq V_o (1 - \exp(-t/T) \cos \omega t) \qquad (1.53)$$

with $\omega \simeq \dfrac{1}{(L_s C_1)^{1/2}}$ (1.54)

and $T \simeq \dfrac{L_s}{2R_s}$ (1.55)

For the capacitor transfer equivalent circuit (figure 1.8 (d)) the circuit equations are

$$I_1 = I_2 + I_3 \tag{1.56}$$

$$\frac{dq_1}{dt} = -I_1, \quad \frac{dq_2}{dt} = -I_2 \tag{1.57}$$

$$I_3 = \left(\frac{dq_2}{dt} - \frac{dq_1}{dt}\right) \tag{1.58}$$

With S_1 only closed

$$L_s \frac{d^2q_1}{dt^2} + R_s \frac{dq_1}{dt} + \frac{q_1}{C_1} + \frac{q_2}{C_2} = 0 \tag{1.59}$$

and with S_2 closed

$$L_T \left(\frac{d^2q_2}{dt^2} - \frac{d^2q_1}{dt^2}\right) + R_T \left(\frac{dq_2}{dt} - \frac{dq_1}{dt}\right) + \frac{q_2}{C_2} = 0 \tag{1.60}$$

Initially S_2 is open and upon closure of S_1, the voltage V_2 may be calculated using the fact that $I_3 = 0$. Consequently $I_1 = I_2$ or $\frac{dq_1}{dt} = \frac{dq_2}{dt}$ hence

$$q_1 = q_2 + Q_o \tag{1.61}$$

where Q_o is a constant. Equation (1.59) then becomes

$$L_s \frac{d^2q_1}{dt^2} + R_s \frac{dq_1}{dt} + \frac{q_1}{C} = V_x \tag{1.62}$$

where $$C = \frac{C_1C_2}{C_1+C_2} \tag{1.63}$$

and $$V_x = \frac{Q_o}{2} \tag{1.64}.$$

The particular solution of this equation applicable to the nitrogen laser is

$$q_1 = \exp(-t/T)\,[c \sin \omega t + d \cos \omega t] \tag{1.65}$$

with $$\omega = \left(\frac{1}{L_sC} - \frac{R_s^2}{4L_s^2}\right)^{1/2} \tag{1.66}$$

and $$T = \frac{2L_s}{R_s} \tag{1.67}$$

At $t = 0$ $I_1 = 0$ due to L_s, hence $dq_1/dt = 0$, also $d^2q_2/dt^2 = 0$ so that $dI_1/dt = L_sV_o$. Using these and assuming $\omega >> 1/T$ gives

$$q_1 = \frac{V_o}{L_s\omega^2} \exp(-t/T) \cos\omega t + \frac{Q_oC}{C_2} \tag{1.68}$$

The voltage across the laser tube V_T (i.e. across S_2 because it is open) is given by $V_T = q_2/C_2$. Using (1.61), (1.63) and the assumption $\omega >> 1/T$, V_T is given by

$$V_T \simeq \frac{V_oC_1}{C_1 + C_2} \exp(-t/T) \cos\omega t - \frac{Q_o}{C_2} \left(\frac{C_2}{C_1+C_2}\right) \tag{1.69}$$

Due to the slow action of R (figure 1.8 (c)) we choose Q_o such that at $t = 0$ $V_T = 0$. Hence

$$V_T \simeq \frac{V_o \ C_1}{C_1 + C_2} \exp(-t/T) \cos\omega t - 1 \tag{1.70}$$

$$\text{with } \omega \simeq \left(\frac{C_1 + C_2}{L_sC_1C_2}\right)^{1/2} \tag{1.71}$$

$$\text{and } T \simeq \frac{2L_s}{R_s}$$

Upon closure of switch S_2 (i.e. after gas breakdown in the laser tube) current I_3 will flow. Solution of the circuit equations for I_3 is complex even under the assumption that

R_T is constant and conventionally I_3 is computed numerically. However the following proportionality holds

$$I_3 \propto V_T \exp(-t/T_D) \sin\omega_D t \qquad (1.73)$$

$$\text{with } \omega_D \propto \frac{1}{\sqrt{L_T C}} \qquad (1.74)$$

$$\text{and } T_D \propto \frac{2L_T}{R_T} \qquad (1.75)$$

From equation (1.38) the inversion density is proportional to the current density and hence I_3. Consequently I_3 needs to be maximised and should have a fast risetime so that most of the energy is deposited in a time short compared to the upper state lifetime (36ns). This means V_T and ω_D have to be maximised. The value of V_T that is reached before breakdown depends on the risetime and consequently on ω, hence ω also needs to be maximised. Physically this means that the inductances L_S and L_T must be as small as possible. Typical values for L_S and L_T are 10-20nH and 2-10nH respectively. For a moderately sized laser $C_1 = C_2 = 20$nF so that $\omega = 5 \times 10^7$ Hz and 7×10^7 Hz for the Blumlein anc C-C circuit respectively. Despite the slightly faster risetime for the C-C circuit the actual voltage V_B reached at breakdown is less than in the case of the Blumlein circuit because the amplitude is less ($0 \rightarrow 2V_0$ for the Blumlein and $0 \rightarrow V_0$ for the C-C (excluding damping and with $C_1 = C_2$)). In addition the C in the

expression for ω_p is larger than in the case of the Blumlein circuit because it includes both C_1 and C_2. Consequently the current risetime and current density reached before lasing are less than in the Blumlein laser and this has a profound effect on the output. Due to the high initial inversion densities produced in the Blumlein circuit large peak powers are produced but because of the self-terminating nature of the lasing transition (pp 20) the output is soon extinguished. However in the C-C circuit the initial inversion densities are not as high and the self termination time not as short leading to longer pulses. Typical pulse durations for lasers using C-C circuits are 8-10ns (FWHM) and 3-5ns for those using Blumlein circuits. The pulse energies produced by the two systems are similar.

The requirement for minimum L_S and L_T means that the nature and layout of the components are critical. Inductance is proportional to the area enclosed by any current loop so that the loops containing I_1 and I_3 must be made as physically small as possible (under the constraint of adequate insulation). All electrical paths should be fashioned as current sheets rather than single lines and the lengths should be kept as short as possible.

For the Blumlein circuit the capacitors C_1 and C_2 usually take one of two forms. They are either a parallel array of ceramic capacitors (Nagata and Kimura (1.18)) or are formed by large area parallel plates separated by a thin insulator (C.P. Wang (1.19). The capacitance of such a capacitor is given by

$$C = 8.85 \times 10^{12} \frac{\varepsilon A}{d} \quad F \qquad (1.76)$$

where A is the area of the plates, d the separation and ε the dielectric constant of the insulator. For a 20nF capacitor made with Mylar (ε = 3.25) designed to hold off 25kV the area required is 250cm^2. This is a large value for convenience and is one drawback of the inexpensive parallel plate capacitor, another is that insulator failure rate is quite high. The first problem can be overcome by wrapping the capacitors round the discharge chamber (Schwab and Hollinger (1.20)) and the second by pulse charging the capacitors (C.P. Wang (1.19)), Bonch-Bouevich et. al. (1.21)). The distributed nature of the capacitor C_1 in either case means that this circuit is amenable to modification to operate with the travelling wave excitation method first reported by Shipman (1.22) and later developed by others (1.23, 1.24). In this method the electrical excitation is induced to travel from one end of the discharge chamber to the other in sychronisation with the light pulse. When using this method higher peak powers and shorter pulse widths are produced. To achieve this by propagating a voltage wave down the distributed capacitance (i.e. transmission line) the current risetime in the high voltage switch, equal to L_s/Z_o (Z_o is the characteristic impedance), must be less than the two way transit time on the transmission line. The velocity of propogation in a

transmission line is given by

$$v = \frac{c}{\sqrt{\varepsilon}} \qquad (1.77)$$

so that for the Mylar capacitor given above $v = 1.65 \times 10^8 ms^{-1}$. Hence the two-way transit time for a 50cm laser is 6ns so that the switch inductance needs to be less than 6nH (for $Z_o = 1\,\Omega$). This is in practice quite difficult to achieve with conventional high voltage switches. Consequently it is easier to achieve the travelling wave excitation by having non parallel electrodes (1.25) or by using a distributed transmission line of various lengths (i.e. graduated parallel cables (1.26)).

For the C-C circuit the storage capacitor C_1 (C_s) is usually one large low inductance paper foil capacitor (Feldman (1.27)) or a parallel array of discrete ceramic capacitors (Woodward et. al. (1.28)). The dumping capacitor C_2 (C_D) most commonly consists of a parallel array of ceramic capacitors. However they are sometimes replaced wholly or partly by a parallel plate transmission line (Geller et. al. (1.29)) or a set of low inductance parallel coaxial cables (Woodward et. al. (1.28), Anderson and Borgstrom (1.30)). Cubeddu and Curry (1.31) report a specially fabricated dumping capacitor which utilises water for the dielectric medium.

The value of C_s, C_D, C_1 or C_2 depends on the length of the electrode to be used. Feldman et. al. (1.30) found experimentally that a suitable value for the dumping capacitor in the C-C circuit is 15-20 nanofarad/metre of electrode length. They also found that the optimum value for the C_D/C_s ratio is between 1/3 and 1/2. There has been no data reported in the literature for the optimum value of C_1 and C_2 in the Blumlein circuit. Increasing C_1 and C_2 increases the stored energy proportionately but because of equations (1.54) and (1.74) leads to lower voltages and current risetimes being achieved. In general there will be some optimum value of C_1 and C_2 which leads to the best efficiency. In all cases C_1 should be equal in value to C_2 (1.32).

The other critical component in the electrical circuit is the high voltage switch. This has to have a hold off voltage of tens of kilovolts, a very low inductance and be able to withstand peak currents of a few kiloamps. There are only two devices capable of satisfying these requirements, the hydrogen thyratron and the spark gap. The main advantages of the spark gap are its simplicity, low cost and its ability to operate either as a simple relaxation oscillator (i.e. triggering by self breakdown) or to be triggered by an external electrical signal. The advantages of the thyratron are that it produces less radio frequency interference and operates with much less jitter (variation of delay in the time between the application

of an electrical trigger pulse and the initiation of switching). Jethwa et. al. (1.33) reduced this jitter to less than one nanosecond by using special triggering circuits (compared to typically 50-100ns with a spark gap). The drawbacks of the thyratron are the cost, the necessity of an auxillary supply for the heater and the difficulty of providing highly conducting electrical paths between it and the storage capacitors whilst minimising the flow of heat.

A final consideration pertaining to the electrical aspects is whether to include preionisation. Preionisation is applied to ensure a stable glow discharge. A simple physical model to determine the requirements of preionisation in effecting a stable glow discharge was proposed by Palmer (1.34) and later developed by Levatter and Lin (1.35). Initially it is assumed that there are a certain number density of primary electrons n_o in the vicinity of the cathode and then a step voltage is applied across the cathode anode gap. The applied electric field induces the electrons to cross the gap. As they do so the number of electrons increases due to ionisation of the gas molecules and reaches a value n_e given by

$$n_e = n_o \exp (\alpha V_d t) \qquad (1.78)$$

where α is the Townsend ionisation coefficient, v_d is the electron drift velocity and t the elapsed time. The electrons are more mobile than the ions and a space charge electric

field develops in each avalanche. After a certain critical time t_c this field becomes comparable to the applied field. When this happens avalanches initiated by secondary electrons (produced by photoionisation) are attracted to the primary avalanches. This field increases the space charge field within each avalanche head. Eventually one avalanche will bridge the gap and an arc will result. However if the number of primary electrons is sufficient such that when the time t_c is reached the avalanche heads overlap then the high local space charge fields of each avalanche are avoided and a homogeneous glow discharge will result. The avalanche head radius is given by (1.35))

$$r = (2\ Dt)^{1/2} \qquad (1.79)$$

where D is the electron diffusion coefficient. There will be some critical radius r_c corresponding to t_c where the space charge field of the avalanche is equivalent to the applied field. The criterion for a stable discharge is that when r_c is reached the initial number density of primary electrons n_o is above some critical value n_c such that the separation of the avalanche heads is less than r_c, or

$$n_c > (r_c)^{-3} \qquad (1.80)$$

Levatter and Lin (1.35) proceeded to show that there is also a maximum allowable risetime to the voltage pulse for efficient glow discharge operation. However this criterion does not affect nitrogen lasers because the voltage risetime is necessarily less than this maximum.

For nitrogen lasers preionisation is not as important as in some other gas lasers (eg. rare gas halide lasers) because they do not necessarily conntain electrophilic gases (eg. HCl, NH_3) which remove electrons from previous discharges. In addition it should be noted that the radius of an avalanche head is inversly proportional to pressure so that at low pressures (<100 torr) preionisation is not usually required. However at high pressures or if an electronegative gas is added it is necessary.

1.3.2 Mechanical Considerations

There are several mechanical aspects which have to be considered when designing a nitrogen laser. Most of these pertain to the layout of the electrical components as described previously; however there are other considerations such as the length and shape of the discharge chamber, electrode geometry and gas handling.

The length of the laser will mainly be defined by the size of capacitors being used as outlined previously. The lasers can be scaled to larger capacitors and longer lengths under three constraints: firstly increasing the capacitors increases the voltage and current risetime, secondly the prediction of the output saturating with length by Richter et. al. (1.11) and thirdly the length can not be longer than the product of the pulse duration and the speed of light (half this if a rear mirror is used). This latter effect arises because the gain is

time varying and becomes negative (i.e. absorption occurs) upon termination of the laser pulse (Hasson and Bergmann (1.36)).

The gain can be defined for the case of a monochromatic plane wave of frequency for ν and intensity I propogating through an inverted medium with an inversion density ΔN. The plane wave will stimulate transitions from the upper level 2 to the lower level 1 at a rate given by $\Delta N \sigma$ where σ is the stimulated emission cross-section. The power per unit volume generated is given by

$$P = \Delta N \sigma h\nu \qquad (1.81)$$

where h is Plancks constant. This radiation is added coherently to that of the travelling wave so that it is equal, in the absence of dissipation mechanisms, to the increase in intensity per unit length or

$$\frac{dI}{dz} = \Delta N \sigma I \qquad (1.82)$$

The product $\Delta N \sigma$ is referred to as the small signal gain coefficient α_0. The solution of (1.82) is

$$I(z) = I(o) \exp [\alpha_s z] \qquad (1.83)$$

This leads to the definition of the small signal (unsaturated) gain G_o of a laser as below

$$G_o = \exp(\alpha_o l) \tag{1.84}$$

where l is the length of the laser. These equations refer to gain in the absence of any large signal and α_o should be redefined for the case of large signals as (1.37)

$$\alpha_s = \frac{\alpha_o}{1 + \frac{I_o}{I_s}} \tag{1.85}$$

where I_s is the saturation intensity and α_s is the saturated gain coefficient (all the above equations are a steady state approximations). Saturation occurs because of the depletion of the population inversion due to the presence of the signal. I_s is defined as the intensity required to reduce the gain coefficient by half. Equation (1.85) modifies equation (1.82) as follows

$$\frac{dI(z)}{dz} = \frac{\alpha_o \quad I_o}{1 + \frac{I(z)}{I_s}} \tag{1.86}$$

The solution for the small signal case ($Iz \ll I_s$) is the same as equation (1.83) and the solution for the large signal case ($I(z) \gg I_s$) is

$$I_1 = I(o) + \alpha_o I_s l \tag{1.87}$$

Equation (1.85) refers to homogeneously broadened systems whereas the nitrogen laser is a mixture of both inhomogeneous and homogeneous broadening. However as pointed out by Allen and Peters (1.38) for an inhomogeneously broadened gain profile subject to an inhomogeneously broadened emission profile (such as amplified spontaneous emission (ASE)) the saturation behaves more like homogeneous broadening. The reason for this, physically, is that although each frequency unit on the emission profile 'burns' a hole in the gain profile, of the order of the natural linewidth, all these holes overlap. The net effect is that the whole gain profile is reduced by saturation as is typical of saturation effects in homogeneously broadened profiles.

For the nitrogen laser as the laser pulse terminates ΔN equals zero (self terminating laser) and because the lower level is metastable α_o becomes negative and absorption occurs. Consequently for Blumlein circuit lasers with pulse widths of 4ns the length is limited to about 60cm when using a rear mirror. At high pressures the pulse widths are even further reduced (due to shorter upper state lifetime (pp18)) to about 1ns so that the maximum length is reduced to 15cm. The restriction on length can only be circumvented by using the travelling wave excitation method mentioned earlier or by using a multistage oscillator-amplifier device (Jitsuno (1.39)).

Most early nitrogen lasers use a confined discharge where the discharge is confined to a small region by the walls of the chamber. This is useful for high repetition rate operation because the metastable molecules can deexcite by collisions with the walls. The diffusion time of the metastables to the chamber walls is given by

$$t = \frac{4d^2}{\pi^2 v_{th} l} \qquad (1.88)$$

where d is the characteristic chamber dimension, v_{th} is the thermal velocity and l is the mean free path. For a nitrogen laser with d equal to 3mm and operating at 30 torr, $t \simeq 2 \times 10^{-3}$ S, permitting operation at a repetition rate up to 500Hz. However the disadvantages of the confined discharge are that it produces an output with a double line profile and the pulse energies are fairly low because the breakdown voltage reached, V_b, is low because breakdown occurs along a surface. For these reasons most modern designs of nitrogen lasers use an unconfined discharge (plate separation $d \simeq 2$cm, $t \simeq 280$ms), which produces higher energies and a more uniform beam profile. To remove unwanted metastable molecules the gas has to be flowed longitudinally or transversly through the laser chamber. For short lasers (<30cm) longitudinal flow is adequate but for longer systems transverse flow is necessary to avoid a pressure gradient along the tube (which would mean that the E/p was optimised in one place only) and to ensure an

even distribution of residual ions and electrons etc. Targ (1.40) achieved a repetition rate of 1.2KHz and an average power of 1.5 watts by using a blower and heat exchanger system. Sealed-off operation has been reported (Armichev et. al. (1.41)) with some success but the low cost of bottled or liquid nitrogen makes this form of operation normally unnecessary.

The electrode separation needs some consideration. The electrode separation will determine the optimum pressure of operation because the output is optimised at some particular value of E/p. With larger electrode separations this means the optimum pressure will decrease (at a constant applied voltage). Alternatively, if very high applied voltages are going to be used, narrow electrode separations should be avoided because of the high pressure needed for optimum E/p and the resultant narrowing of the pulse width. The structure of the electrodes is not critical, for most low pressure devices each electrode is a cylindrical surface (Fitzsimmons et. al. (1.6)). Other structures have been used including knife edges (Schmidt (1.42)), copper foil edges (Small and Ashari (1.43)) and one or more hacksaw blades (Levatter and Lin (1.44)). One special case of electrode structure is the use of a helix of pins for each electrode (Khrahn (1.45) and (1.46), Sze and Scott (1.47)). This electrode structure generates a circular beam geometry (as opposed to the more normal rectangular) and is thus more suitable for spherical optics.

1.3.3 Other considerations

The other main consideration concerns the optics used with the laser. Conventional stable resonators are generally superfluous due to the very high gain of the system and the short inversion lifetime. The small signal gain coefficient of the system is given by

$$\alpha_o = \Delta N \sigma \qquad (1.89)$$

The stimulated emission cross section σ is given by (1.39)

$$\sigma = \frac{c^2}{8\pi n^2 \nu^2 T_r \Delta\nu} \qquad (1.90$$

where c is the velocity of light, n is the refractive index in the medium, ν is the frequency, T_r is the radiative lifetime and $\Delta\nu$ is the half width (FWHM) of the lineshape function. The radiative lifetime is given by

$$T_r = \frac{\varepsilon_o}{2\pi} \frac{m_e c^3}{f_{12} e^2 \nu_o^2} \qquad (1.91)$$

Where ε_o is the electric permittivity of a vacuum, m_e is the electron rest mass, c is the speed of light, e is the electronic charge, ν_o is the line centre frequency and f_{12} is the oscillator strength of the transition. For the

transition involved $f_{12} = 0.047$ (J. Desquelles et. al. (1.48)) and $\nu_o = 8.84 \times 10^{14}$Hz so that $T_r = 36$ns.

The nitrogen laser transition is both Doppler and pressure broadened but the pressure broadening does not become significant until the pressure approaches atmospheric. The Doppler half width per rotational line is given by (1.39)

$$\Delta\nu = 2\nu_o \left(\frac{2kT \ln 2}{Mc^2}\right)^{1/2} \qquad (1.92)$$

where k is Boltzmanns constant, T is the temperature and M is the mass of the molecule. The mass of the nitrogen molecule is 4.65×10^{-26} kg so that for a temperature of 300°K the half width is 2.1×10^9Hz. Substituting this value along with n = 1 and c = $2.98 \times 10^8 ms^{-1}$ into equation (1.90) gives a value for σ of $1.2 \times 10^{-13} cm^{-2}$ (assuming 5 rotational lines (1.6)). Inserting this value for σ and the value calculated for ΔN previously ($10^{13} cm^{-3}$) into equation (1.89) gives a value of $1.2 cm^{-1}$ for the small signal gain coefficient which is similar to measured values (1.49).

The resulting high value for the gain ensures that the laser is rapidly saturated by ASE. The saturation intensity is given approximately by

$$I_s = \frac{h\nu}{\sigma T_s} \qquad (1.93)$$

where T_s is the spontaneous lifetime. Substitution of the appropriate values for nitrogen gives a value for I_s of 122 Wcm^{-2}. This value is quite small compared to experimentally measured values ($\sim 1 kWcm^{-2}$) indicating that the steady state approximation may not be a good one for nitrogen lasers.

A condition for saturation of the gain by ASE can be formulated (Linford et. al. (1.50)). The spontaneous optical power within a frequency interval $d\nu$, from a volume elenent dV, is taken to be

$$dP_s = \frac{h\nu \, \Delta N \, d\nu dV}{T_s \, \Delta\nu} \qquad (1.94)$$

If only those photons emitted within $d\Omega$ are considered then equation (1.94) becomes

$$dP_s = \frac{h\nu \, \Delta N}{T_s \, \Delta\nu} \frac{d\Omega}{4\pi} d\nu dV \qquad (1.95)$$

The expression for ASE output power is given by

$$P_s = \int_0^{\pi} \int_{-\infty}^{\infty} \int_0^{1} \frac{h\nu}{T \, \Delta\nu} \, \Delta N \exp\left(\sigma \, \Delta N \, (1-z)\right) \left[\frac{d\Omega}{4\pi}\right] d\nu dV \qquad (1.96)$$

The solution of this equation is

$$P_s = I_s \, A \, \frac{\Omega}{4} \, \frac{[\exp(\sigma \, \Delta N l) - 1]^{3/2}}{[\sigma \, \Delta N l \exp(\sigma \, \Delta N l)]^{1/2}} \qquad (1.97)$$

where $I_s(\simeq h\nu/\sigma T_s)$ is the saturation intensity and A is the cross-sectional area of the laser. For saturation of the output by ASE the output power due to ASE is equal to the product I_sA. Hence the condition for this to occur is given by the following inequality (with $G_o = \exp(\sigma\Delta N l)$.

$$\frac{4\,(G_o \ln G_o)^{1/2}}{(G_o-1)^{3/2}} < \Omega \qquad (1.98)$$

For high gain lasers with small active solid angles this reduces to

$$\frac{4\,(\ln G_o)^{1/2}}{G_o} < \Omega \qquad (1.99)$$

Most high gain lasers operate with a mirror placed at one end which essentially doubles the active length and consequently squares the optical gain. Hence equation (1.97) should be written as

$$\frac{4\,(\ln(G_o)^2)^{1/2}}{G_o^{\,2}} < \Omega \qquad (1.100)$$

For a nitrogen laser 50cm long with discharge dimensions of 0.5 x 2cm^2 Ω has a value of 4 x 10^{-4}sr. Hence the gain length product required for saturation is 5.18 corresponding to an inversion density of 10^{12}cm^{-3}. Conversley for a typical inversion density of 10^{13}cm^3 the length required for saturation is 4.3 cm which is comparable to experimentally measured values (1.49). Consequently most nitrogen lasers are saturated by ASE and this combined with the very short inversion lifetimes means that the laser pulses are developed in only a few cavity round trips. This number of round trips is too small to establish conventional stable resonator modes

and the beam qualities are determined by the properties of ASE emission ie. lacking directionality and spatial coherence. The beam divergence will in fact only be controlled by the size of the solid angle Ω so that for the 50cm long laser mentioned previously the beam divergence will be approximately 20 mrad in the horizontal direction and 5 mrad in the vertical direction.

As most nitrogen lasers are used for transverse pumping of dye lasers the beam quality is quite adequate. However for other applications it is not and some way of controlling the beam divergence is required. Ischenko et. al. (1.49) approached the problem by inserting a series of raster diaphragms into the cavity (similar in principle to the an x-ray collimator) which were separated by less than the length required for saturation by ASE. This system was successful in decreasing the beam divergence from 10 mrad to 1 mrad for a decrease in power of 80% but the spatial coherence was still poor. An alternative approach tried by them and other workers (eg. Bergmann (1.51), is the utilisation of an unstable resonator. The analysis of mode build up in unstable resonator for high gain short pulse laser has been presented in a series of papers by Zemskov et al. (1.52) and Isaev et al. (1.53) (1.54) (1.55). The important points which emerge from this analysis are that the magnification of the unstable resonator, M, must be sufficiently large to enable a diffraction-limited resonator mode to become the dominant mode in the resonator in a time t which is less than t_g, the positive gain time, and that

the small signal gain coefficient of the laser medium must be sufficiently small so that the threshold of lasing is not reached before such a mode has had time to build up. In summary

$$t_g > t \tag{1.101}$$

and $$\alpha_o < \alpha_{cr} \tag{1.102}$$

where t and α_{cr} are given, for a confocal positive branch unstable resonator (Isaev et. al. (1.53)) by

$$t = \frac{2L}{c}\left(1 + \frac{\ln M_o}{\ln M}\right) \tag{1.103}$$

$$\alpha_{cr} = \frac{\ln M}{L_a}\left(\frac{A}{2\ln (MM_o)} + 1\right) \tag{1.102}$$

in which $M_o = 2a^2/\lambda f_1$ where a is the radius of the laser aperture, f_1 is the focal length of the output mirror, L is the resonator length and L_a is the length of the gain medium. The quantity A is the gain-length product for which ASE becomes observable. The only other limitation on M is the maximum permissible output coupling. The fractional output coupling in the geometrical limit at large equivalent Fresnel numbers is given by (Siegman (1.56))

$$\delta = 1 - M^{-2} \qquad (1.105)$$

Equation (1.101) can be written in an alternative form (Anan'ev (1.57)) shown below which relates the number of round trips n which are required to transform the ASE into a diffraction limited unstable resonator mode

$$n = \frac{\ln M_o}{\ln M} \qquad (1.106)$$

Use of equations (1.99 - 1.104) enables one to design unstable resonators to produce one to two times diffraction limited output beams for a variety of high gain laser systems.

The remaining consideration pertains to the quality and nature of the laser gas. The quality of the nitrogen is not critical and in general technical grade bottled gas of boiled off liquid nitrogen is quite adequate. Other gases may be added to improve the output power. These include SF_s (Willet and Litynski (1.58), Akins and Lin (1.59)), F_2 (Sumida et al. (1.60)), CF_4 (Collier et. al. (1.61)) and NF_3 (Armandillo and Kearsley (1.62). Power increases have been in the range 10-50% and have been attributed by Judd (1.13) to an increase in the E/p value obtained in the discharge. The main problem in utilising these gases is that they are all electrophilic and can lead to instabilities in the discharge unless adequate preionisation is provided.

1.4 CONCLUSION

From the previous sections it is clear that a large amount of development has been carried out on nitrogen lasers and many design alternatives have been reported in the literature. The most significant and important of these are (1.7, 1.9-1.12, 1.16-1.18, 1.20, 1.22-1.24, 1.27, 1.28, 1.35, 1.36, 1.40, 1.41, 1.44, 1.46, 1.49, 1.58 and 1.62).

Despite this attention the nitrogen laser still has some undesirable output characteristics for some applications. These include the rectangular output beam geometry with the concomitant large and inequal beam divergence, the fixed pulsed width (for a particular laser) and in particular the unpolarised output. The Mark II and III lasers with their subsequent coupling together as an oscillator-amplifier system (as described in later chapters) were designed to improve these characteristics.

CHAPTER II

Mk I LASER

2.1 DESCRIPTION

This laser is based on an unpublished design by B Dunning and co-workers at Rice University. A cross-section of the laser is shown in figure 2.1. The laser operates using a capacitor transfer circuit but with the addition of an inductance L between the spark gap and the storage capacitor. The storage capacitor C_S has a nominal capacitance of 43.2nF and consists of a bank of 12 ceramic capacitors. The dumping capacitor C_D comprises a bank of fourteen and a bank of eighteen 500pF ceramic capacitors, giving a total capacitance of 16nF. The inductance is formed from two straight pieces of low inductance wire each of length approximately 20cm connected from the spark gap to the storage capacitors. The purpose of the inductor is to limit the discharge rate of the storage capacitors and hence reduce the electrostrictive force on the ceramic dielectric within the capacitors. However the limiting of the discharge rate also limits the voltage rise across the laser electrodes, hence the breakdown voltage is lower and the output power is decreased. According to Dunning the decrease is less than 20% and the inclusion of the inductance prevents failure of the ceramic capacitors. The spark gap is a three electrode device and is pressurised with nitrogen. The trigger pulses for all lasers are provided by a Hartley Measurements Ltd. trigger unit

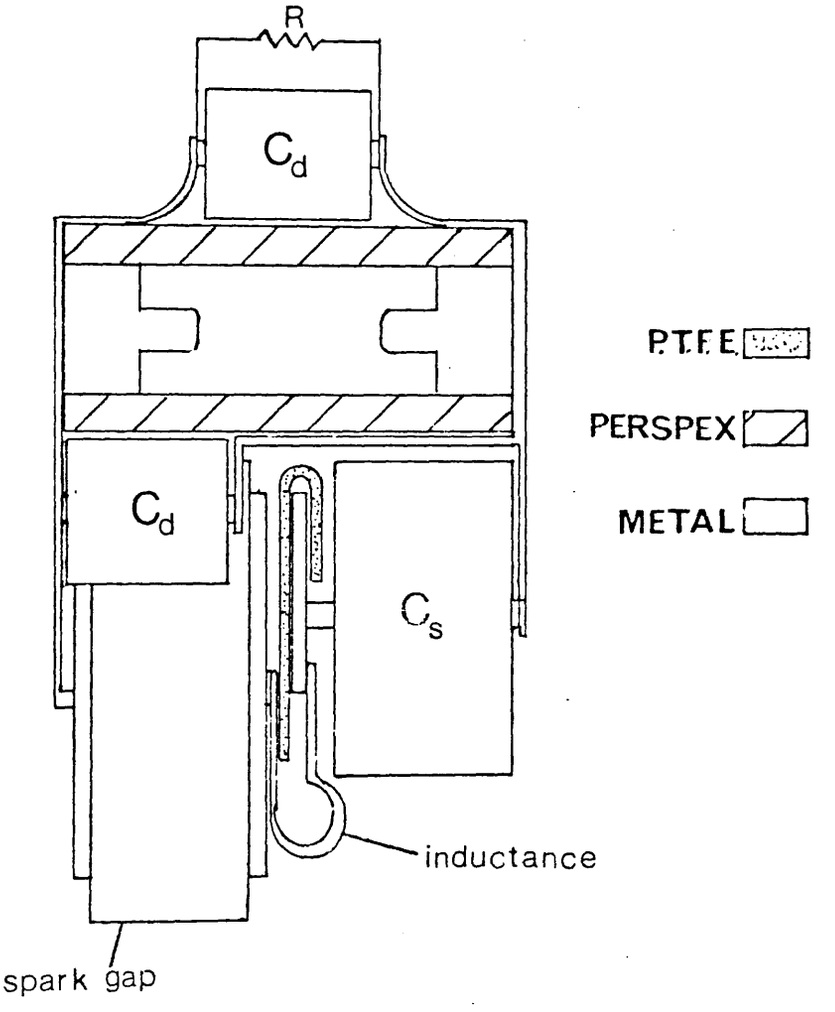

FIGURE 2.1 Cross-section of the Mk I Laser.

model 350 in combination with a pulse transformer of ratio 1:100. Together they produce 30 kV pulses with a repetition rate variable between 1-100Hz. For all lasers the high (<25 kV) DC voltage was supplied by a Hartley Measurements Ltd. capacitor charging unit model 411-2225 which is rated at 200 watts.

The electrodes are separated by a distance of 2.5cm, have an active length of 118cm and a circular profile of radius 4.8mm. The gas flow is longitudinal with the pressure being controlled by a flow valve prior to entering the tube; the gas is exhausted by means of a rotary vacuum pump. The pressure is monitored with an Edwards aneroid type pressure gauge. There were some initial problems in sealing the perspex walls to the aluminium electrodes; attempts were made using RTV silicone seal but the vacuum attainable was not satisfactory. This problem has been overcome by cutting grooves along the top and bottom of the electrodes and placing 'O' ring rubber in the grooves. Also the number of screws along the electrodes has been doubled and only the last few mm at either end is sealed with silicone seal. The ends of the tube are terminated with two fused silica flats, one of which is coated on the outside with aluminium. Each flat can be adjusted to be perpendicular to the laser axis by means of three screws which press a perspex plate onto the flat, which in turn is pressing on to an 'O' ring.

2.2 OPERATION

The output characteristics of this laser are similar to other nitrogen lasers using a capacitor transfer circuit and an open discharge chamber (see for example 1.26). The pulse energy as a function of gas pressure for two different applied voltages is shown in figure 2.2. The experimental method and errors used throughout this work are outlined in Appendix I and unless otherwise stated all results have been taken using this method. The pressure for maximum pulse energy increases with increasing applied voltage; this is because the output energy peaks at a particular value of the electric field to pressure ratio (E/p). This and other characteristics of the operation of nitrogen lasers will be discussed fully in chapters 3 and 4.

The output pulse shape with an applied voltage of 15kV, a repetition rate of 10Hz and a gas pressure of 38 torr is shown in figure 2.3. The figure shows ten pulses superimposed indicating good pulse to pulse stability. The pulse width (FWHM) is approximately 6ns.

This laser has some problems associated with it which make it unsuitable for dye laser pumping or for further development. In particular the discrete ceramic storage capacitors are very prone to failure which makes the laser very unreliable and hence unsuitable for long term operation (ie. more than a few hours at 10Hz). The replacement capacitors, although available, have to come from America (Sprague Electric Company)

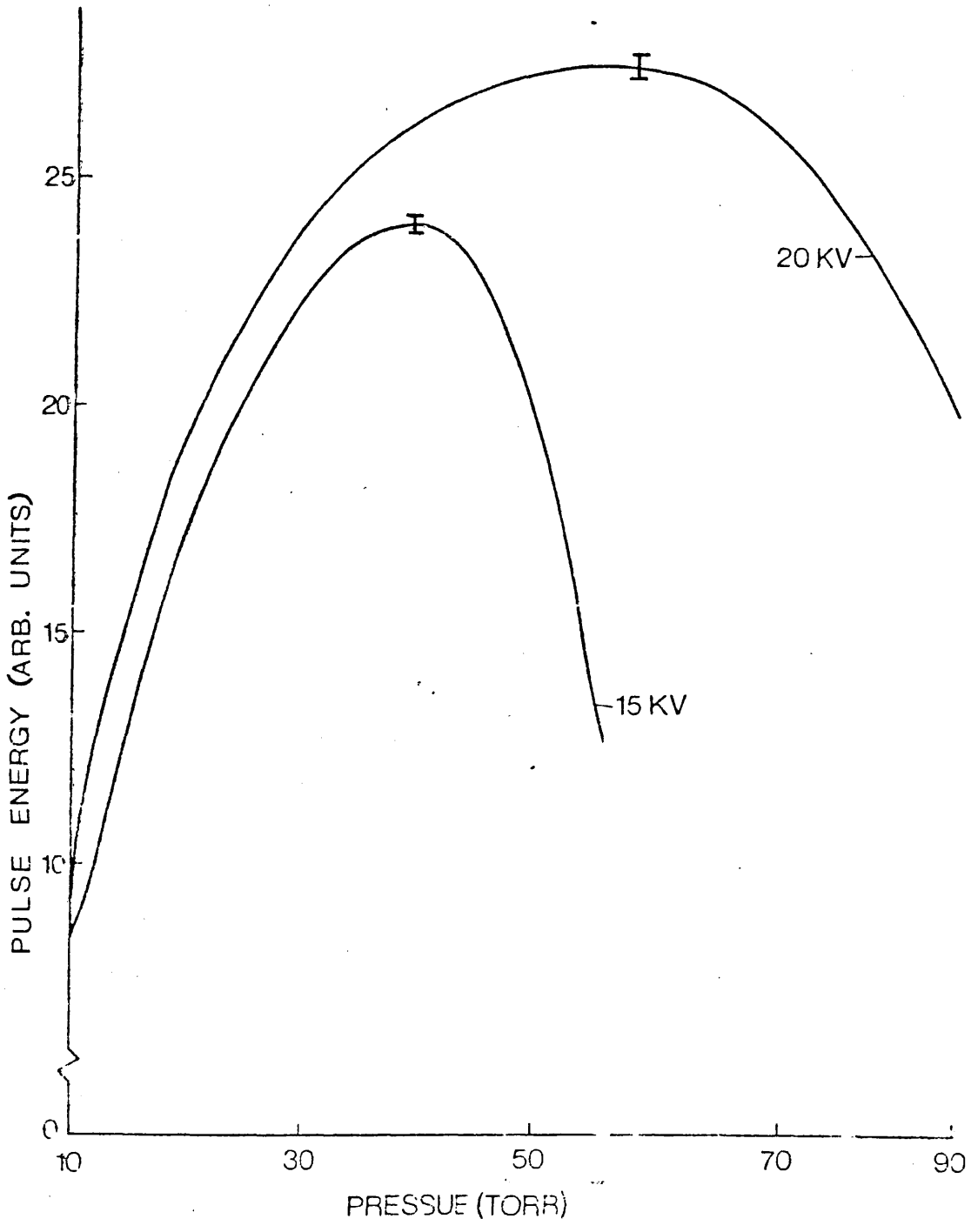

FIGURE 2.2 Variation of pulse energy with pressure for the Mk I Laser. (Repetition rate (RR) = 10Hz).

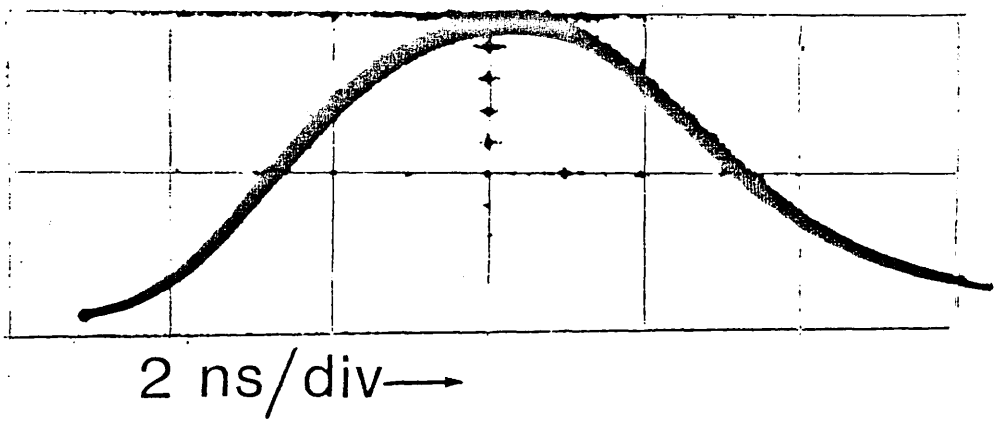

FIGURE 2.3 Output pulse shape of the Mk I laser.
(Applied potential (V) = 15kV, RR = 10Hz, pressure (P) = 38 torr).

and delivery times are greater than nine months. Various methods were tried to prevent the failures, including increasing the inductance between the spark gap and the storage capacitors, moving the location of the connection of the inductance to the storage capacitors, and looking for any spikes or oscillations affecting the capacitors. It was concluded that the cause is probably a combination of poor quality capacitors and the design of the laser, which does not allow sufficient cooling of the capacitors despite forced air ventilation. Another problem associated with the design of this laser is that it is very inflexible and as such is difficult to develop the laser in any way. When a British supplier of a similar type of capacitor was found it was decided to design and build a new laser rather than try to modify the existing one.

The MkI laser is currently being used for plasma diagnostics. It is being operated with a laser triggered spark gap at very low repetition rates and the short pulse width is being utilised to produce time resolved shadowgrams of a plasma produced by a TEA CO_2 laser.

CHAPTER III

Mk II LASER

3.1 DESCRIPTION

This laser was originally designed solely for dye laser pumping. Hence the requirements were a long pulse width (Chapter 6) and possible operation at high repetition rates for a high average power.

The electrical circuit used for the laser is shown in figure 3.1 and is identical to the capacitor transfer circuit shown in figure 1.8 (page 42)except for the addition of the two preionizing wires, and the preionizing capacitor C_p. The circuit operates in the manner described previously except that prior to the main discharge the preionizing capacitor, which is switched in the same way as C_S, discharges to ground via the two preionizing wires. This happens before the main discharge for three reasons: firstly the voltage rise on C_p is greater than that of the C_S/C_D combination because of the absence of a dumping capacitor, secondly, the separation of the preionizing wires can be adjusted to be less than that of the main electrodes and thirdly, the preionizing discharge takes place along a surface and consequently breaks down at a lower voltage. This discharge provides ultraviolet photons which preionize the gas between the main electrodes, ensuring a stable and homogeneous main discharge. Preionization is not

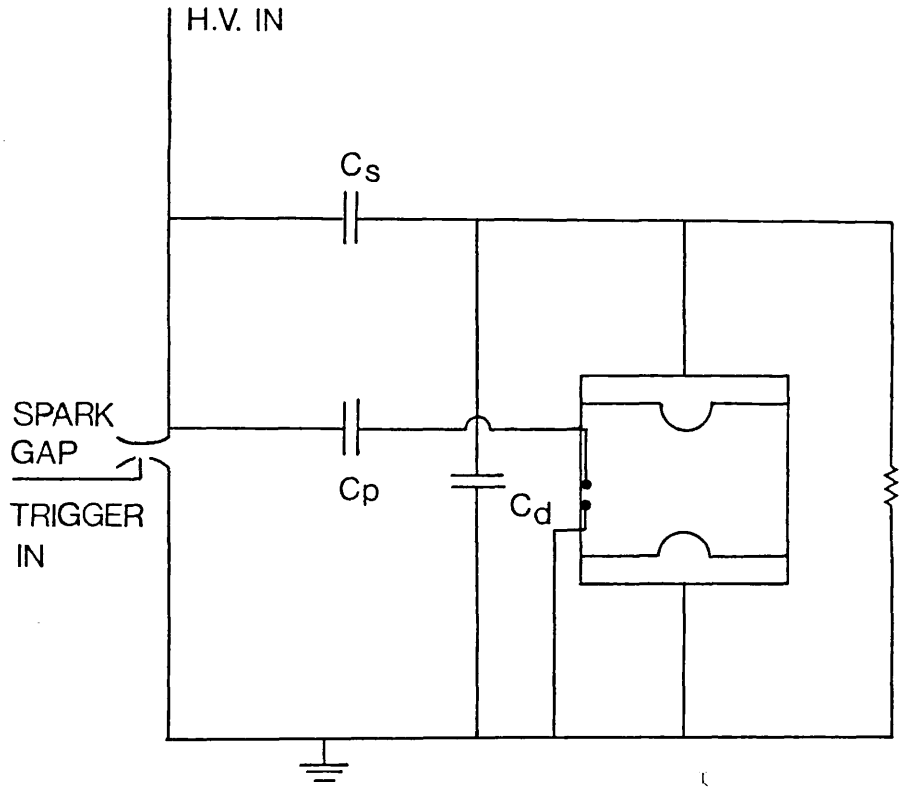

FIGURE 3.1 Electrical circuit of the Mk II laser.

essential with this laser but the discharge appears more uniform when it is utilized.

A cross-section of the laser is shown in figure 3.2. The length of the tube is 110cm whilst the discharge and preionizing electrodes have active lengths of 106cm. The discharge electrodes are interchangeable so providing the facility to change the electrode separation and/or geometry. Unless otherwise specified the electrode profile was circular with a radius of 4.8mm and a separation of 19mm. The preionizing wires run along the top of the tube and were usually 32 gauge copper wire separated by 12.7mm. The sealing of the electrodes to the perspex spacers and of the end windows to the tube is achieved in the same manner as on the Mk I laser. Transverse gas flow is employed and for this purpose plenum chambers are constructed in the electrode mounts. Holes connecting the plenum chambers and the discharge chambers are regularly placed along the electrode mounts. To achieve maximum gas flow rate for any particular rotary vacuum pump it was ensured that there are no constrictions between the pump and the flow control valve. Differential pumping was also avoided by having pipes of equal length connecting the pump to the nozzles on the exit plenum chamber.

Forced air cooling is achieved with two fans placed above the spark gap which is located centrally on the high voltage bar. The P.T.F.E. prevents arcing between the high voltage bar and the screws securing the perspex spacer to the electrode mounts.

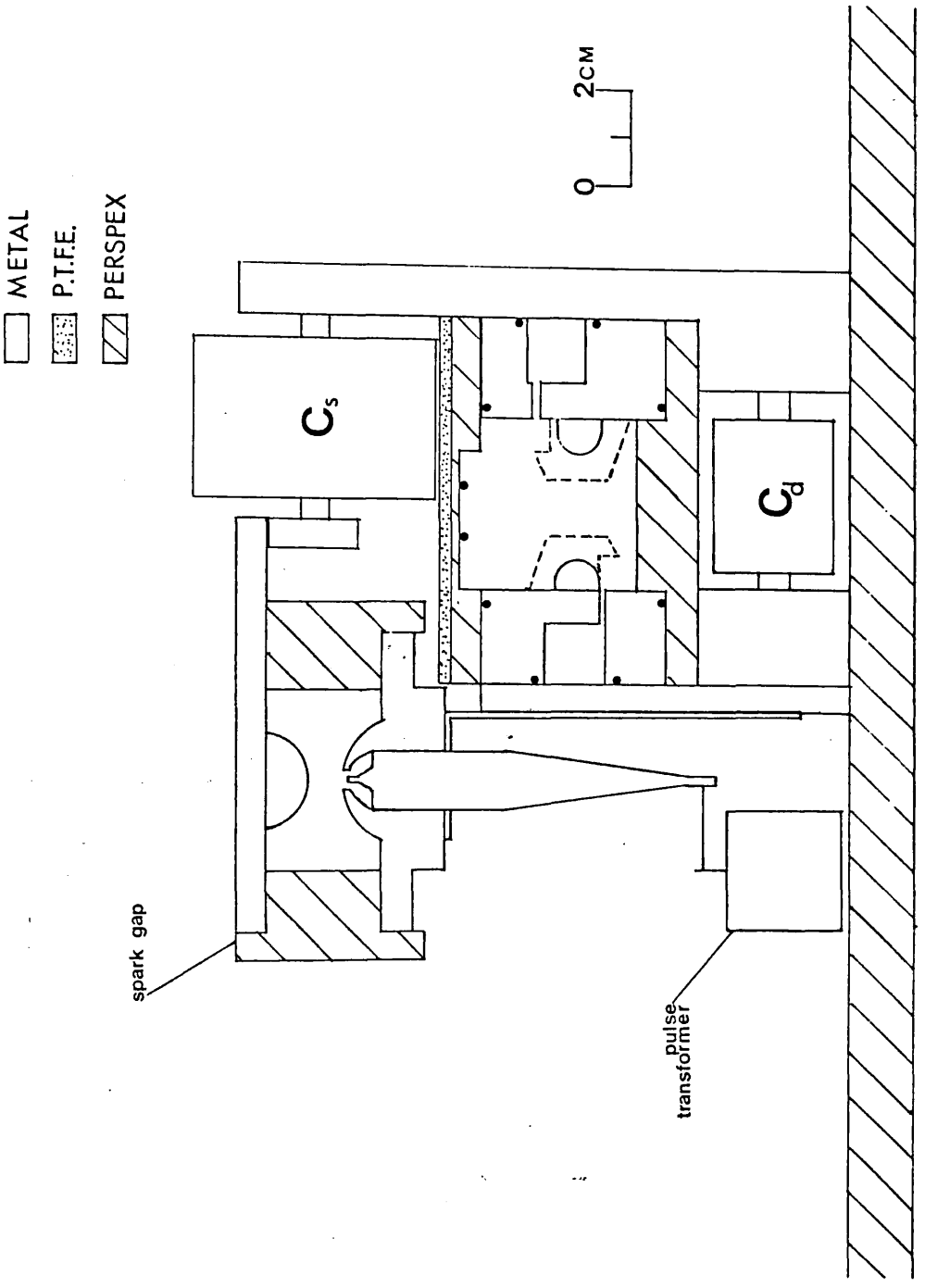

FIGURE 3.2 Cross-section of the Mk II laser.

3.2 OPERATION

The variation of output energy with pressure at three different applied voltages is shown in figure 3.3. As predicted (Chapter 1) the pulse energy peaks at a particular value of gas pressure for a certain applied voltage. This value increases with applied voltage indicating that a higher breakdown voltage is being achieved. A similar effect was reported by Woodward et al. (1.28) and Basting et al. (1.23).

At pressures below that for maximum output the pulse energy for different applied voltages is similar indicating that the breakdown voltage reached is also similar. The maximum pulse energy increases with increasing applied voltage and figure 3.4 shows a plot of applied voltage against pulse energy; for each reading the pressure was adjusted for maximum output. The straight line fit is good but is probably not significant because the relationship between pulse energy and applied voltage is most likely a summation of several factors. These include the facts that the stored energy is proportional to the square of the applied voltage; it is the voltage applied to the gas (breakdown voltage) that is significant and that the capacitance of the capacitors changes with the applied voltage. The latter factor will affect both the amount of stored energy and the voltage risetime across the electrodes.

Figure 3.5 shows the effect of both the applied voltage and the temperature upon the capacitance of the capacitors. This figure

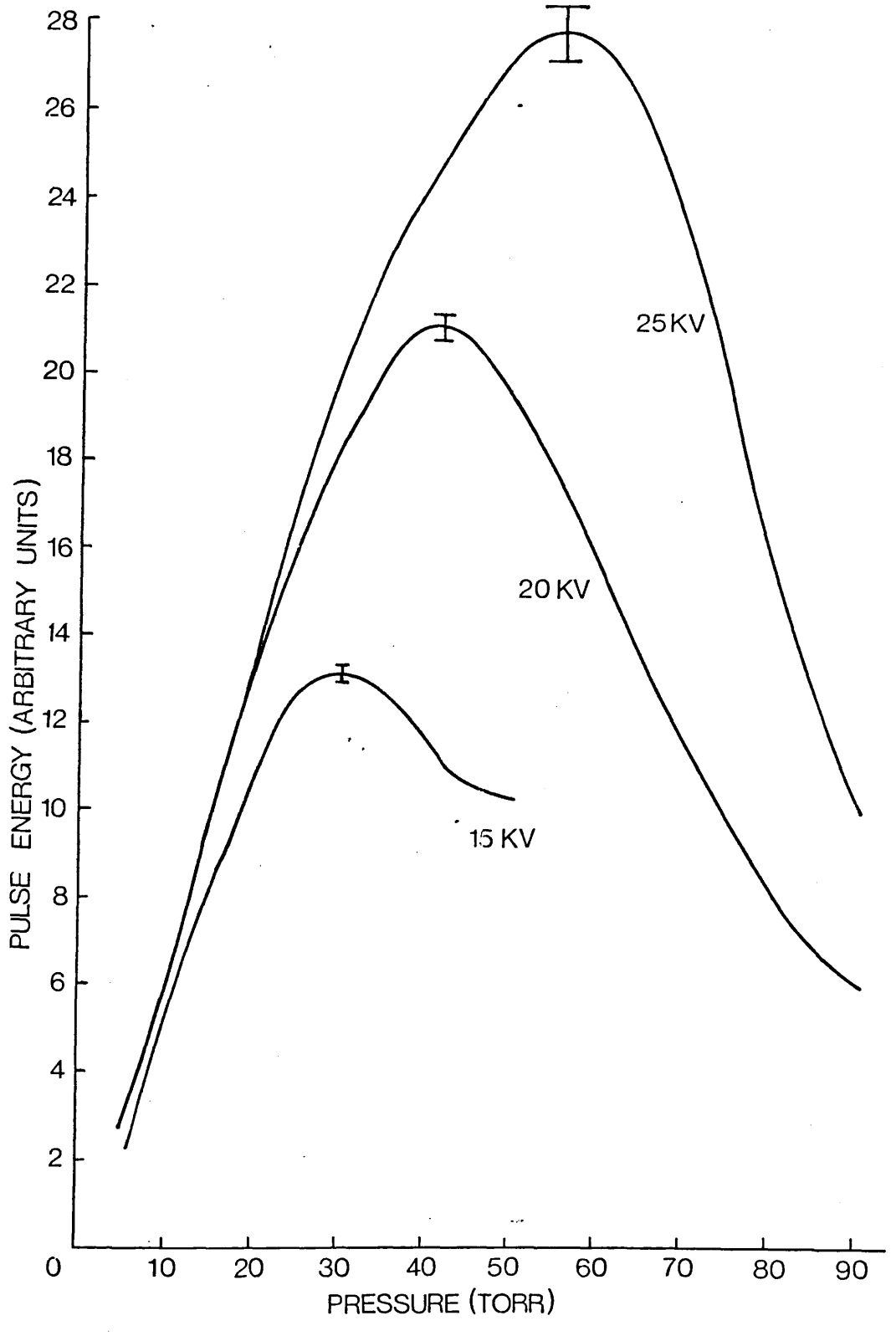

FIGURE 3.3 Variation of pulse energy with pressure of the Mk II laser. (RR = 10Hz)

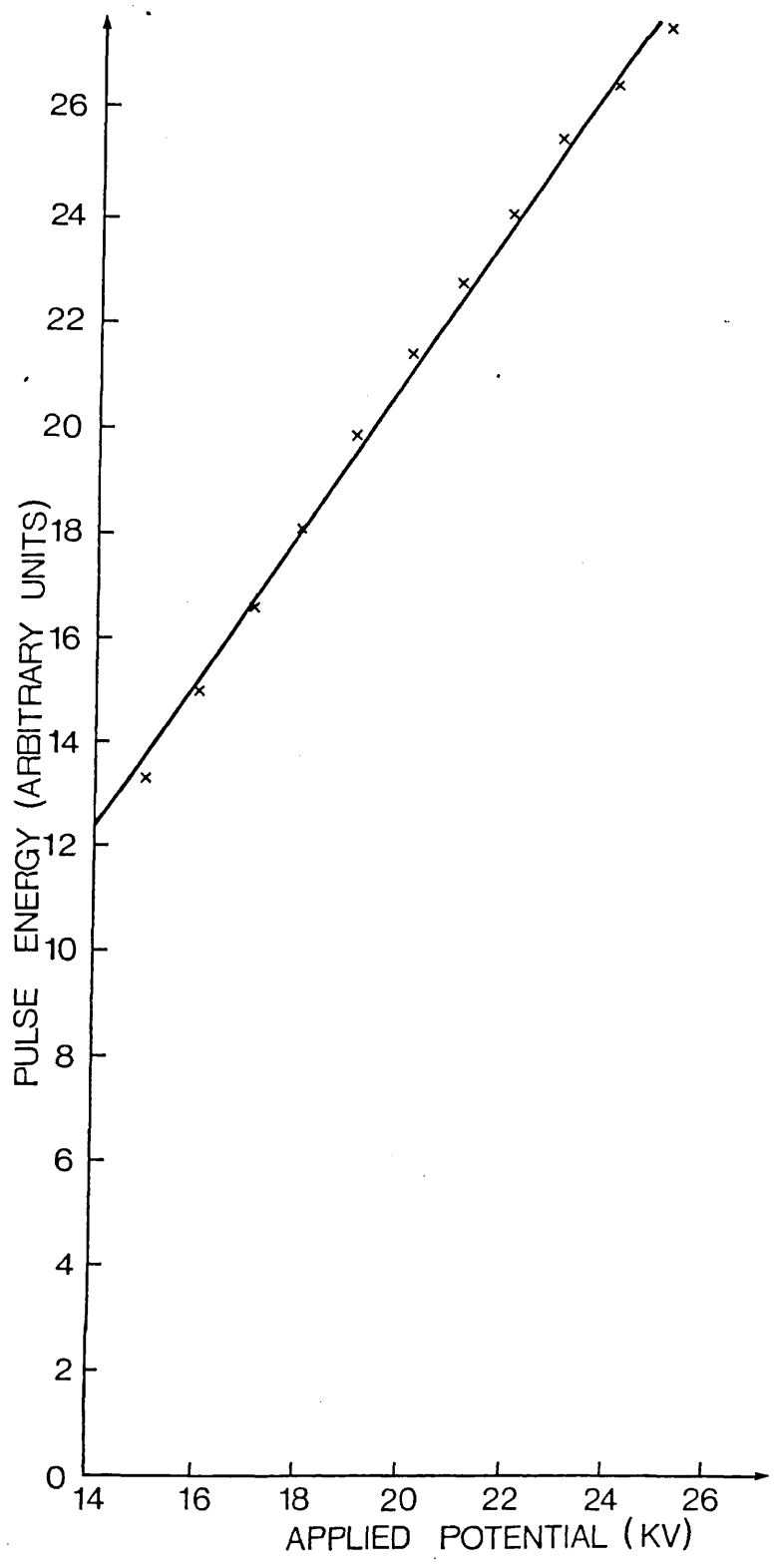

FIGURE 3.4 Variation of pulse energy with applied voltage of the Mk II laser.
(RR = 10Hz)

TYPICAL CURVES FOR CAPACITORS INCORPORATING K2000 AND K3000 MATERIALS (44m.m DIA. x 20m.m THICK)

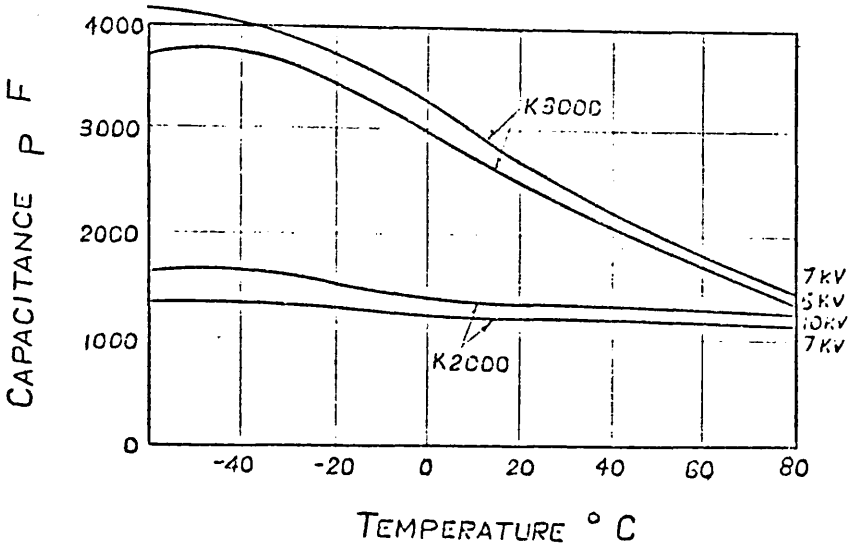

CAPACITANCE / TEMPERATURE CHARACTERISTICS

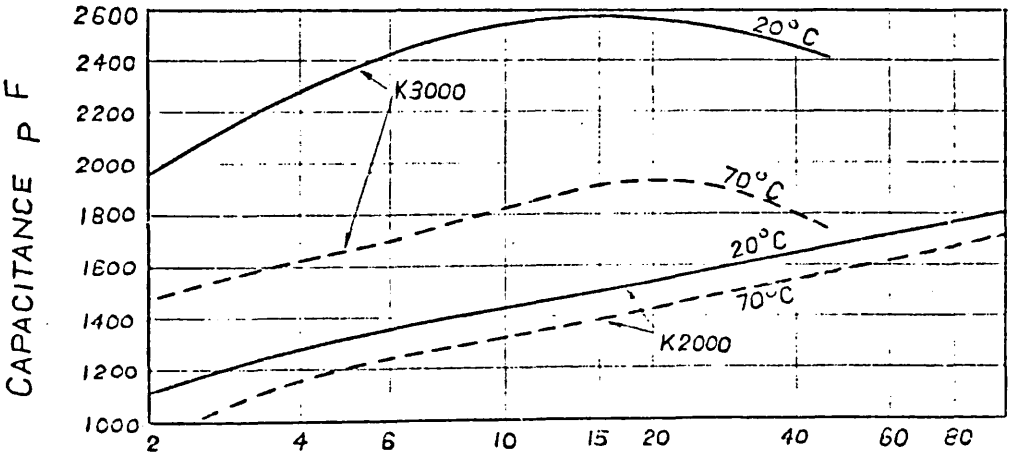

CAPACITANCE / VOLTAGE CHARACTERISTICS

FIGURE 3.5 Effect of voltage and temperature on the capacitance of the capacitors.

was reproduced from a catalogue provided by Steatite and Porcelain Products Ltd; the capacitors used on this laser incorporate the K3000 type material. With the strong dependence of the capacitance upon temperature it was expected that there would be a warm up period whilst the capacitors reached an equilibrium temperature and that the output energy would decrease during this time. An experiment was performed using the arrangement described in Appendix 1 with the output from the voltmeter connected to a chart recorder. In this manner the long term changes in average power were recorded and the result is shown in figure 3.6. The graph shows that the warm up time is about 40 mins. and allowance was made for this before performing all experiments. Variations in power over periods of less than one minute were ignored because these were caused by either non-firing or self breakdown of the spark gap which in this case was pressurised with non-flowing nitrogen.

The variation of average power and pulse energy with repetition rate is shown in figure 3.7. The decrease in pulse energy towards the higher repetition rates is caused by the power capabilities of the power supply being exceeded and the applied voltage not reaching the set value.

Pulse shape at maximum pulse energy is shown in figure 3.8 (a), with the figure showing twelve pulses superimposed. The pulse width (FWHM) is 12ns, a figure better than the design goal. The FWHM can be lengthened by decreasing the gas pressure or by adding a front coupler with a higher reflectivity. Figure

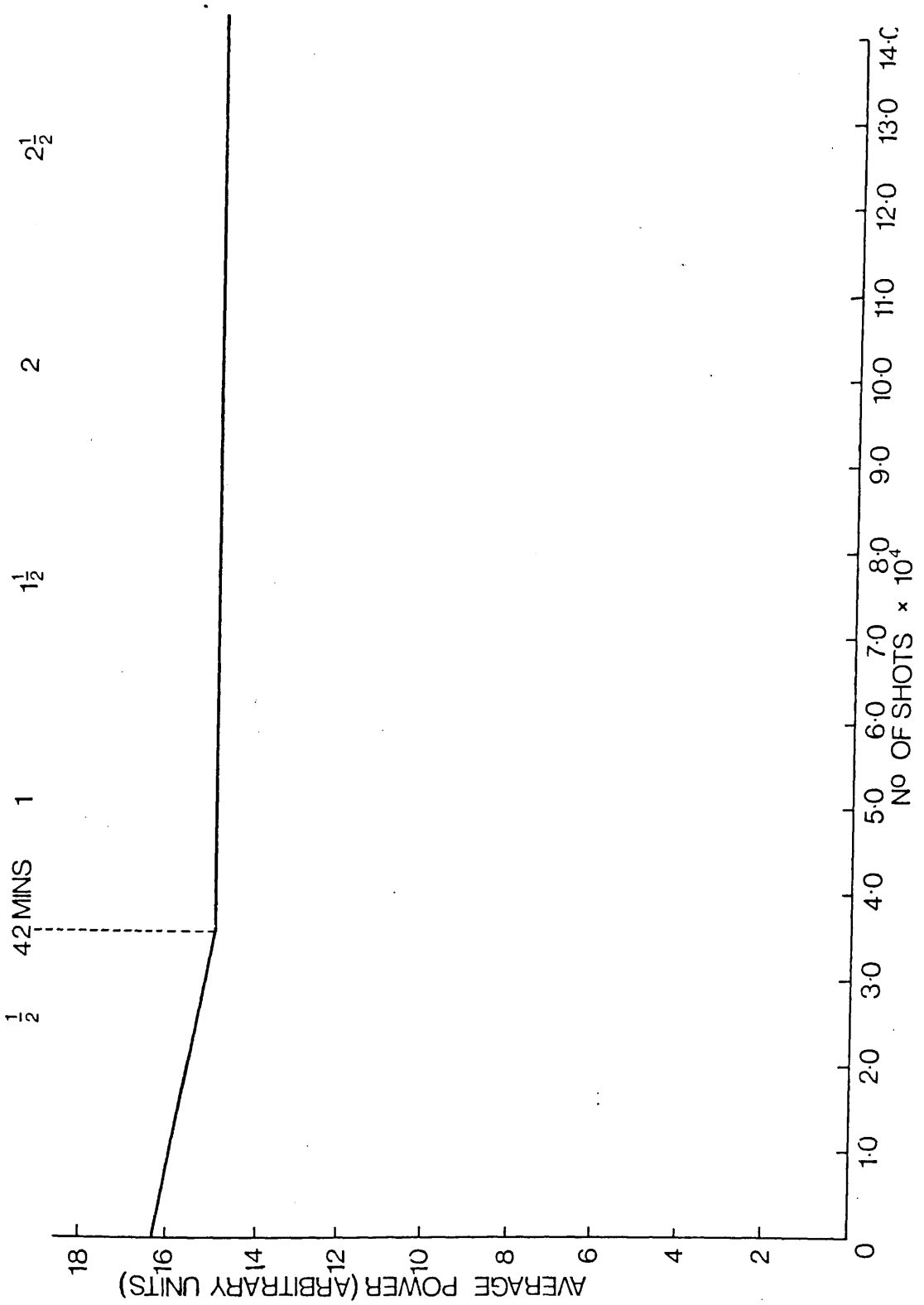

FIGURE 3.6 Long term variations of average power of the Mk II laser. (V = 22kV, RR = 14Hz, P = 50 torr).

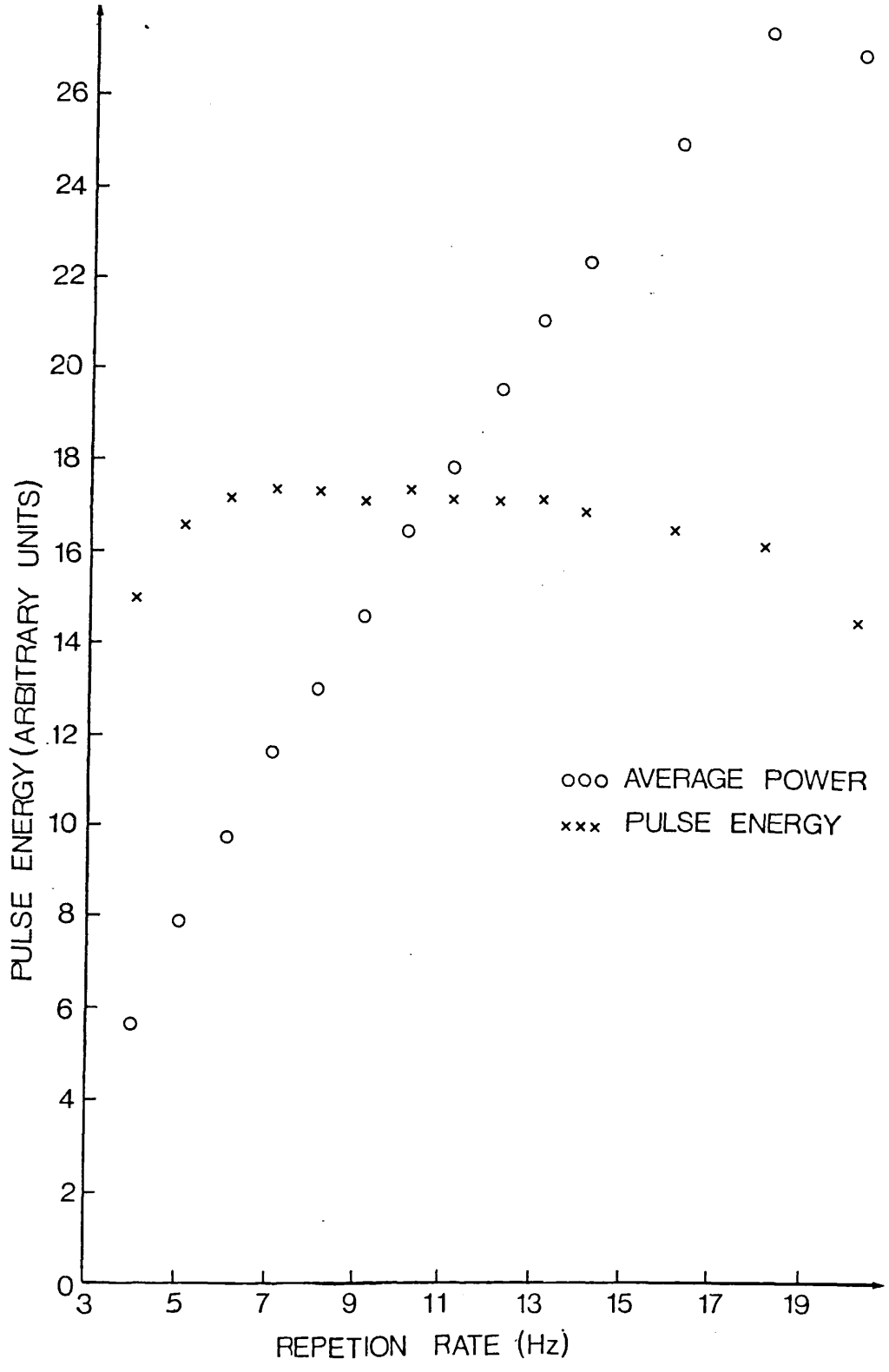

FIGURE 3.7 Variation of pulse energy and average power with repetition rate of the Mk II laser.
(V = 25kV, P = 52 torr).

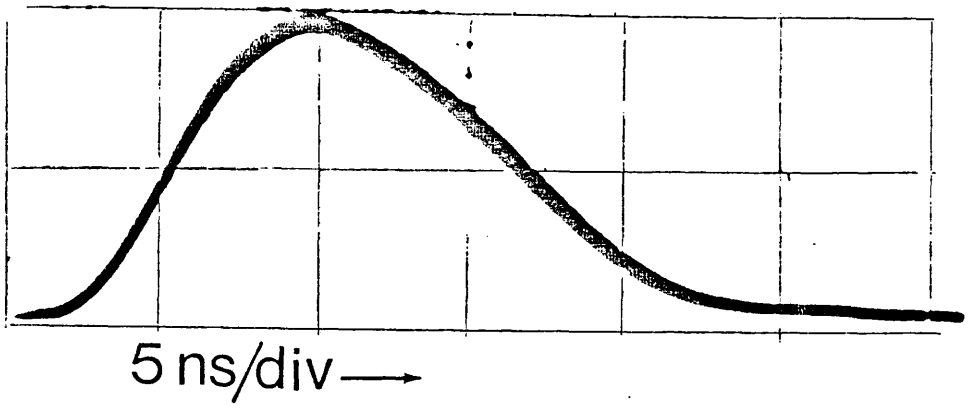

(a)

(V = 25kV, RR = 12Hz, P = 50 torr, coupler transmission (CT) = 92%).

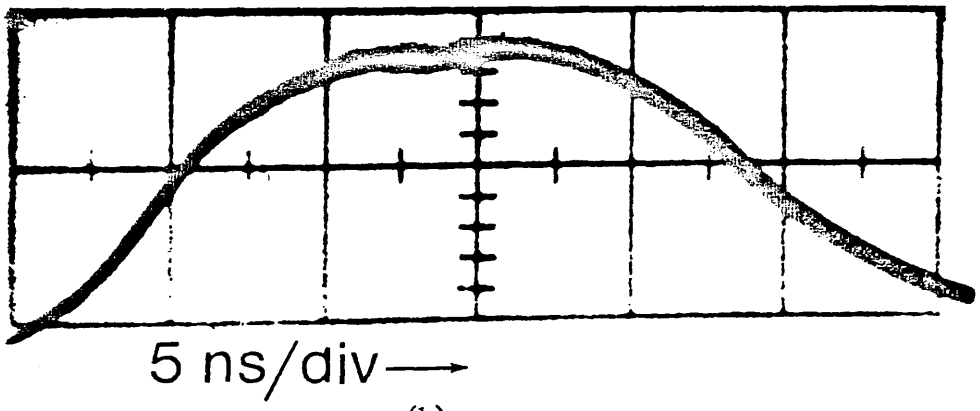

(b)

(V = 25kV, RR = 12Hz, P = 20 torr, CT = 15%).

FIGURE 3.8 Output pulse shapes of the Mk III laser.

3.8(b) shows pulses obtained under the same conditions as previously, except the gas pressure has been reduced to 20 torr and the plain output coupler has been coated with aluminium such that its transmission is about 15%. The FWHM has increased to 20ns but the pulse energy has decreased substantially. Addition of the low transmission coupler decreases the energy by 85% whilst decreasing the pressure reduces the pulse energy by about 50% (from figure 3.3 page 82). The FWHM at 20 torr with a plain output coupler is 16ns whilst the FWHM at 50 torr, with the low transmission coupler, is 15ns.

Whilst observing the pulse shapes a second pulse was observed about 20ns after the first as shown in figure 3.9 (a). The relative heights of the two pulses are not significant due to the varying spectral sensitivity of the photodiode and the attenuators. The wavelengths of the pulses were analysed by passing the radiation through a Spex 'Minimate' monochromator before illuminating the photodiode. The resolution of the monochromator is 1nm. For identification of which wavelength belonged to which pulse the beam was sampled with a beamsplitter prior to entering the monochromator and the sampled portion was directed to a silicon photodiode (Hewlett Packard type 4220). The output from this diode was then used for external triggering of the oscilloscope on which the output of the vacuum photodiode was being observed. This experiment revealed that the first pulse is the desired uv pulse at 337nm whilst the second pulse corresponds to two lines in the infrared with wavelengths of 872nm and 892nm. These wavelengths

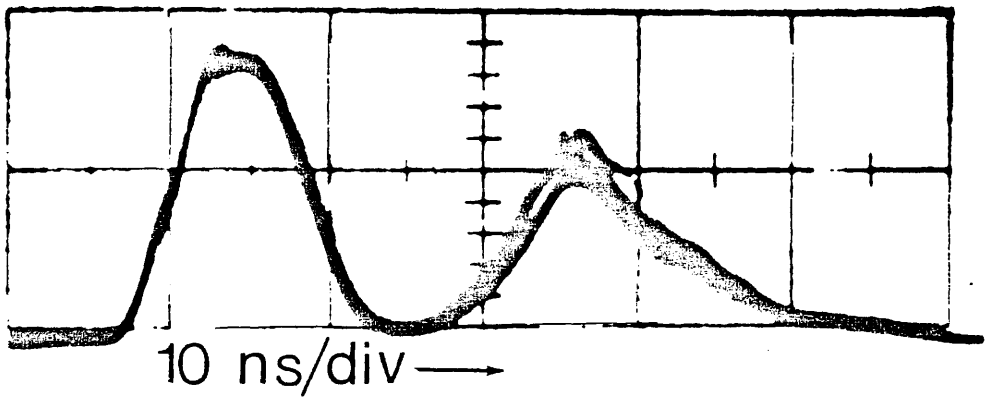

(a)

(V=24kV, RR=10Hz, P = 35 torr, CT = 92%.

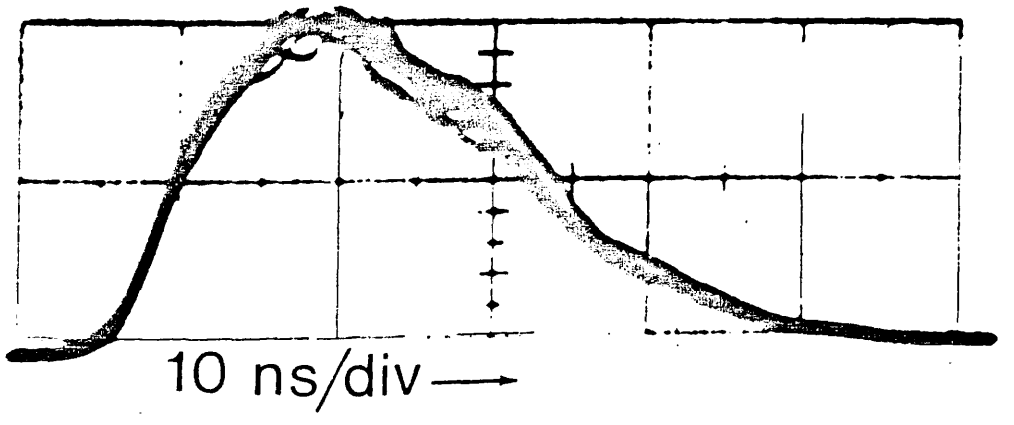

(b)

(V=25kV, RR=12Hz, P = 50 torr, CT = 42%).

FIGURE 3.9 IR output pulse shapes of the Mk II laser.

correspond to transitions in the first positive system ($B^3\pi_g - A^3\Sigma_u^+$). Referring to figure 1.1 (page 17) it can be seen that the upper laser level for the first positive system could be the lower laser level of the second positive system and one might suspect that a cascade process is responsible for population inversion in the first positive system. However this is not the case because the IR wavelengths correspond to transitions from the $V'' = 1$ to $V' = 0$ vibronic states whilst the second positive transition is from $V'' = 0$ to $V' = 0$ states. Hence the upper laser level of the first positive system is not the lower laser level of the second positive system.

The mechanisms proposed for population inversion in the first positive system in a longitudinal discharge by Yasuda et al. (3.2) are the cascade process, direct electron impact and collisional transfer from the metastable $a\,^1\pi_g$ singlet state. As outlined above the cascade process does not occur here and the excitation must occur by the other two methods. Inspection of the Frank-Condon factors in Table 1.2 (pp.19) indicate that the vibrational level in the $B\,^3\pi_g$ state most likely to be populated by direct electron impact is the $V'' = 1$ level, and this explains why radiation is only observed from the 1-0 transition.

Simultaneous laser action in the infra-red and ultraviolet was first reported by Allen et al. (3.3) and subsequently by Woodward et al. (1.26) and Tarasenko and Bychkov (3.4). The

power ratio (UV to IR) in this laser with the plain output coupler is about 20:1 compared with 4:1 in (1.28) and 50:1 in (3.4). The IR output is enhanced by the addition of a coupler with a higher reflectivity; figure 3.9 (b) shows a pulse using an output coupler with a transmission of 42% and with the pressure adjusted for maximum IR output (50 torr). The FWHM is 24ns and although it is lost in the 12 pulse superposition of figure 3.9 (b) there is some evidence of the partial modelocking observed by Gleason et al (3.5). Although the IR output is interesting it is of limited use and no further optimization studies were carried out (however Hocker (3.6) does report the use of the IR N_2 laser for pumping IR dyes).

The energy distribution in the beam was measured by scanning a calibrated Molectron J3-02 pyroelectric detector through the beam. The detector was held in adjustable horizontal and vertical mounts, one of which was calibrated in 0.1mm steps. The detector was moved through the beam in 0.5mm steps and the output monitored on an oscilloscope. The result is shown in figure 3.10. The upper line shows the total output (UV + IR) whilst the lower line shows the IR output only (mulitplied by a factor of 10). The IR output was isolated using a Kodak filter number K29, and the detector was positioned 18cm from the front output window of the laser. The horizontal cross-section is uniform to within 10% across most of beam. The slight asymmetry is most likely caused by a slight misalignment of the rear mirror and front output coupler. The IR vertical beam cross-section is almost identical to that shown in figure 3.10b but

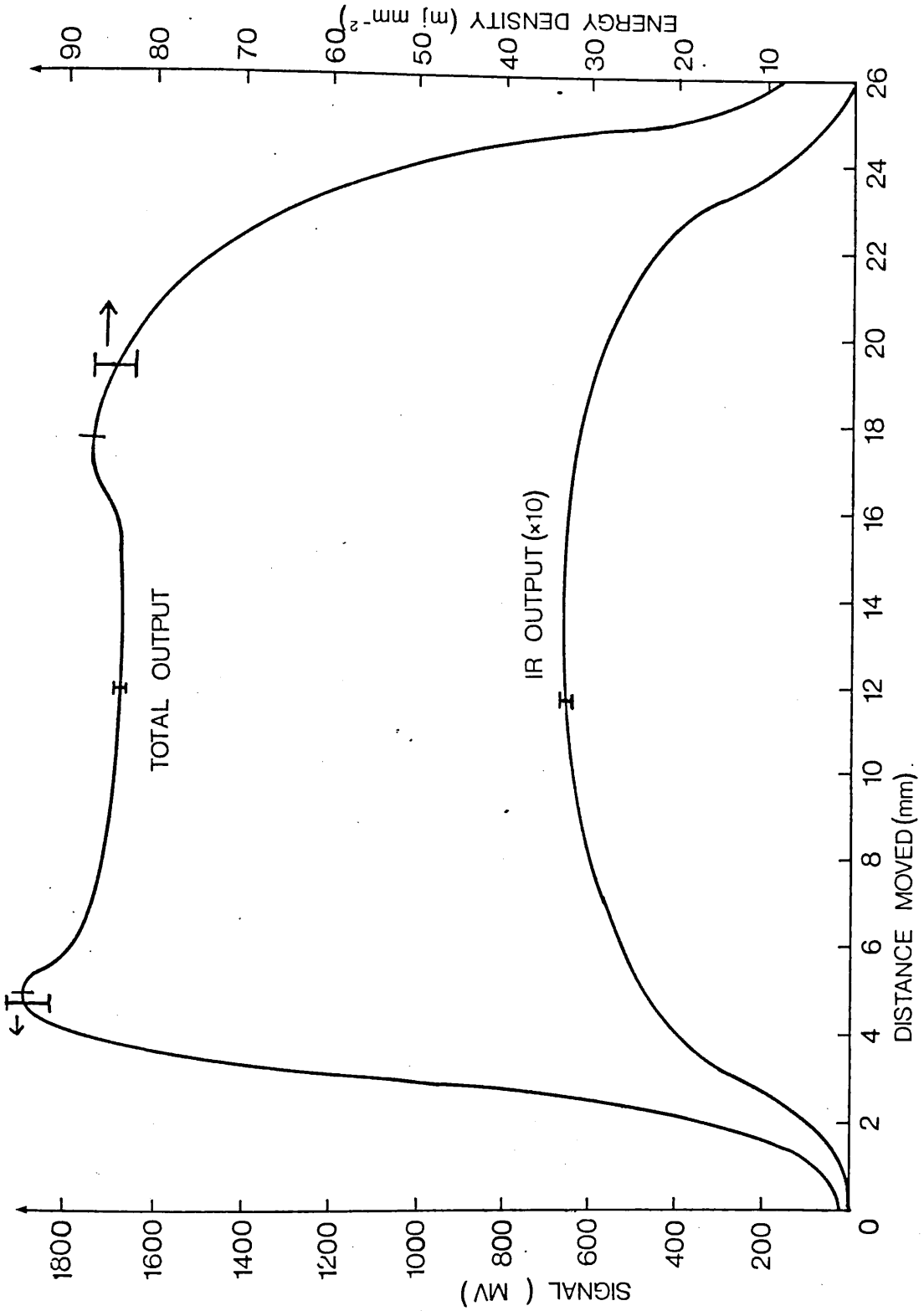

(a) Horizontal distribution

FIGURE 3.10 (a) & (b) Horizontal and vertical output energy distribution of the Mk II laser.

(V = 27.5kV, RR = 10Hz, P = 54 torr)

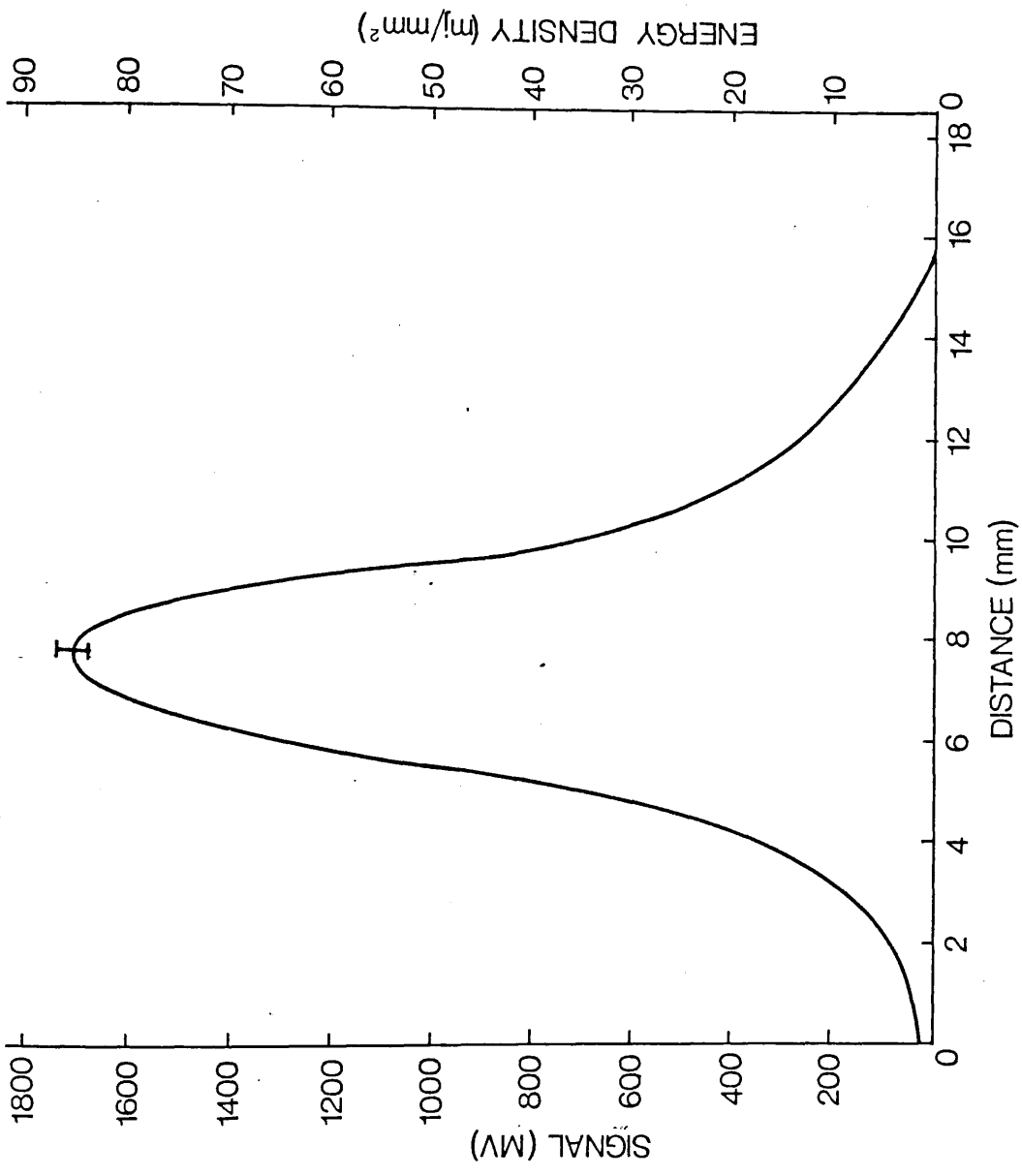

FIGURE 3.10 (b) Vertical Distribution.

reduced by a factor of 20. Because the readings were taken off an oscilloscope the resolution varied depending on the size of the input signal; the resolution at the top of the curve was at best 5% Because the detector had a rather large active area (2mm diameter) the slopes of the vertical lines are steeper than indicated and the shortest distance of travel for a 0-100% intensity rise or fall is 2mm. The wings in the vertical cross-section (figure 3.10 (b)) are due to large amounts of spontaneous emission. Both curves in figure 3.10 (a) were recorded with the detector adjusted in the vertical direction for maximum signal. Similar curves recorded in different vertical positions had similar shapes but different peak values in accord with figure 3.10 (b). The vertical cross-section was recorded in the horizontal centre of the beam, but again curves recorded in different horizontal positions had the same shapes but different peak values consistent with figure 3.10 (a). Using the data from these curves an estimate was made of the pulse energy using the following formula:-

$$E = \frac{W \times h \times P}{A \times S} \quad J \qquad (3.1)$$

where W and h are the width and height of the horizontal and vertical cross-sections (measured at the half maximum points), P is the average peak signal in the horizontal direction, A is the detector active area and S the detector sensitivity. The result is that the total pulse energy is about 5mJ, of which 4-5% is in the infra-red. Measurement of W and h at a distance of 110cm from the laser reveal that the half angle beam

divergences are 0.9 mrad and 3.5mrad in the vertical and horizontal planes respectively.

To try and equalize the beam divergences and so provide easier beam control a pair of electrodes were designed to produce a discharge with a square cross-section. These are the electrodes shown by the dotted lines in figure 3.2 (page 80) and have flat front surfaces of width 12.7mm which taper back to rear surfaces of width 19mm. The edges between the front surfaces and the tapered surfaces were given a circular profile and an indentation was made in the rear surfaces for gas flow. The electrodes are separated by 12.7mm and a uniform square discharge is produced. Preionization is essential with this electrode configuration. The beam profile in the horizontal and vertical directions was measured as previously (except the detector was at a distance of 30cm from the laser) and the results are shown in figure 3.11 (a & b). The beam dimensions in the two directions are similar, however the horizontal cross-section has a narrower peak and broader base than previously. This is readily explained when one examines the half angle beam divergences, which in the horizontal direction is 4.5 mrad and in the vertical direction 2.2 mrad. The increase in the vertical divergence is expected because of the larger plasma size in that direction whilst the large increase in the horizontal divergence, instead of the expected decrease, is caused by the kaleidoscope effect described by Godard and Vannier (3.7). The kaleidoscope effect is multiple reflections off the electrodes and is particularly severe with this

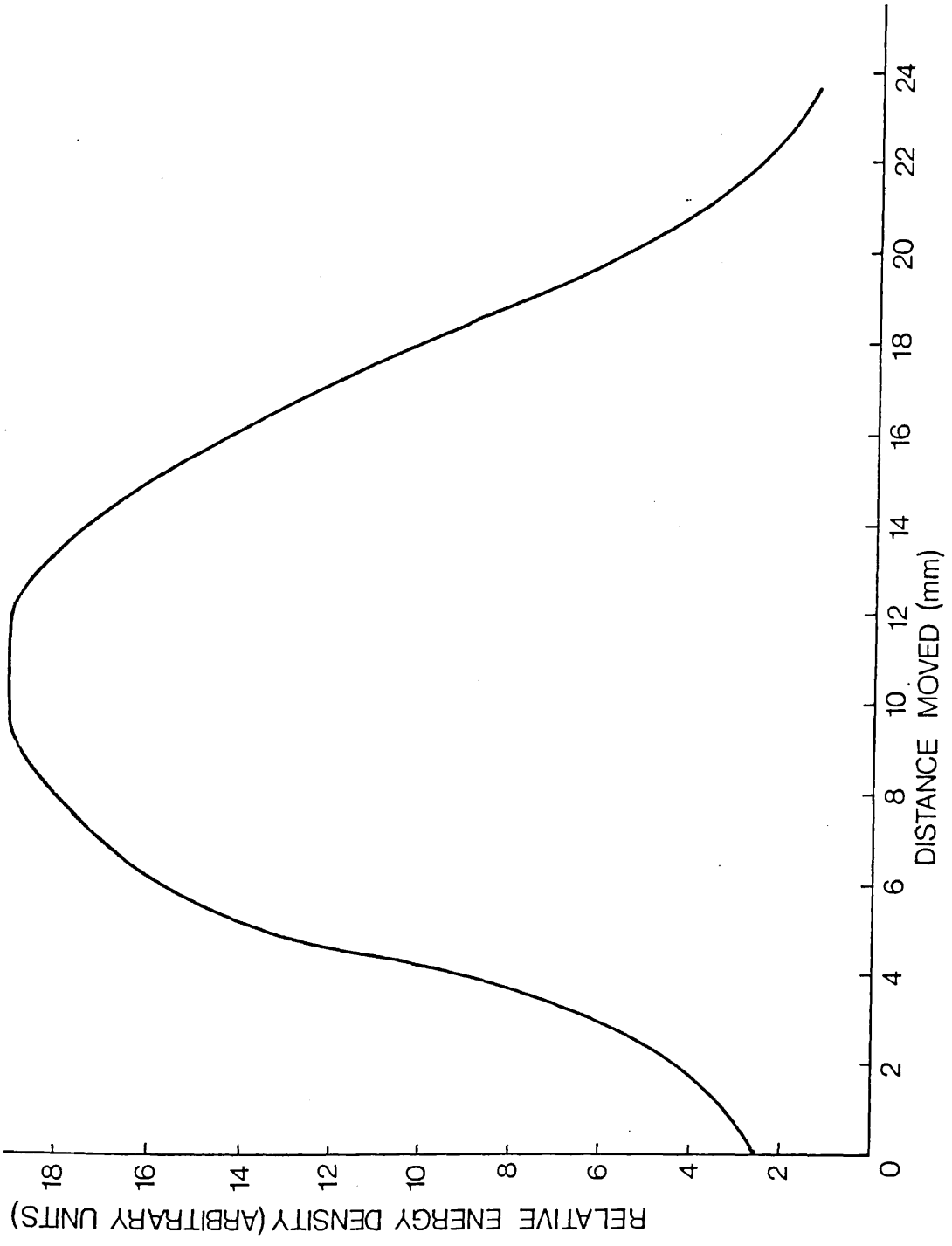

(a) Horizontal distriubtion

FIGURE 3.11 (a) & (b) Horizontal and vertical output energy distribution of the Mk II laser with square profile electrodes.
(V = 22.5kV, RR = 10Hz, P = 55 torr).

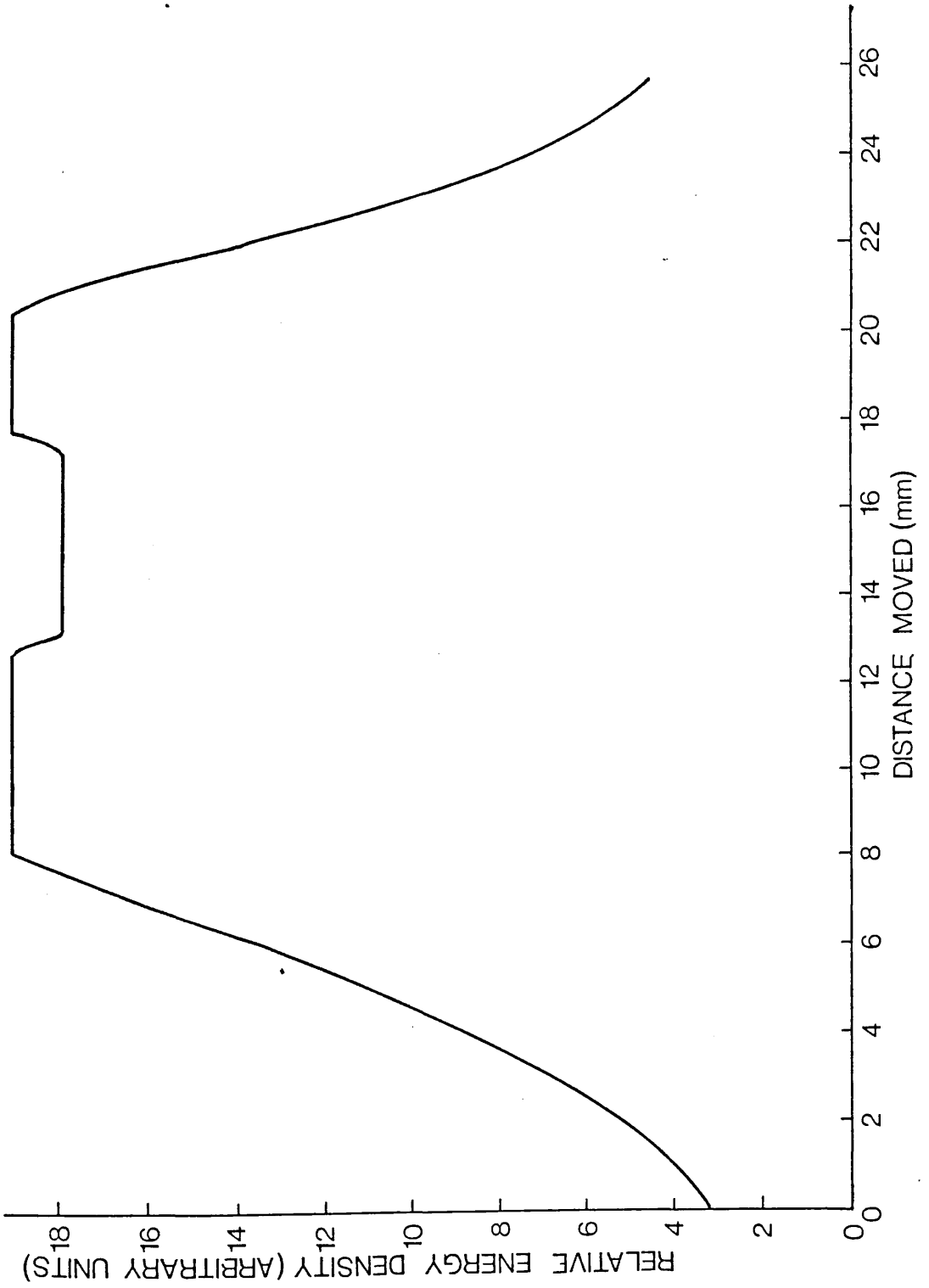

FIGURE 3.11 (b) Vertical Distribution.

electrode geometry because the electrodes present large flat parallel surfaces to the beam. In another nitrogen laser using a similar electrode geometry (3.8) there was no report of this differing beam divergence. In this reference graphite electrodes with a low coefficient of reflection at this wavelength were used.

3.3 SUMMARY

The design goal of producing a nitrogen laser with a long (10ns) pulse width for dye laser pumping was achieved. The laser was demonstrated to have characteristics similar to those using the same design principles. In addition pulse stretching by the addition of higher reflectivity output couplers was demonstrated and pulses with half widths of 20ns were produced. The simultaneous outputs in the ultraviolet and infra-red were studied. Finally a discharge with a square cross-section was produced and it was demonstrated that it was not possible to produce equal divergences in the horizontal and vertical directions by this method when using metal electrodes.

CHAPTER IV

MkIII LASER

4.1 INTRODUCTION

This laser was designed with a view to it becoming the oscillator part of an oscillator - amplifier configuration and hence was designed to allow variations and modifications to be made. In particular it has an electrode structure which allows the separation to be varied over a wide range and the effect of this has been investigated. The laser was initially designed for operation with a Blumlein circuit but was later converted for operation with a Blumlein or capacitor transfer circuit.

4.2 OPERATION USING A BLUMLEIN CIRCUIT

4.2.1 Description

A cross-section of the laser is shown in figure 4.1. The laser has an active length of 24cm and employs longitudinal gas flow. The electrode separation can be varied (from a maximum of 25.4mm) by inserting spacers between the right hand electrode and the block of aluminium in which it is held. The electrode profile is circular with a radius of 4.8mm. The method of sealing the discharge chamber and the gas manipulation system are the same as that on the MkI and II lasers. The electrical circuit is shown in figure 4.2 and is the same as the Blumlein

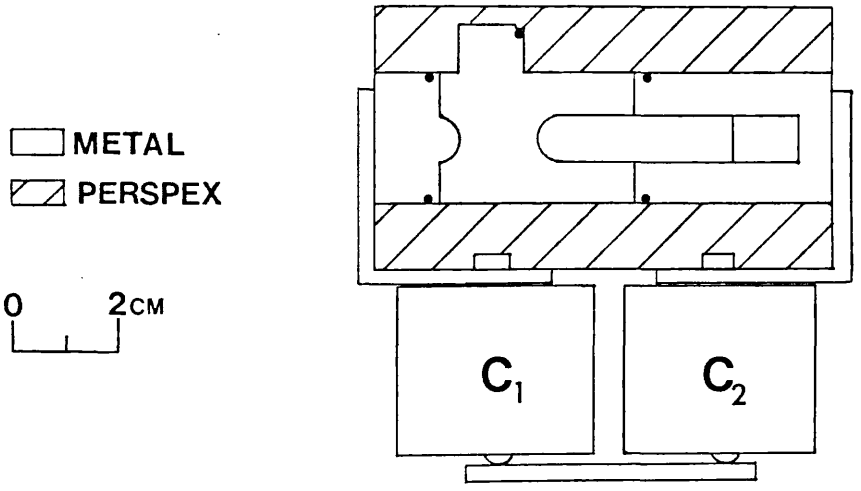

FIGURE 4.1 Cross-section of the Mk III laser when using a Blumlein circuit.

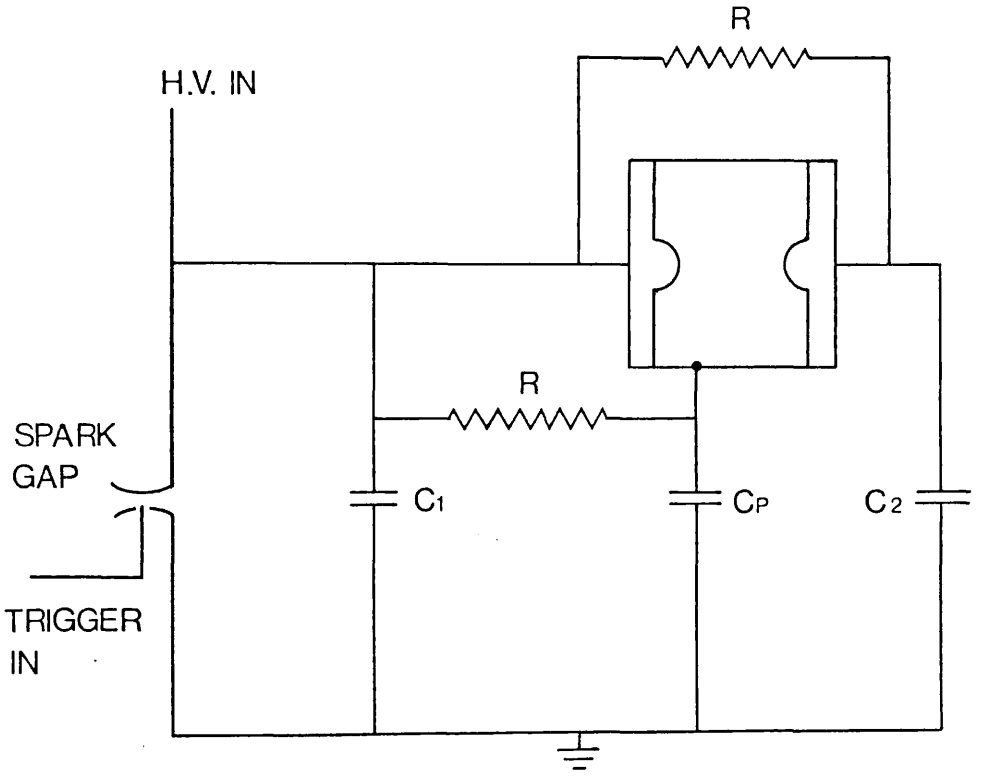

FIGURE 4.2 Electrical circuit of the Mk III laser when using a Blumlein circuit.

circuit shown in figure 1.8 (pp 40) with the addition of the preionizing capacitor Cp and the preionizing wire. The laser was initially designed without preionization but at all electrode separations the discharge was non-uniform, so preionization was incorporated as shown. When the spark gap fires, the voltage on the left hand electrode changes and the preionizing capacitor discharges to this electrode; because of both its proximity and because the discharge takes place across a surface it occurs before the main discharge and provides uv preionizing photons. Unless otherwise specified C_1 and C_2 each comprise of a bank of ten 500pF ceramic capacitors giving a total value of 5nF for each bank. The preionizing capacitor comprises three 500pF capacitors connected in series giving a capacitance of 166pF. A three electrode triggered spark gap is connected to C_1 for switching purposes.

4.2.2 Operation

With an electrode separation of 25.4mm the laser produces pulses as shown in figure 4.3. The FWHM is 4ns and good pulse to pulse stability is evident (the figure shows 12 pulses superimposed).

The variation of output pulse energy with pressure is shown in figure 4.4. The figure illustrates the effect of the preionization which is most necessary at higher pressures where the electric field strengths are greater.

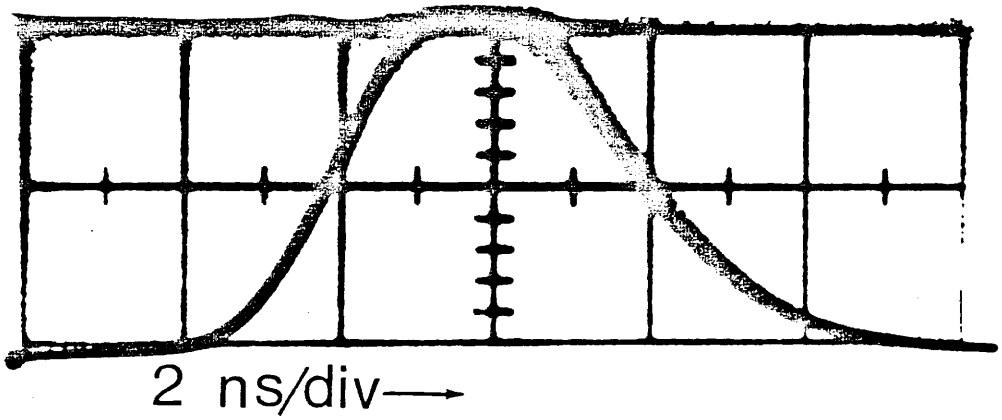

FIGURE 4.3 Output pulse shape of the Mk III laser.
(V = 15kV, RR = 25Hz, P = 84 torr, electrode separation (D) = 25.4mm).

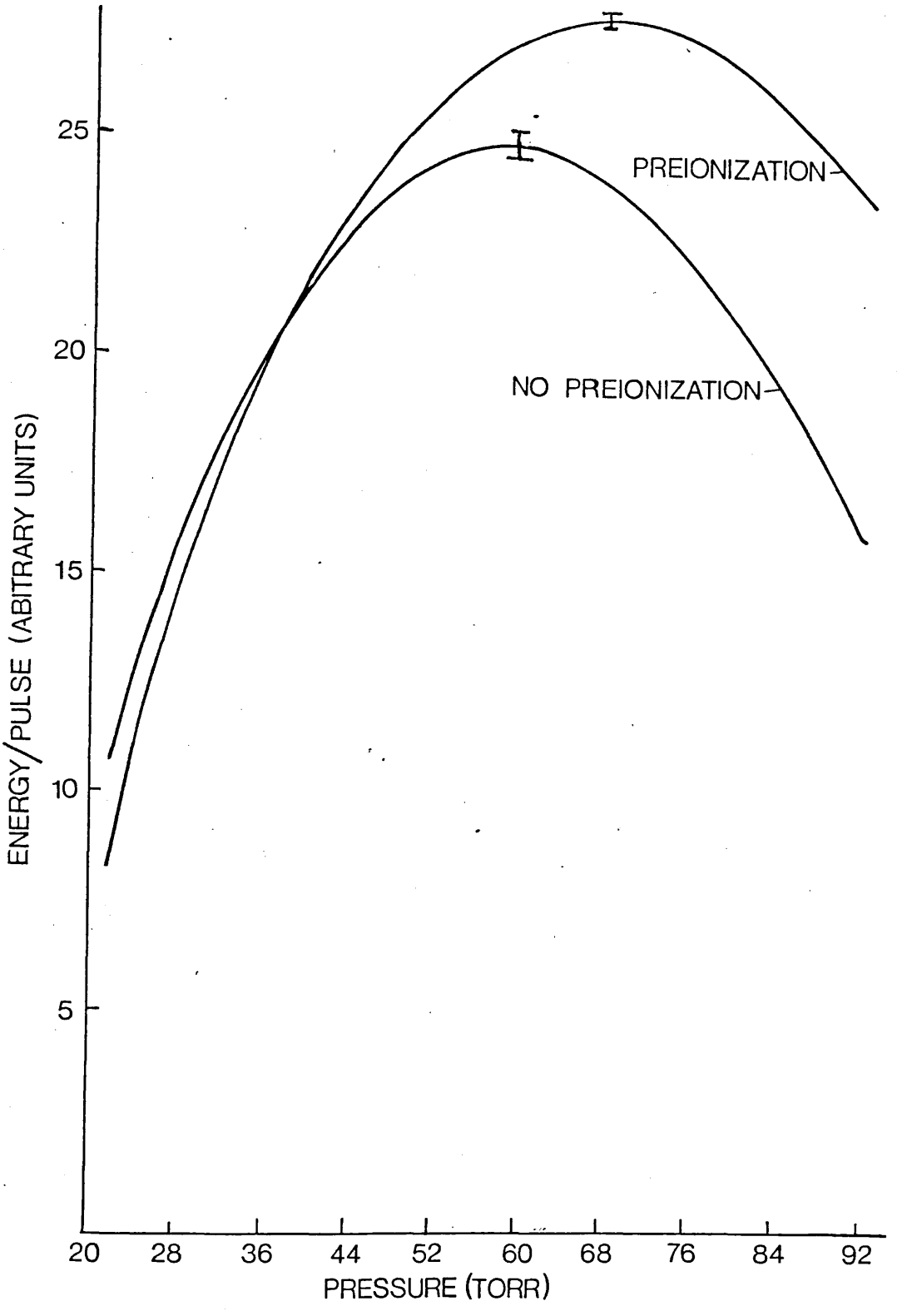

FIGURE 4.4 Variation of pulse energy with pressure of the Mk III laser. (V = 15kV, RR = 40Hz, D = 25.4mm).

The variation of average power and pulse energy with repetition rate is shown in figures 4.5 and 4.6. The two curves on each figure correspond to operation with two different size vacuum pumps and hence two different flow rates of gas through the laser. The average power peaks at 75Hz for the larger pump and 60Hz for the smaller. The difference arises because at high repetition rates the stability of the discharge is affected by contaminants such as ions and free electrons left from previous discharges and there are more of these present with the smaller pump. With the smaller pump operation above 80Hz is not possible due to arcing in the region where the gas exits.

The variation of pulse energy with pressure for an electrode separation of 12.7mm is shown in figure 4.7. The upper curve was recorded with the usual arrangement of capacitors whilst for the lower curve two capacitors were removed from C_1 and three from C_2 giving values of 4nF and 3.4nF respectively. The particular capacitors that were removed extended beyond the length of the discharge tube and it was thought that their use might be superfluous. Their removal decreases the pulse energy by about 9% but the efficiency in relation to stored energy increases by 21%. These effects are similar to those predicted by Ali (1.9). Decreasing the capacitance moves the peak of the curve from 105 torr to 120 torr. This is because the decrease means less charge has to pass through the spark gap and a shorter voltage risetime is produced. (i.e. the time constant of the C_1/spark gap combination is decreased). The shorter

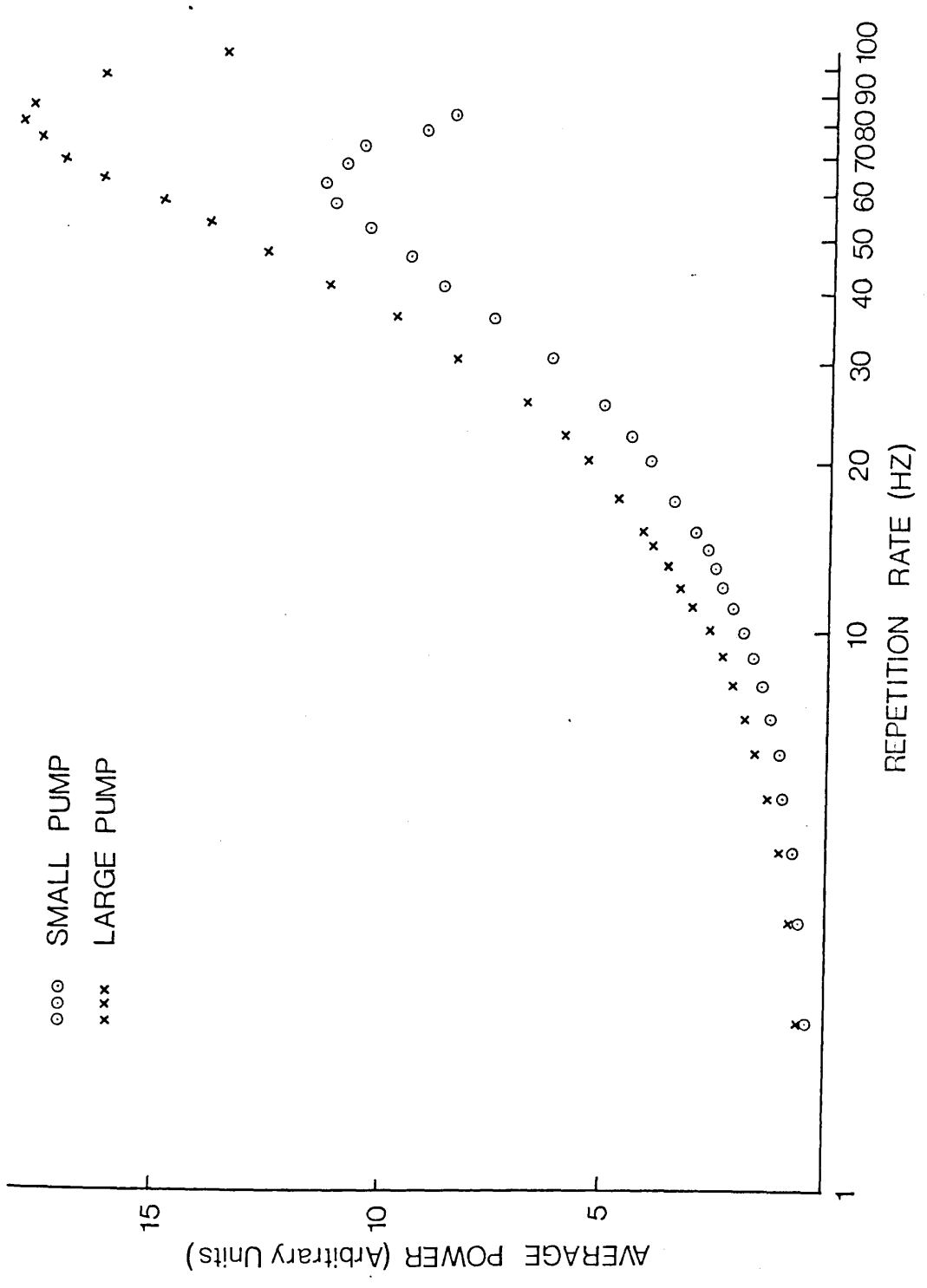

FIGURE 4.5 Variation of average power with repetition rate of the Mk III laser.
(V = 15kV, P = 80 torr, E = 25.4mm).

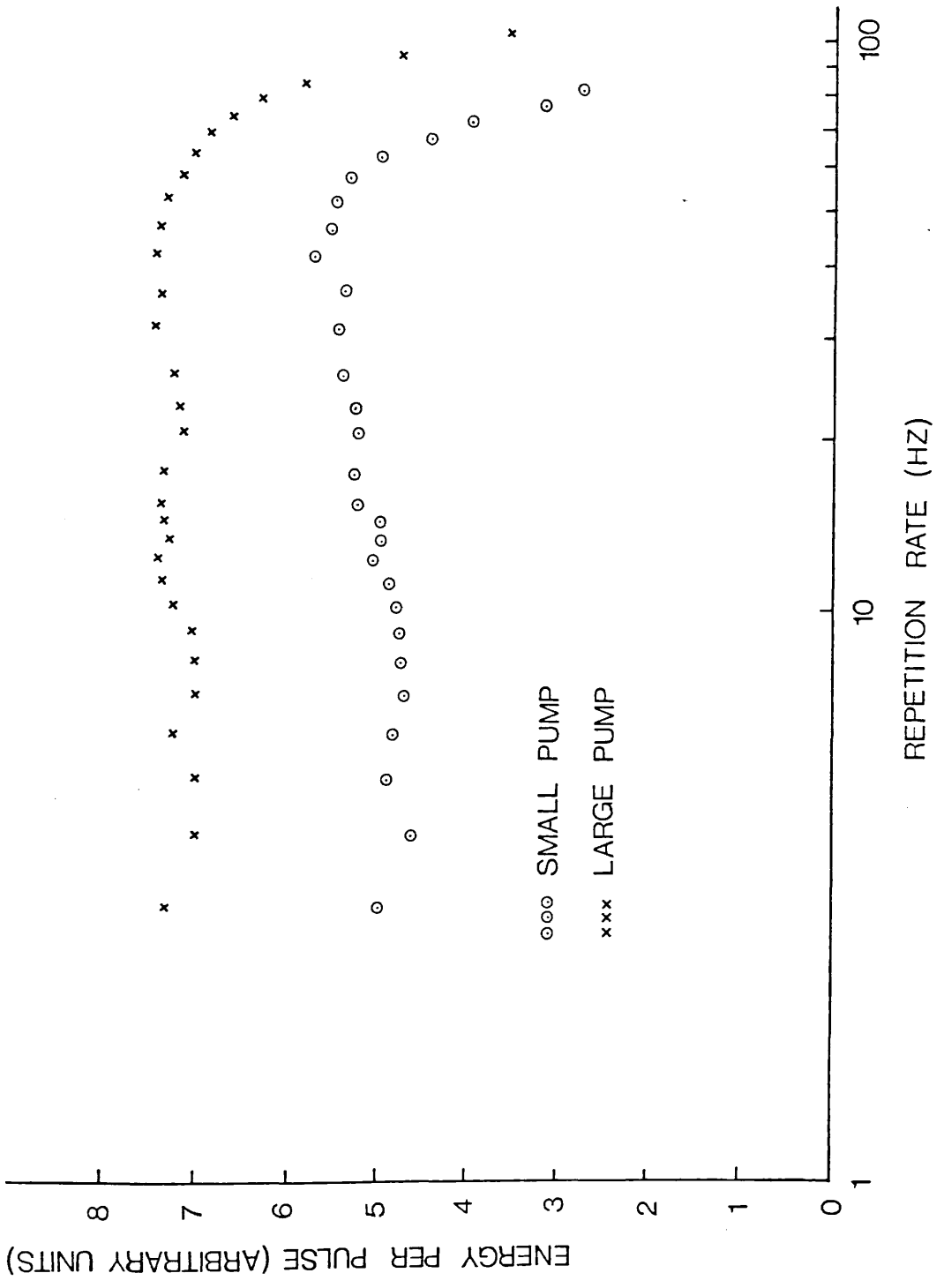

FIGURE 4.6 Variation of pulse energy with repetition rate of the Mk III laser.
(V = 15kV, P = 80 torr, D = 25.4mm).

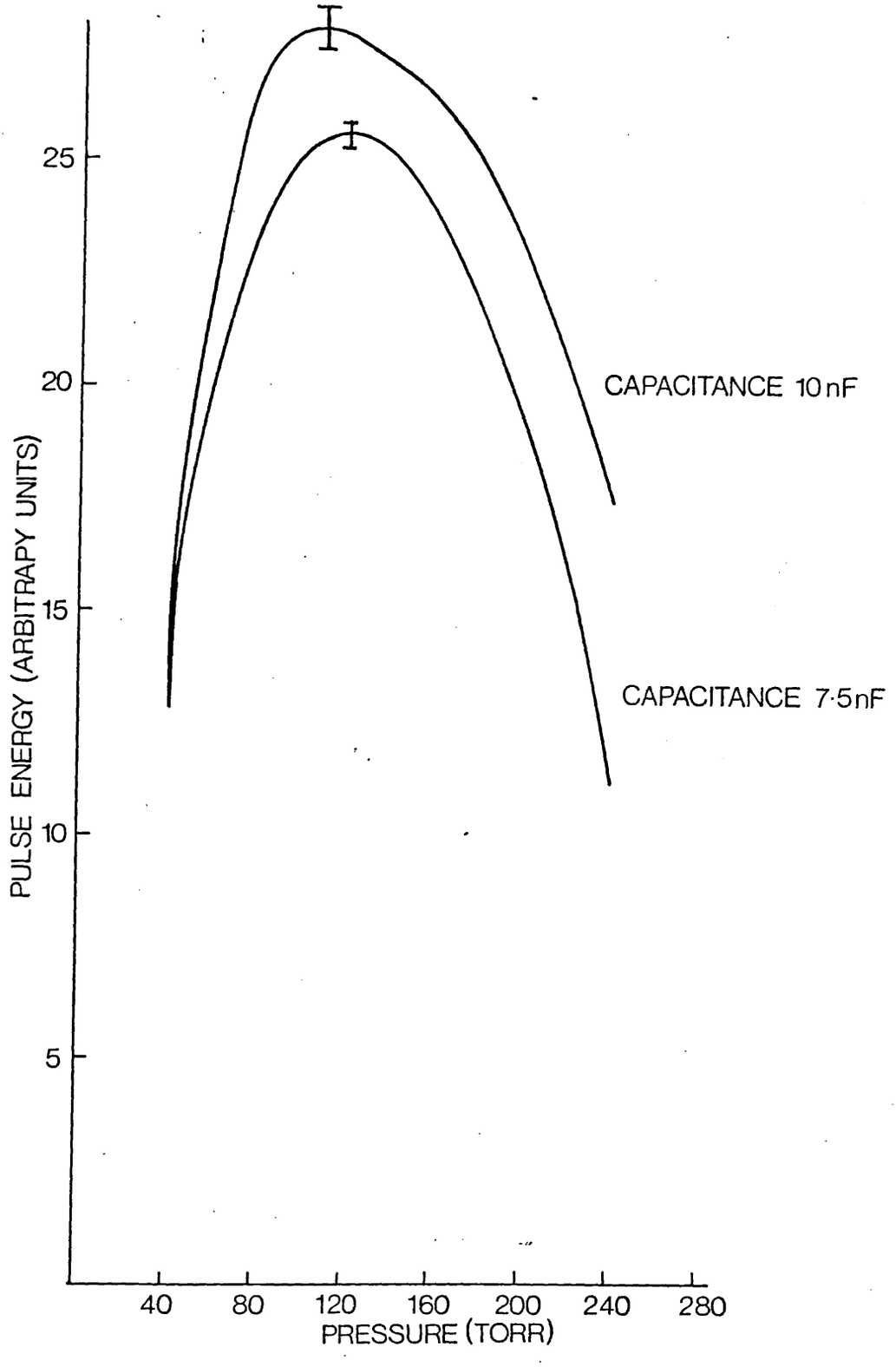

FIGURE 4.7 Variation of pulse energy with pressure of the Mk III laser. (V = 20kV, RR = 20Hz, D = 12.7mm).

voltage risetime means that a higher breakdown voltage is reached and consequently a higher pressure is required to maintain the optimum E/p value. A similar effect was reported by Fitzsimmons et al. (1.6). At this electrode separation the pressure for maximum pulse energy with an applied voltage of 15kV is 90 torr compared to 72 torr for an electrode separation of 25.4mm. The difference arises because the narrower electrode separation produces higher electric field strengths, and hence the pressure has to be increased to maintain the optimum E/p value. Although the electrode separation is halved the pressure does not have to be doubled because the higher electric field strength (for a particular voltage) means that the breakdown voltage achieved is lower (i.e. the E/p value is maintained at that for optimum by a combination of the pressure rising and a lowering of the voltage being reached before breakdown).

The variation of peak power and pulse width with pressure is shown in figure 4.8 for an electrode separation of 12.7mm. The FWHM at maximum pulse energy is about 3.8ns. The FWHM varies from 4.0ns at 60 torr to 3.2ns at 180 torr, again this effect was predicted by Ali (1.8). The pressure for maximum peak power is 120 torr, which is different to that for maximum pulse energy. The difference is because at high pressures higher breakdown voltages are reached; hence breakdown occurs more rapidly producing more high energy electrons and hence a high peak power results. However the E/p value falls more quickly to a value insufficient to provide electrons with enough energy to produce a population inversion and combined with the fact that

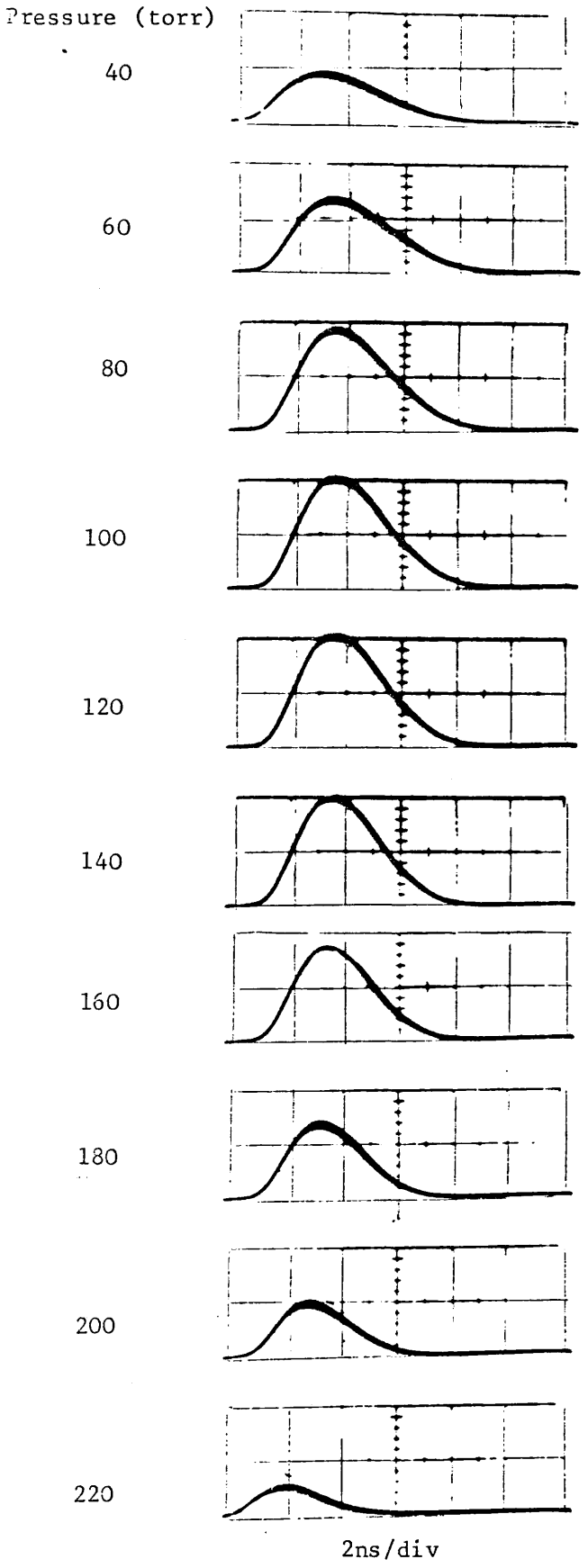

FIGURE 4.8 Variation of peak power and pulse width with pressure of the Mk III laser.
(V = 15kV, RR = 10Hz, D = 12.7MM).

the nitrogen laser is a self-terminating laser a shorter pulse width results. The pulse energy is the convolution of the peak power and pulse width.

The output energy distribution has been measured in the same manner as previously and the result is shown in figure 4.9 (a & b) for an electrode separation of 12.7mm. The upper curve was recorded with the detector at a distance of 10cm from the laser whilst for the lower curve this distance was 108cm. The half angle beam divergences have been obtained from these curves and they are 3.9mrad in the horizontal plane and 1.55mrad in the vertical plane. The horizontal distribution is not quite symmetrical at 108cm indicating a slight misalignment of the mirrors. The energy distribution is fairly uniform and the edges are sharply defined in the near field. An estimate of the pulse energy using these curves gives a value of 0.54mJ.

Shown in figure 4.10 is the variation of pulse energy with pressure for an electrode separation of about 8mm. The two traces correspond to operation with the large rotary vacuum pump and with a compressor pump. Operation above 300 torr with the large pump is not possible because the flow control valve was fully open at this pressure. The peaks of the two curves are in different places because the compressor pump does not have a linear relationship between flow rate and pressure, hence increasing the pressure increases the amount of gas exchanged between pulses raising the relative pulse energy at higher pressures. The graph demonstrates the large pressure

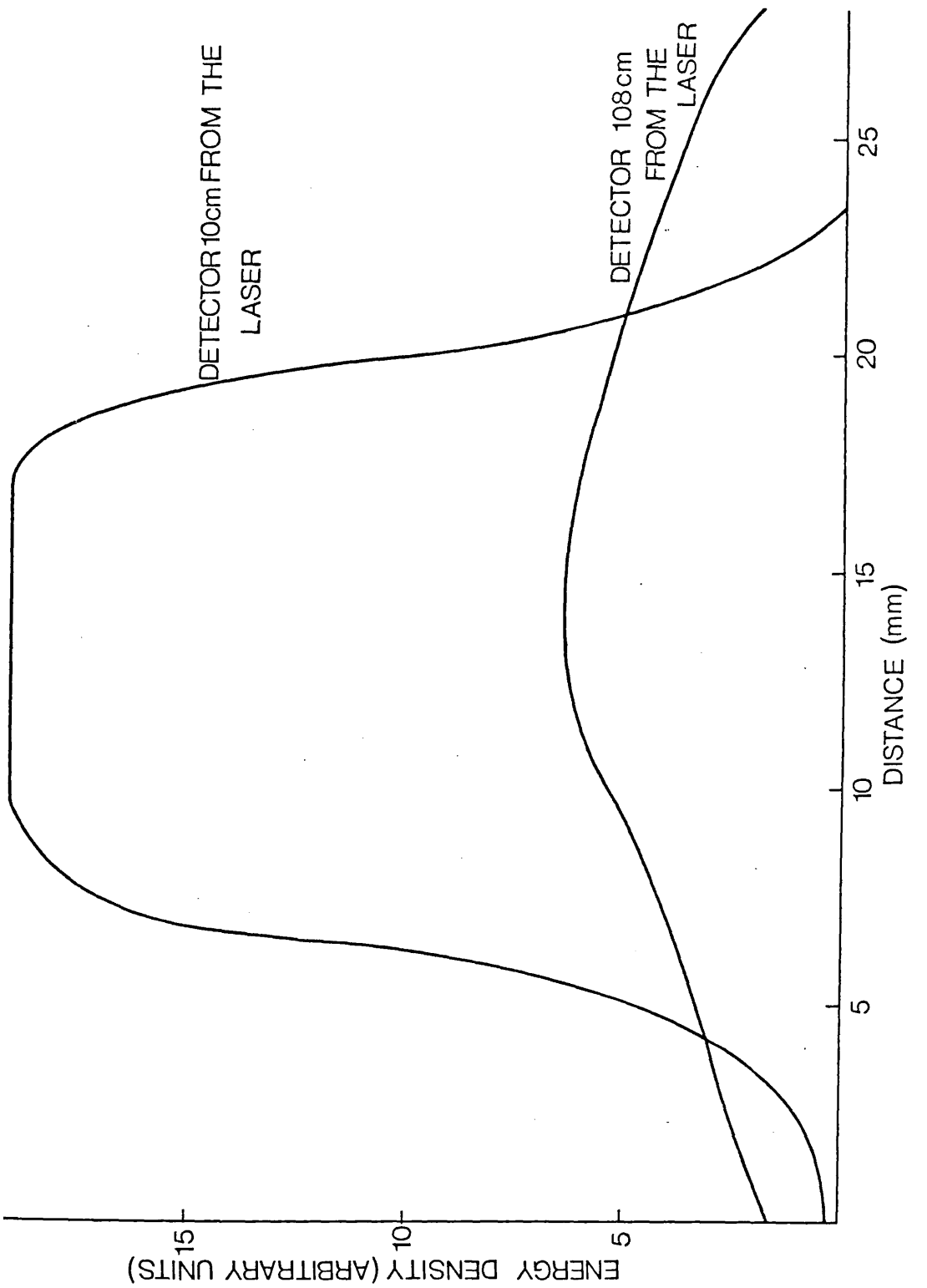

(a) Horizontal Distribution

FIGURE 4.9 Horizontal and vertical output energy distribution of the Mk III laser.
(V = 20kV, RR = 20Hz, P = 110 torr, D = 12.7mm).

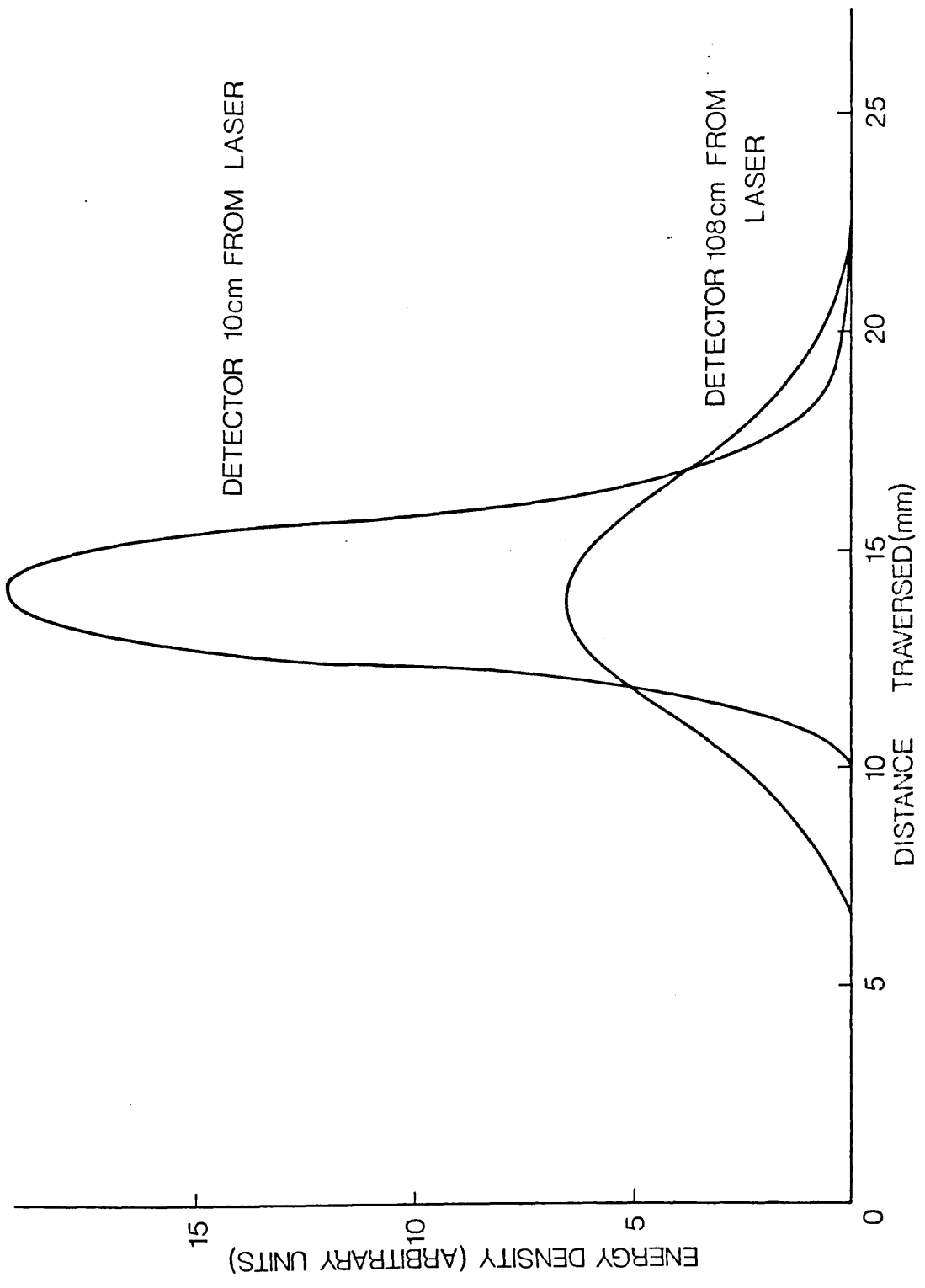

FIGURE 4.9 (b) Vertical Distribution

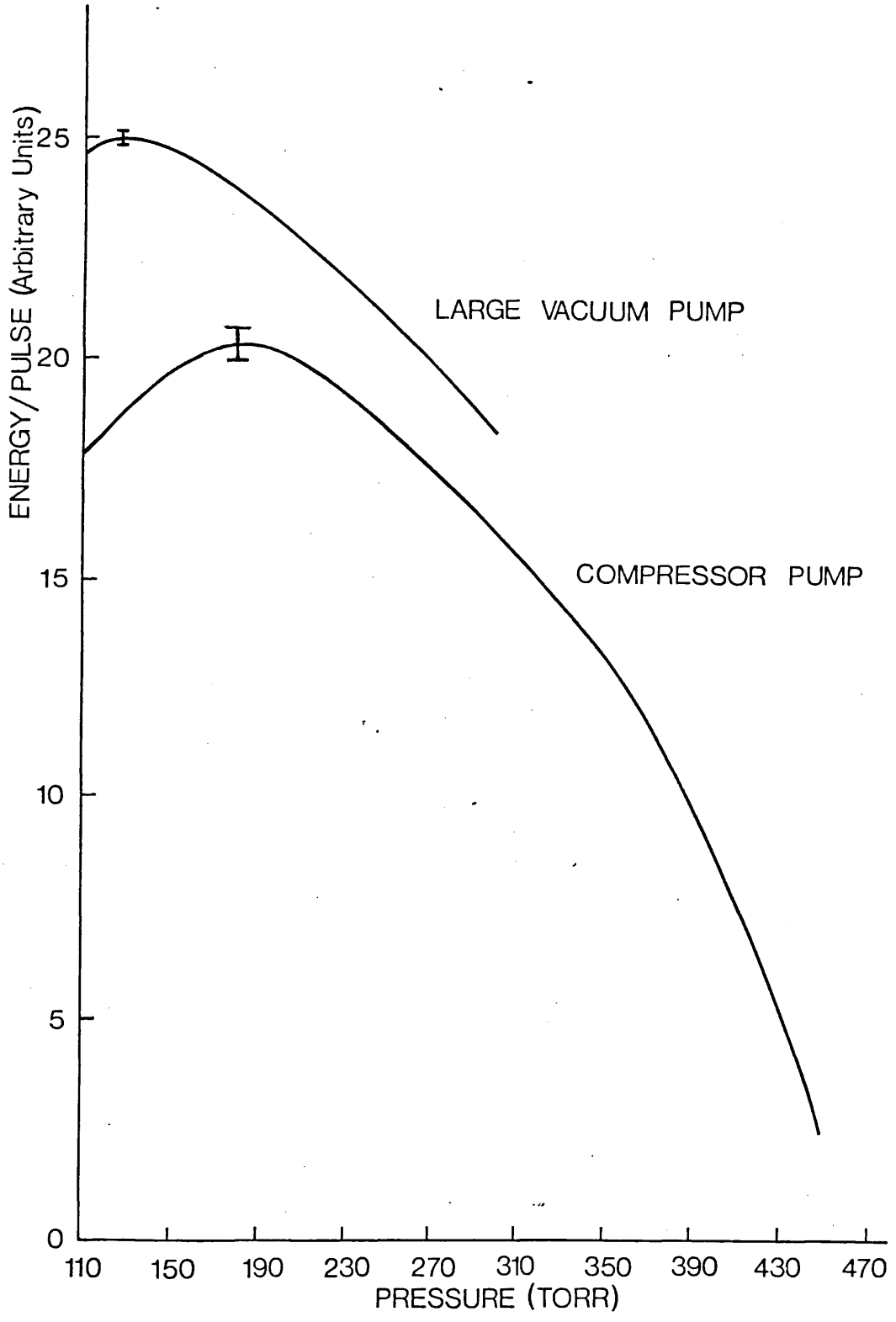

FIGURE 4.10 Variation of output pulse energy with pressure of the Mk II laser.
(V = 15kV, RR = 16Hz, D = 8.2mm).

range over which this laser will operate with this electrode separation.

The variation of peak power and pulse width with pressure at this electrode separation is shown in figure 4.11. The FWHM varies from 3.2ns to 2.2ns and is 2.8ns at maximum pulse energy. The maximum peak power occurs at a pressure of 270 torr.

The effect of the repetition rate on the pulse energy and average power is shown in 4.12. The average power is seen to increase up to 80Hz and the pulse energy remains fairly constant because the narrow electrode separation reduces the tube volume, hence more gas exchanges occur per second; additionally the proximity of the electrodes means that the metastable molecules are more likely to deexcite by collisions with the electrodes.

The laser was also operated with an electrode seperation of approximately 3.2mm. This is narrow enough to allow stable operation at atmospheric pressure and figure 4.13 (a) shows a pulse produced at this pressure. The FWHM is 1.4ns but is the convolution of the laser pulse width and the risetime of the oscilloscope/photodiode combination (0.6ns). Assuming a Gaussian pulse profile the deconvoluted width is 1.3ns. The pressure for maximum pulse energy with this electrode separation is 570 torr and the pulse shape for this pressure is shown in figure 4.13(b).

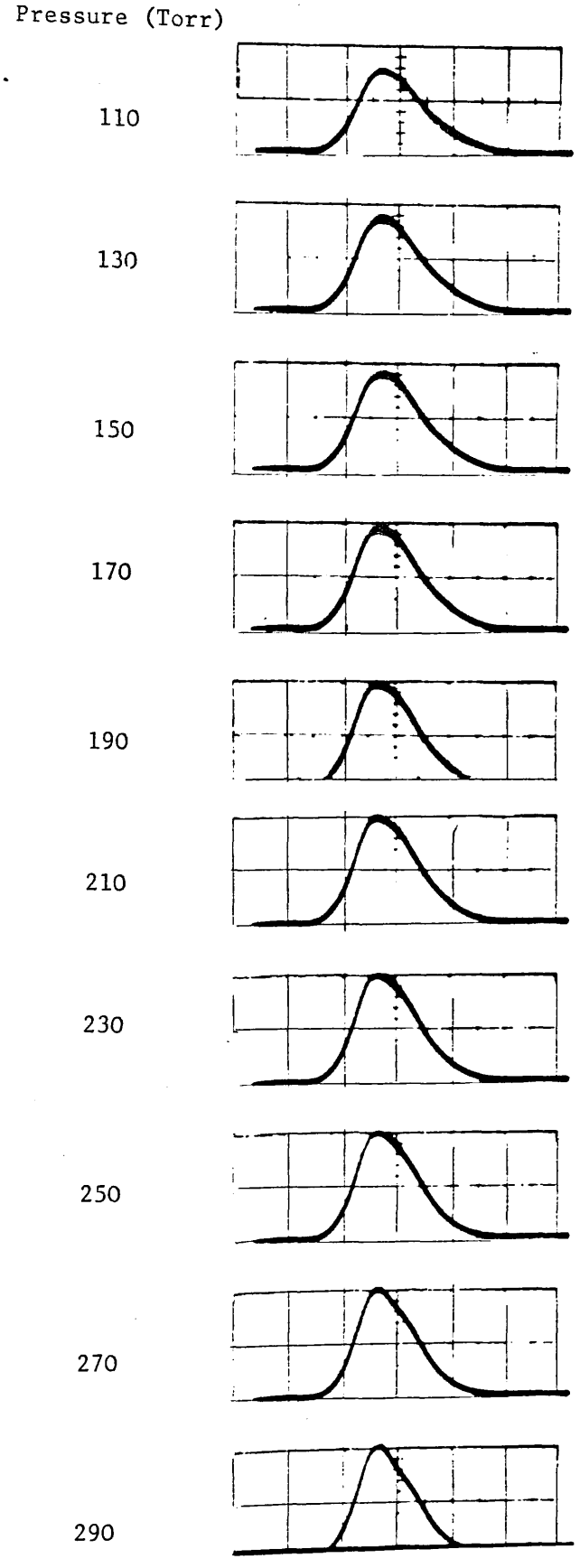

FIGURE 4.11 Variation of peak power and pulse width with pressure of the Mk III laser.
(V = 17.5kV, RR = 18Hz, D = 8.2mm).

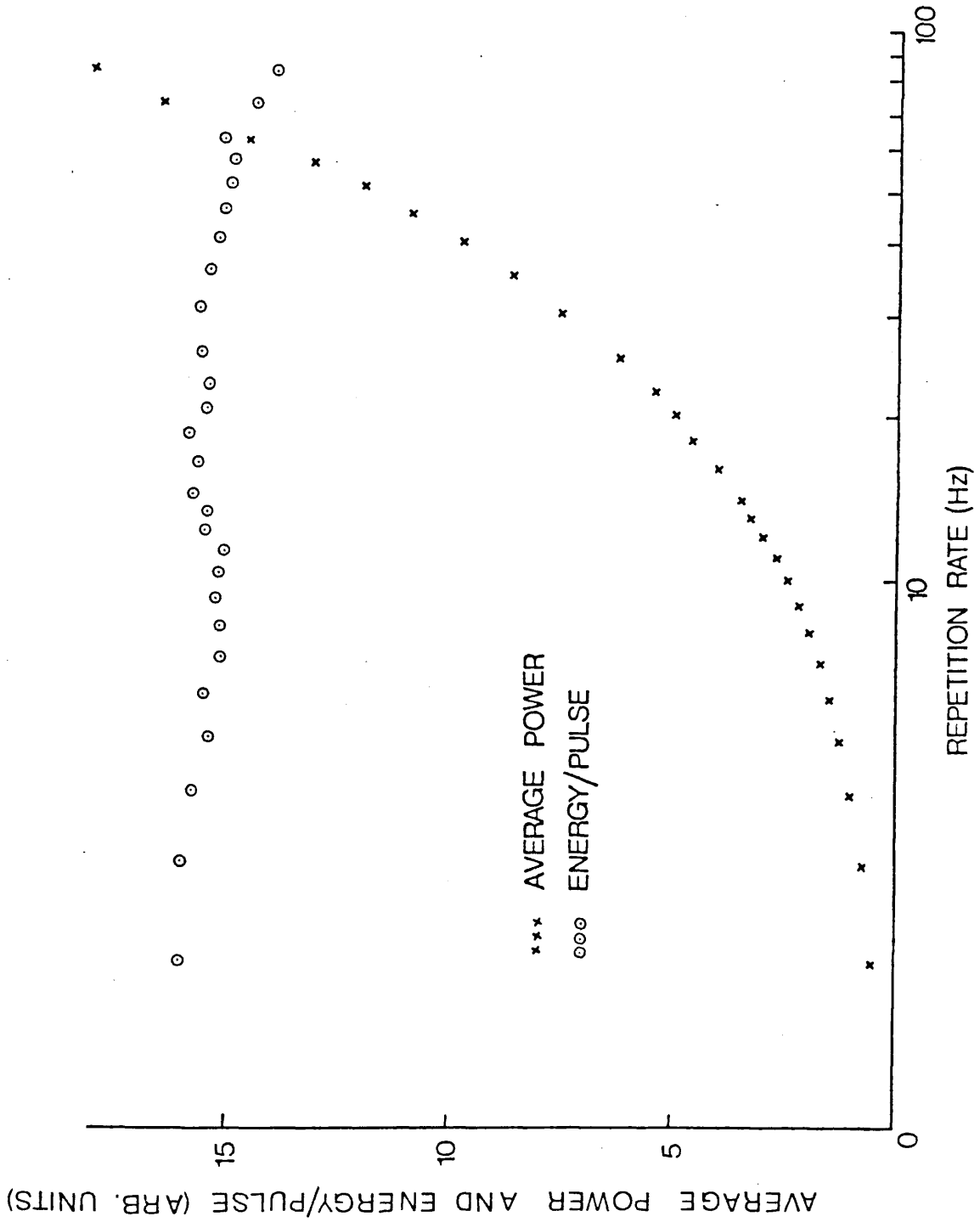

FIGURE 4.12 Variation of average power and energy/pulse with repition rate of the Mk III laser.
(V = 17.5kV, P = 210 torr, E = 8.2mm).

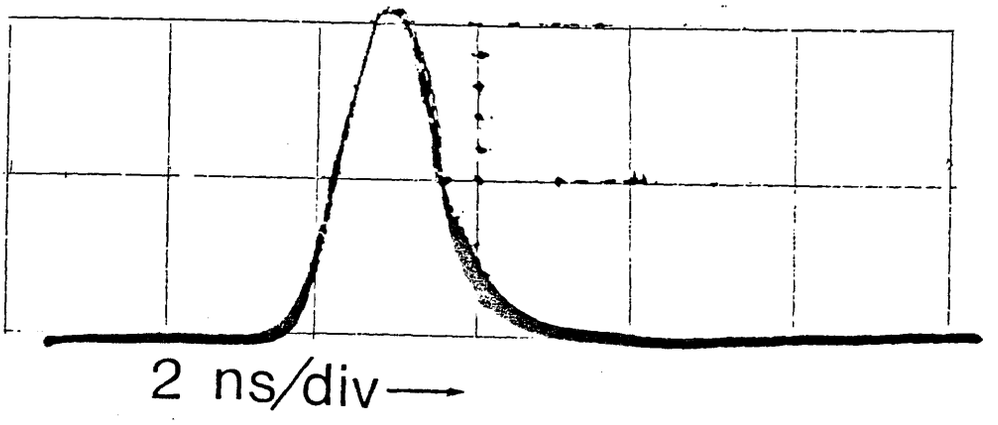

(a) (V = 14kV, RR = 10Hz, P = atmospheric, D = 3.2mm).

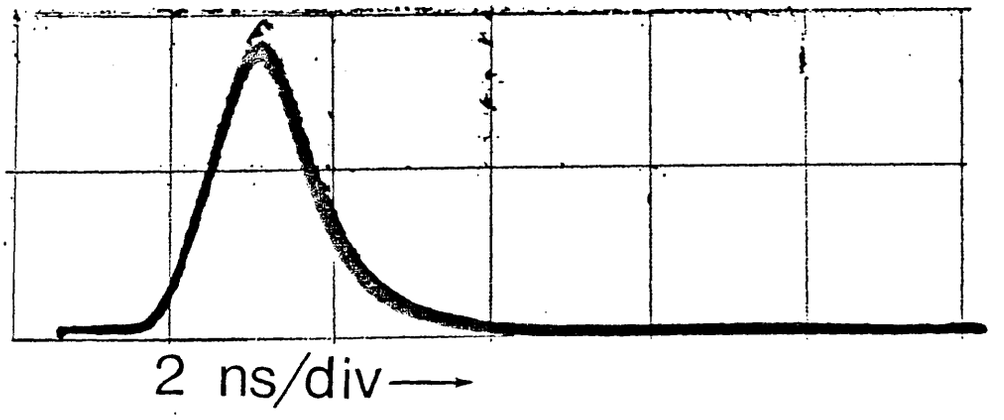

(b) (V = 13kV, RR = 10Hz P = 570 torr, D = 3.2mm).

FIGURE 4.13 Output pulse shapes of the Mk III laser.

It was decided that for operation as an oscillator in a MOPA configuration that the separation of the electrodes would be kept at 12.7mm. The reason for this is that the beam dimensions of this laser (12.7 x 4mm) are then well matched to that of the Mk II laser after allowing for expansion due to beam divergence.

4.3 OPERATION USING A CAPACITOR TRANSFER CIRCUIT

4.3.1 Description

Conversion to operation with a capacitor transfer circuit was fairly straightforward. The tube is unaltered apart from a different position for the third preionizing electrode, holes were tapped in the right hand electrode for mounting the storage capacitors and two new mounting plates were made. In addition new mountings had to be made for the three electrode triggered spark gap.

The electric circuit for the laser used in this manner is similar to that shown in figure 3.1 (pp 78). The only difference is that the grounded preionization wire is not needed, with the preionizing discharge proceeding from the preionizing wire to the grounded electrode. The storage capacitor comprises five 2.5nF capacitors giving a total capacitance of 12.5nF. Unless otherwise specified the dumping capacitor consisted of eight 625pF capacitors with a total capacitance of 5nF. The preionizing capacitor has a value of

166pF and the electrode separation was kept constant at 12.7mm.

4.3.2 Operation

Some of the output characteristics of the laser are similar to when it is operated with a Blumlein circuit. The variation of pulse energy with repetition rate was measured up to a repetition rate of 35Hz and was found to be constant. The pressure for maximum pulse energy at an applied voltage of 20kV was 100 torr, somewhat less than in the case of the Blumlein circuit. The relatively small difference is probably because the make of capacitors, mountings and connections are all different for the two circuits which means that the inductances and impedances will also be different.

The main differences between operation with the two circuits are the beam divergence and pulse widths. The output energy density was measured in the same manner as previously and the half angle beam divergence was obtained from the resulting curves. It is 1.6mrad and 2.7mrad in the vertical and horizontal planes respectively. This is a decrease of 1.2mrad in the horizontal plane when compared to operation with the Blumlein circuit. The decrease is caused by the beam being able to make more passes up and down the tube due to the longer pulse widths (see later). There is no decrease in the vertical plane because the plasma has a larger height; at 10cm the heights are 3.7mm and 4.1mm for the Blumlein and capacitor transfer circuits respectively. The larger plasma volume is

probably caused by more efficient preionization in the capacitor transfer circuit.

The pulse shape is shown in figure 4.14. The FWHM is 5.4ns which represents an increase of 1.7ns over that when using the Blumlein circuit under the same conditions. This demonstrates well how the fast Blumlein circuit produces shorter pulse widths than the slower capacitor transfer circuit. An additional point to note is that this laser produces shorter pulses than the Mk II laser despite operating with the same circuit. This is the effect predicted by Richter et al. (1.9) whereby the pulse width decreases with decreasing discharge length (page 30). Due to the different mountings etc. it is also probable that the initial inversion densities are not the same and this will also affect the pulse width (1.9). The pulse width can be extended further by the addition of a front coupler with a higher reflectivity. Shown in figure 4.15 (a) & (b) are the pulse shapes produced under the same conditions except that the output couplers had transmissions of 25% and 10%; the FWHM's are 5.6ns and 6.2ns respectively. The decrease in pulse energy with the low transmission output couplers is less severe than in the case of the Mk II laser. For example, the decrease in pulse energy when using a coupler with a transmission of 27% is only 50%. The higher reflectivity couplers also cause a decrease in beam divergence; the beam divergence when using the 10% transmission coupler is reduced to 1.1mrad and 1.8mrad in the vertical and horizontal planes respectively. The energy in this case is decreased by 75% so there is no increase in brightness.

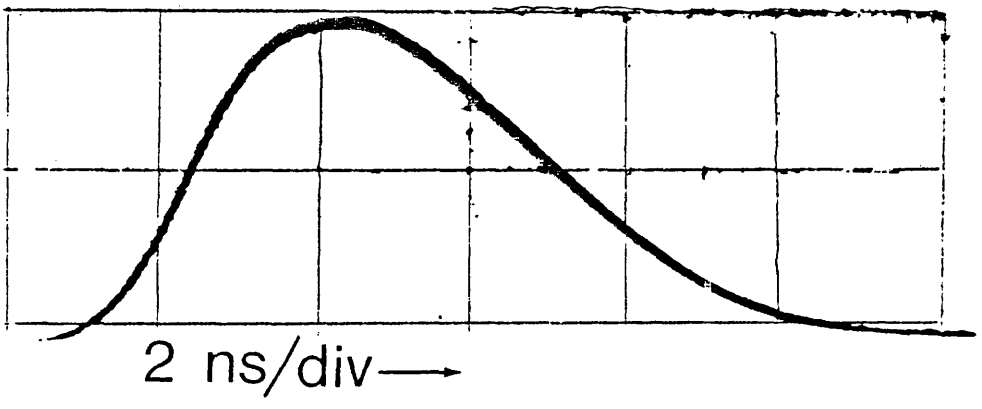

FIGURE 4.14 Output pulse shape of Mk III laser using a capacitor transfer circuit
(V = 25kV, RR = 10Hz, P = 110 torr,
D = 12.7MM, CT = 92%).

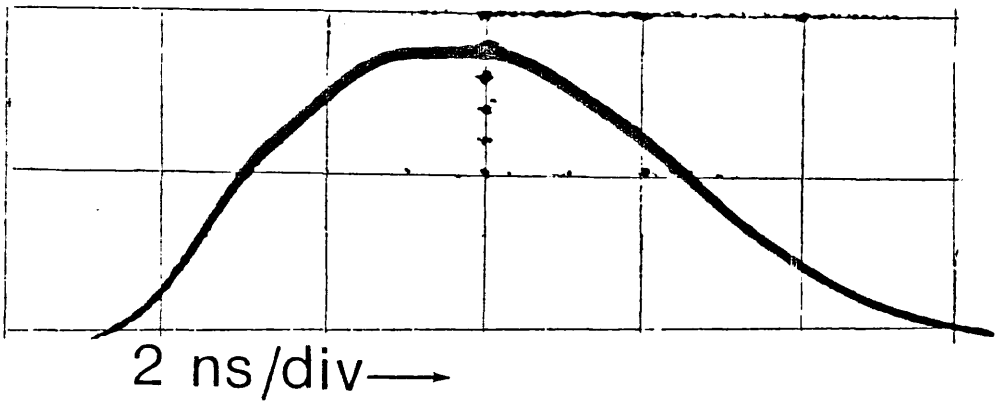

(a) (V = 25kV, RR = 10Hz, P = 110 torr, D = 12.7mm CT = 25%).

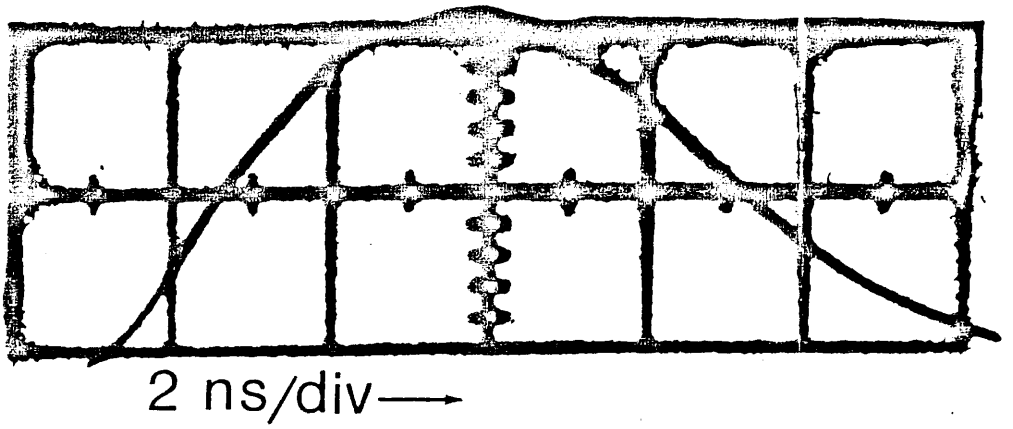

(b) (V = 25kV, RR = 10Hz, P = 110 torr, E = 12.7mm, CT = 10%).

FIGURE 4.15 Output pulse shapes with low transmission couplers of the Mk III laser.

4.4 SUMMARY

This laser has been demonstrated to be extremely versatile. It operates with repetition rates from single shot to 100Hz and with applied voltages from 10kV to 25kV. It has the unusual feature of a widely variable electrode separation which allows operation with gas pressures ranging from 20 torr to atmospheric. This feature has been used to investigate the variation of pulse width with pressure and the pulse widths (FWHM) have varied from 4.0ns at 20 torr to 1.4ns at atmospheric pressure. There have been other reports of N_2 lasers with variable electrode separations but most have been designed for operation at atmospheric pressure or greater and consequently only operate with narrow separations. Bergmann et al. (4.1) described a laser with a variable electrode separation which is designed for low pressure operation but they do not give any data on the variation of the pulse width.

The laser operates with two types of circuit and the increased pulse width when using the capacitor transfer circuit has been well illustrated. Additionally the pulse width has been shown to be less in this short laser than in the longer Mk II laser when using a similar circuit.

To the author's knowledge this is the first report that the pulse energy maximum and the peak power maximum occur at significantly different gas pressures. The flexibility of this laser means that it is a very useful tool. In addition to its

use as an oscillator in an oscillator-amplifier system it has been used for triggering a laser triggered spark gap and for dye laser pumping.

CHAPTER V

OSCILLATOR - AMPLIFIER OPERATION OF THE Mk II AND MkIII LASERS

5.1 PREVIOUS REPORTS OF OSCILLATOR - AMPLIFIER NITROGEN LASER SYSTEMS

There have been few reports of master oscillator power amplifier (MOPA) nitrogen laser systems. The main reason for this is that the majority of nitrogen lasers are used for dye laser pumping, for which the superior beam characteristics of MOPA systems are not usually required. Despite this nitrogen laser MOPA systems have uses such as plasma interferometry (5.1), plasma holography (5.2), high speed photography (5.3), flash photolysis experiments (5.4) and they could also be used for longitudinal pumping of dye lasers.

The main technical difficulty in constructing nitrogen laser MOPA systems lies in the very short population inversion times which mean that the synchronization of the oscillator and amplifier sections must have a jitter of less than one nanosecond. Conventional spark gaps have a delay of about 500ns and jitters of between 10 and 50ns between the application of an external electrical trigger signal and the firing of the gap, making them unsuitable for switching each channel. However, Thomas et al. (5.5) report limited success with conventional spark gaps by using a multiple gap arrangement.

An alternative method is to use laser triggered spark gaps which have delays of a few nanoseconds and jitters of a few tenths of a nanosecond (5.6). Most laser triggered spark gaps are triggered with lasers of high power (5.6). However, Pinnekamp et al (5.7) report using a laser with a peak power of 400W whilst Schildbach and Basting (5.8) used a dye laser with a peak power of 10kW to switch a spark gap on a nitrogen laser with a delay of 10ns and subnanosecond jitter.

Instead of spark gaps thyratrons can be used; these also have fairly long delays but the jitter can be reduced to 1 or 2 ns (1.33). This however does require 'fine tuning' of their operating conditions. In addition Santa et al. (5.9) report that the delay in switching thyratrons drifts with time and that resynchronization is required every 10 to 20 minutes.

Two groups (5.10 and 5.11) report synchronization by using one switch and then letting the oscillator discharge act as the switch for the amplifier section. In this way the delay between the output of each section is about 20ns with negligible jitter. Hugenschmidt and Volbrath (5.12) extended this technique to a multichannel system with one initiating switch and five discharge channels.

The most common way of achieving synchronization is to use one switch for both discharges thus eliminating all problems of jitter. All that is then required is to adjust the relative timing of the oscillator and amplifier sections so as to

compensate for the time of flight of the light pulse between them. The main difference between systems employing one master switch is in the way this is achieved.

One technique is to use identical oscillator and amplifier sections and then adjust them so that the breakdown voltage is higher in the amplifier section. For low pressure lasers this is most conviently achieved by decreasing the pressure in the oscillator (Kagawa et al. (5.13, 5.14)), whilst for high pressure (atmospheric) lasers reduction of the electrode separation has the same effect (Bergmann (5.15)) and is simpler. Nakamura et al. (5.15) achieved the correct timing by using parallel plate transmission lines to connect the spark gap to the oscillator and amplifier sections and then arranging for the propagation time of the voltage pulse to be greater to the amplifier. In a similar system Santa et al. (5.9) produced the required delay by introducting inductances into the amplifier arm of the transmission line. An alternative method is the use of an adjustable timing switch (Bergmann and Hasson (1.36)). Jitsuno (1.34) used a combination of adjustable timing switches and varying electrode separations in an 8 stage MOPA system.

5.2 COMBINATION OF THE Mk II AND Mk III LASERS AS A MOPA SYSTEM

The first method conceived for the system was to use a laser triggered spark gap on the amplifier (Mk II laser) and to trigger this with part of the light produced from the

oscillator (Mk III laser). An optical delay line would then be used to compensate for the switching delay. However the results of initial experiments showed that there was an intrinsic delay of about 75ns between switching of the gap and light output from the amplifier and this delay is too long for optical compensation. The experiments did reveal the usefullness of the Mk III laser for switching spark gaps with a jitter of about 2ns and a delay before switching of about 10ns.

Because this method was unsatisfactory it was decided to use a common switch for both sections. With both sections utilizing capacitor transfer circuits the device is similar to the KrF MOPA system described by Caro et al. (5.17) except in their case the oscillator and amplifier sections were of equal size. In addition they achieve correct timing by inserting higher inductance between C_S and C_D whereas the more convenient method used here is to vary the pressure in the oscillator. All previous nitrogen laser MOPA systems have utilized Blumlein circuits for both sections.

It was at this point that the Mk III laser was converted to operation with a capacitor transfer circuit and its C_D/C_S ratio was chosen to be the same as that of Mk II laser and was therefore 0.4. This was to ensure that the voltage risetime was the same across both sets of electrodes and the relative timing would then be adjusted as described previously. The complete circuit of the MOPA system is show in figure 5.1 (excluding preionization). The layout used is shown in figure 5.2 and a

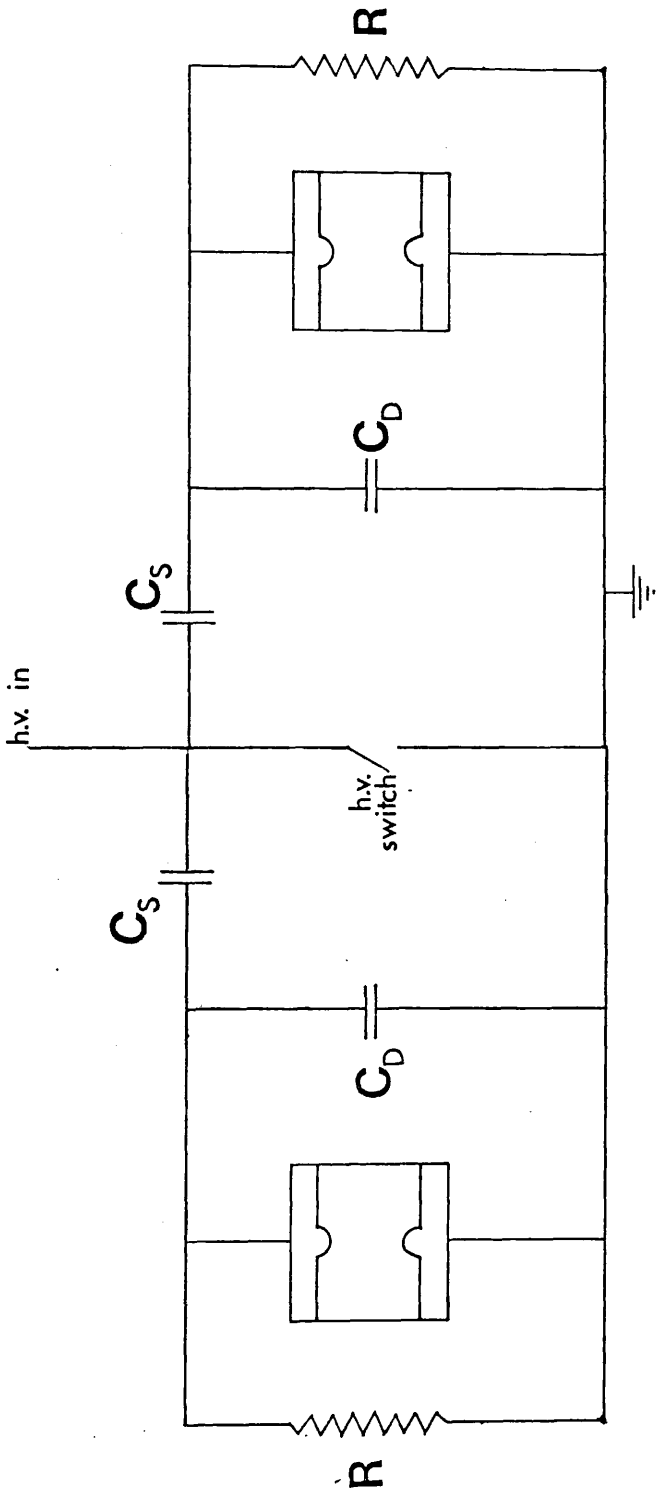

FIGURE 5.1 Electrical circuit of the MOPA system.

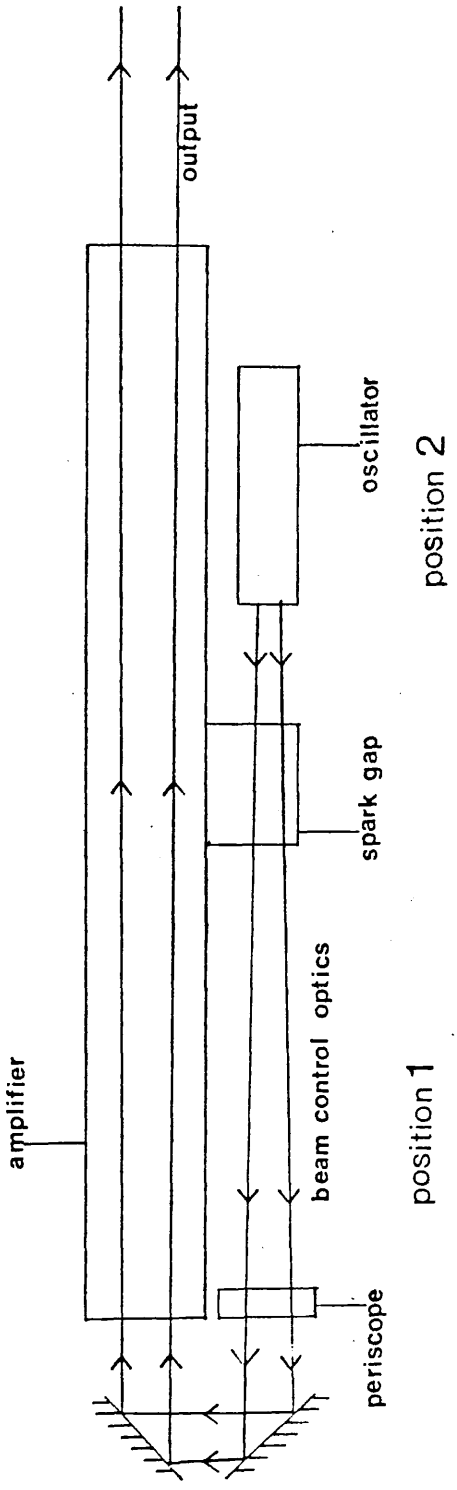

FIGURE 5.2 Schematic layout of the MOPA system.

cross section of the combined laser is shown in figure 5.3. The oscillator can be placed in position 1 or 2 depending on whether beam control optics are required. The light from the oscillator passes over the spark gap (when in position 2); the height is corrected by means of a periscope and the beam is then aligned to pass down the optical axis of the amplifier by means of two front aluminised mirrors held in precision kinematic mounts. The following technique was adopted for measuring the relative timing between the oscillator and amplifier discharges. The light pulses from both the oscillator and the amplifier were suitably attenuated and directed on to the same biplanar vacuum photodiode. The output from this was displayed on a Tektronix 519 oscilloscope whose timebase trigger was derived externally from a silicon PIN photodiode illuminated by a sampled portion of the amplifier pulse. The output from the oscillator was blocked and the trigger hold off adjusted so that the peak of the amplifier pulse was in a suitable position which was then noted. The beam from the amplifier was then blocked (after the sampling beamsplitter) whilst unblocking the beam from the oscillator. The pressure in the oscillator was then adjusted to some value and then increased in 10 torr steps. For each set of measurements all the other variables were kept constant and photographs were taken at each pressure, and from these photographs the variation of relative timing with pressure in the oscillator was found. For these measurements the amplifier was operated as an oscillator, ie. with a fully coated rear mirror. Operation of the oscillator in position 2 required that it discharged

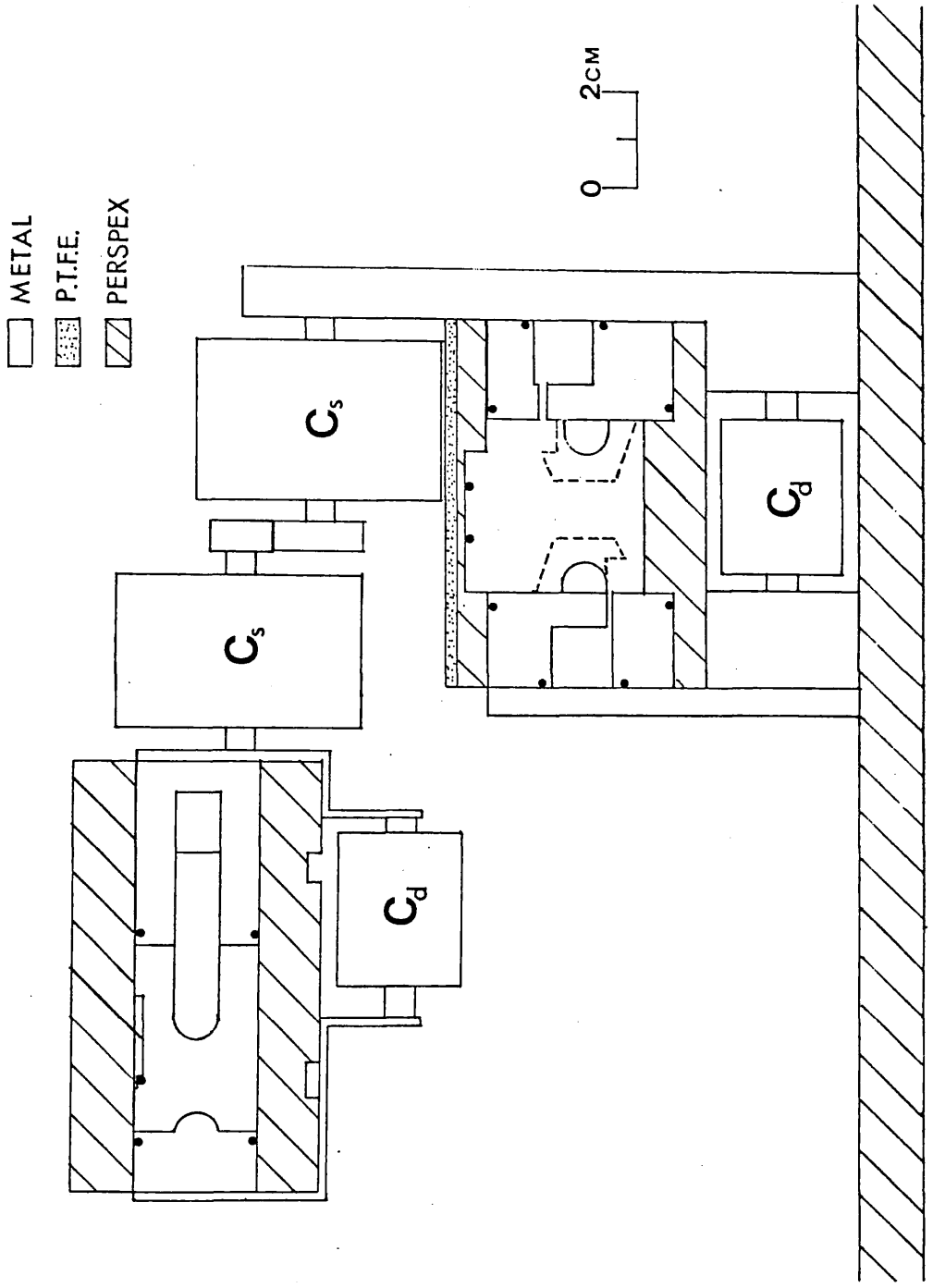

FIGURE 5.3 Cross-section of the MOPA system.

about 6ns before the amplifier. For all results the oscillator electrode separation was kept at 12.7mm and at this time the amplifier had the large area electrodes also with a separation of 12.7mm. The results of initial experiments showed that with equal pressures the amplifier discharged 5ns before oscillator. It was not clear why this was so and attempts were made at improvement. The C_D/C_S ratio on the oscillator was decreased by removing some dumping capacitors so as to increase the voltage risetime across the electrodes. This had the desired effect of advancing the discharge time of the oscillator but it also decreased the pulse energy. The decrease in pulse energy was greater than that obtained by decreasing the pressure sufficiently to advance the timing by the same amount.

In addition to the poor relative timing the amplifier discharge was having a pronounced effect on the oscillator output. The variation of pulse energy from the oscillator as a function of pressure in the amplifier is shown in figure 5.4. With an amplifier pressure below 35 torr arcing in the oscillator was so severe that no output was observed. The effect is more severe at higher oscillator pressures as shown by figure 5.5 which shows pulse energy/pressure curves for the oscillator at various amplifier pressures. With atmospheric pressure in the amplifier no discharge occurs and the curve is the usual shape with the peak (not shown) occurring at 95 torr. The effect of the oscillator on the amplifier was les severe, decreasing the output by 10% in the worst case.

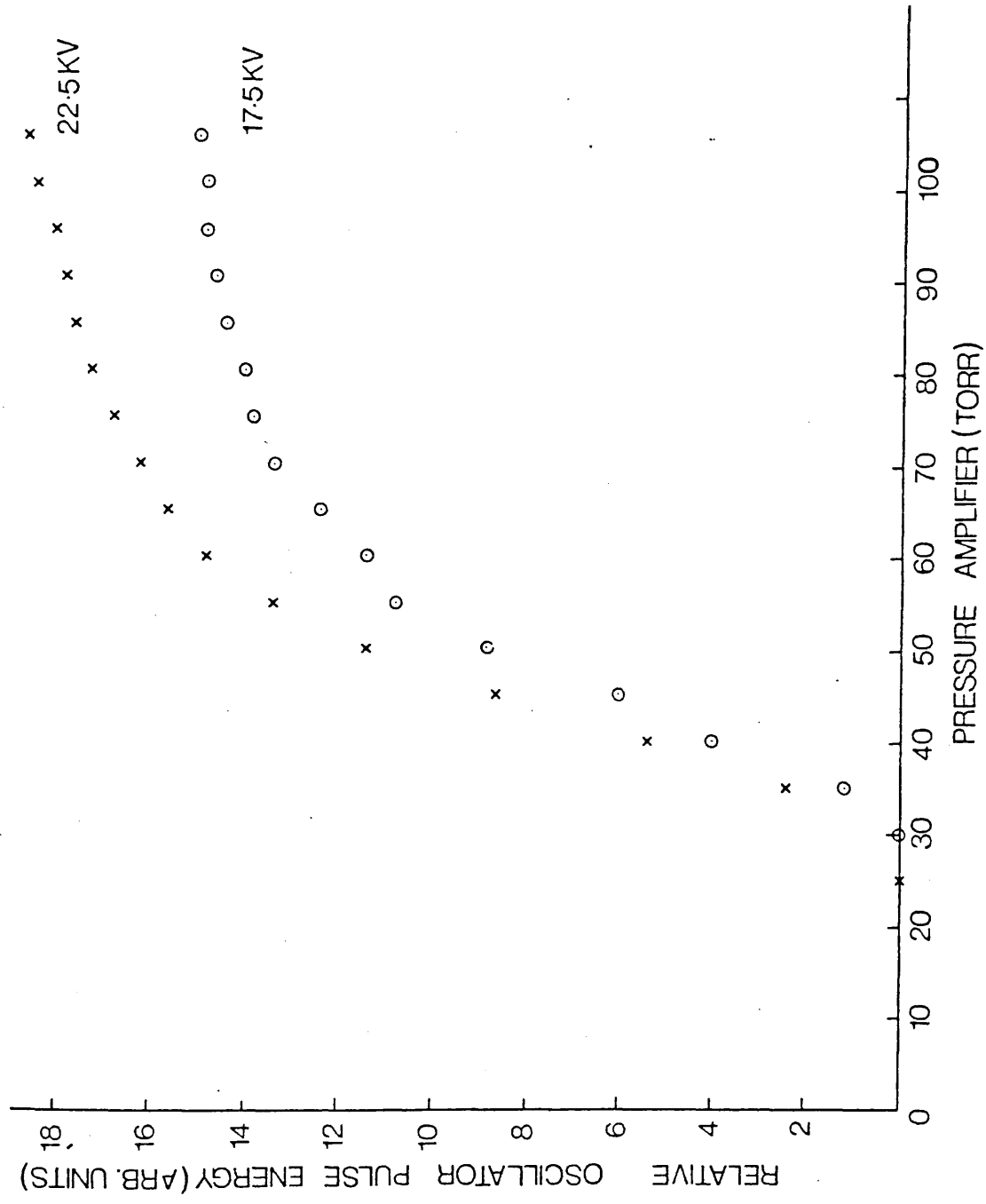

FIGURE 5.4 Variation of oscillator pulse energy with pressure in the amplifier.
(RR = 10Hz, Oscillator Pressure (OP) = 90 torr).

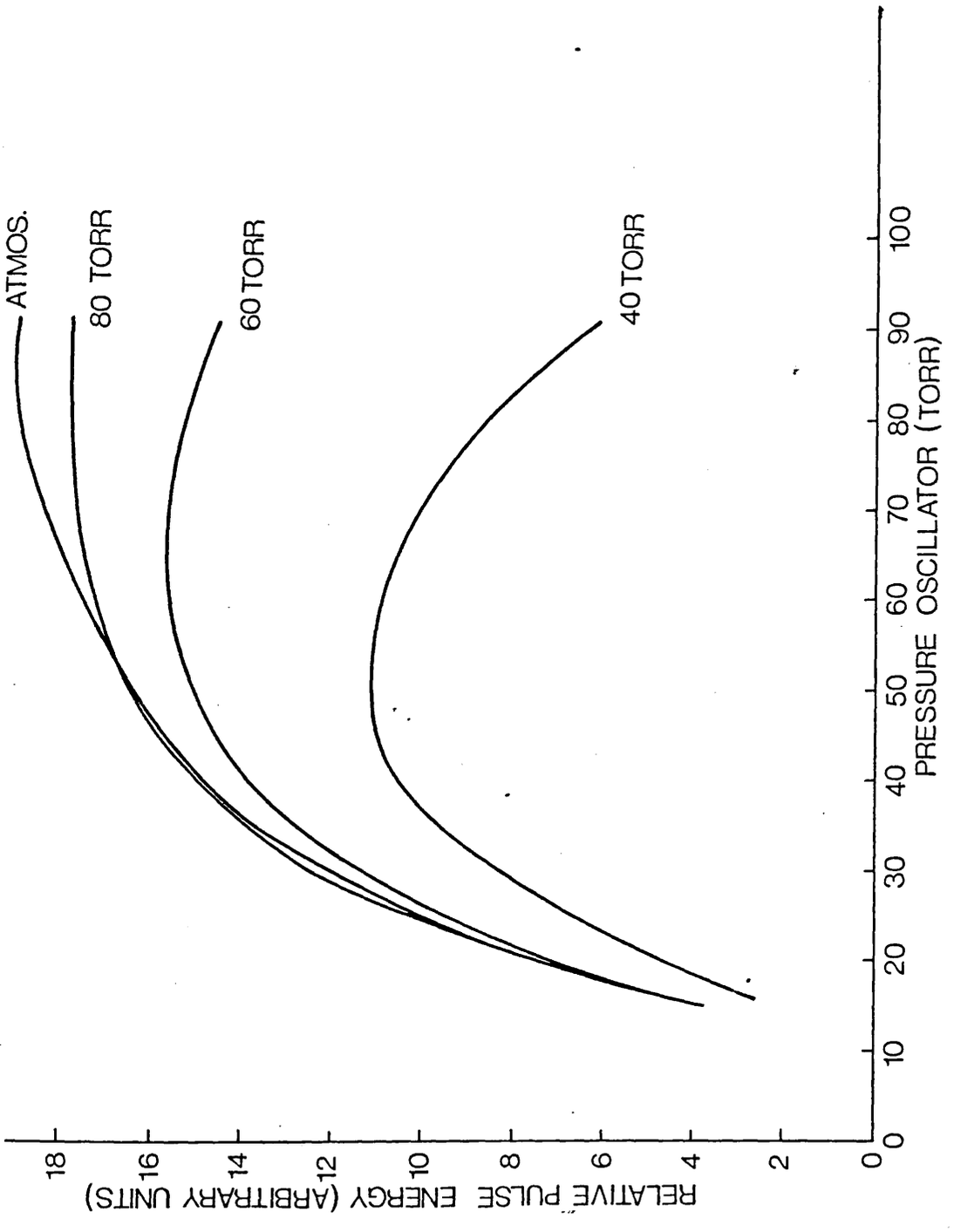

FIGURE 5.5 Variation of oscillator pulse energy with oscillator pressure at various amplifier pressures. (V = 22.5kV, RR = 10Hz).

Fitzsimmons et al. (1.6) reported that nitrogen lasers using Blumlein circuits produce output pulses in a shorter time (relative to the firing of the spark gap) than those using capacitor transfer circuits so it was decided to change the oscillator back to operating with a Blumlein circuit. A mounting plate was made to connect the high voltage bar on the amplifier to the oscillator; this plate has dimensions such that the oscillator remained in the same location. The capacitors C_1 and C_2 were changed from the Eerie capacitors used previously to 6 Steatite and Porcelain type C7061 with nominal capacitances of 625pF. Operation with the Blumlein circuit produced a slight improvement in relative timing of about 4ns over the case with a capacitor transfer circuit. Two typical relative timing results are shown in figure 5.6; the amplifier pressure was 65 torr. The lower line corresponds to operation with the oscillator using the Blumlein circuit and the upper line to that using the capacitor transfer circuit with a C_D/C_S ratio reduced from 0.4 to 0.26. For operation with the required delay of 6ns the oscillator has to have a pressure of 50 torr (Blumlein case) which is a value well below that for optimum output. More importantly the amplifier pressure is substantially higher than that for optimum output. The accuracy of the relative timing experiments is not that high. The pressure gauge on the oscillator has divisions separated by 20 torr so the best resolution is about $\pm$ 5 torr whilst the oscilloscope timebase was set at 2ns per division providing a resolution of $\pm$ 0.5ns. The jitter of the relative timing was generally of the order 0.5ns but was greater

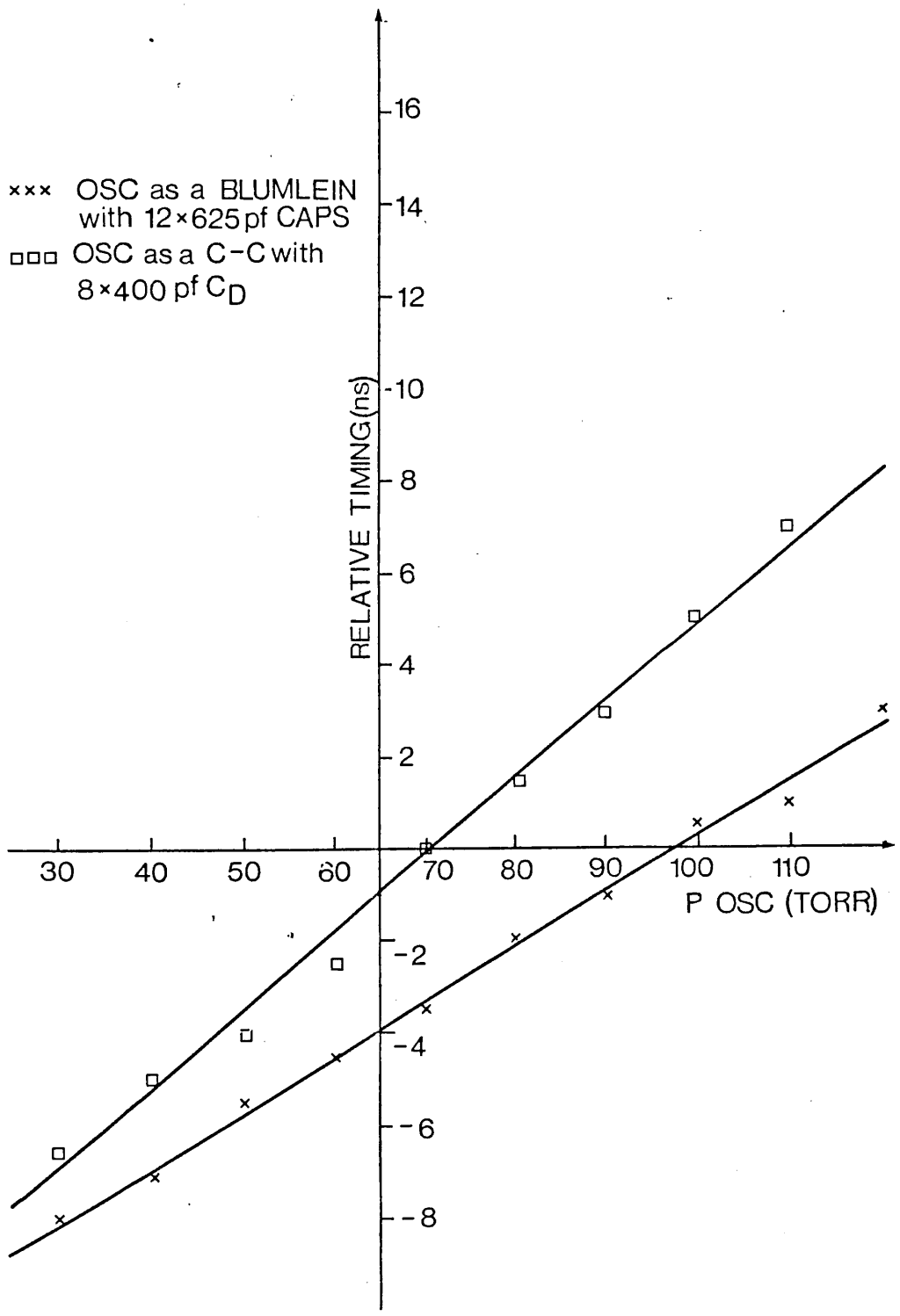

FIGURE 5.6 Relative timing of the oscillator output pulse as a function of oscillator pressure.
(V = 22.5kV, RR = 10Hz, Amplifier pressure (AP) = 65 torr).

(approx. 3ns) when the oscillator discharged a long time (approx. 4ns) after the amplifier.

Various other parameters were investigated to find their effect on relative timing to see if improvements could be made. When using the Blumlein circuit the capacitance of C_1 and C_2 was increased to try and provide more energy but this adversly affected the relative timing and any gain in energy was offset by having to work at a lower pressure. The preionization separations were varied in both the amplifier and oscillator but with little effect. The effect of electrode geometry in the amplifier was also examined and a slight improvement was obtained by reverting to the electrodes with a cylindrical profile (radius of curvature 4.8mm) and a separation of 19mm.

The solution to the problem was discovered when the oscillator was moved from position 2 to position 1 . This move had a very deleterious effect on the relative timing, with the oscillator discharging after the amplifier for all combinations of pressure. It was realised that the only difference between positions 1 and 2 lay in the grounding. The amplifier was grounded by a copper sheet connected to the outer case and the ground electrode; in position 2 the oscillator was grounded by a similar copper sheet attached to the outer casing at the same point. Moving the oscillator to position 1 meant that the grounding sheets were attached to the case at different points. In addition to this when the oscillator was operated with a capacitor transfer circuit (with the same C_D/C_S as

the amplifier) the only difference between the two lasers was that the spark gap was 'grounded' by a copper sheet from its low voltage electrode to the 'ground' electrode of the amplifier. It was suspected that the charge being switched through the spark gap was not going straight to the ground but was being stored on the dumping capacitors of the amplifier and hence raising the voltage of the 'grounded' electrode (ie. increasing the voltage across the electrodes). This was confirmed by holding an earthed lead close to the 'grounded' electrode and observing that a discharge occurred. To equalise the effect of the charging of the dumping capacitors by the spark gap the grounding plate from the spark gap to the amplifier was removed and replaced with 4 low inductance high voltage cables, two connected to the amplifier and two to the oscillator. This affected the relative timing in a dramatic way and figure 5.7 shows the relative timing at three different amplifier pressures and with the osillator in position 1. The oscillator was operated with the capacitor transfer circuit with a C_D/C_S ratio of 0.4 and the amplifier did not have any preionization (all subsequent results were taken with this combination). The oscilloscope timebase was set at 5ns/div. so the best resolution was about 1 ns. Note that in comparison to figure 5.6 the vertical scale has been changed by a factor two, and the horizontal scale has been moved to the left by 10 torr and the amplifier pressure in that case was 65 torr. With an optimum amplifier pressure of 50 torr the oscillator pressure needs to be 100 torr (close to that for maximum output) for a time difference of 6ns. The slope of the lines is greater than

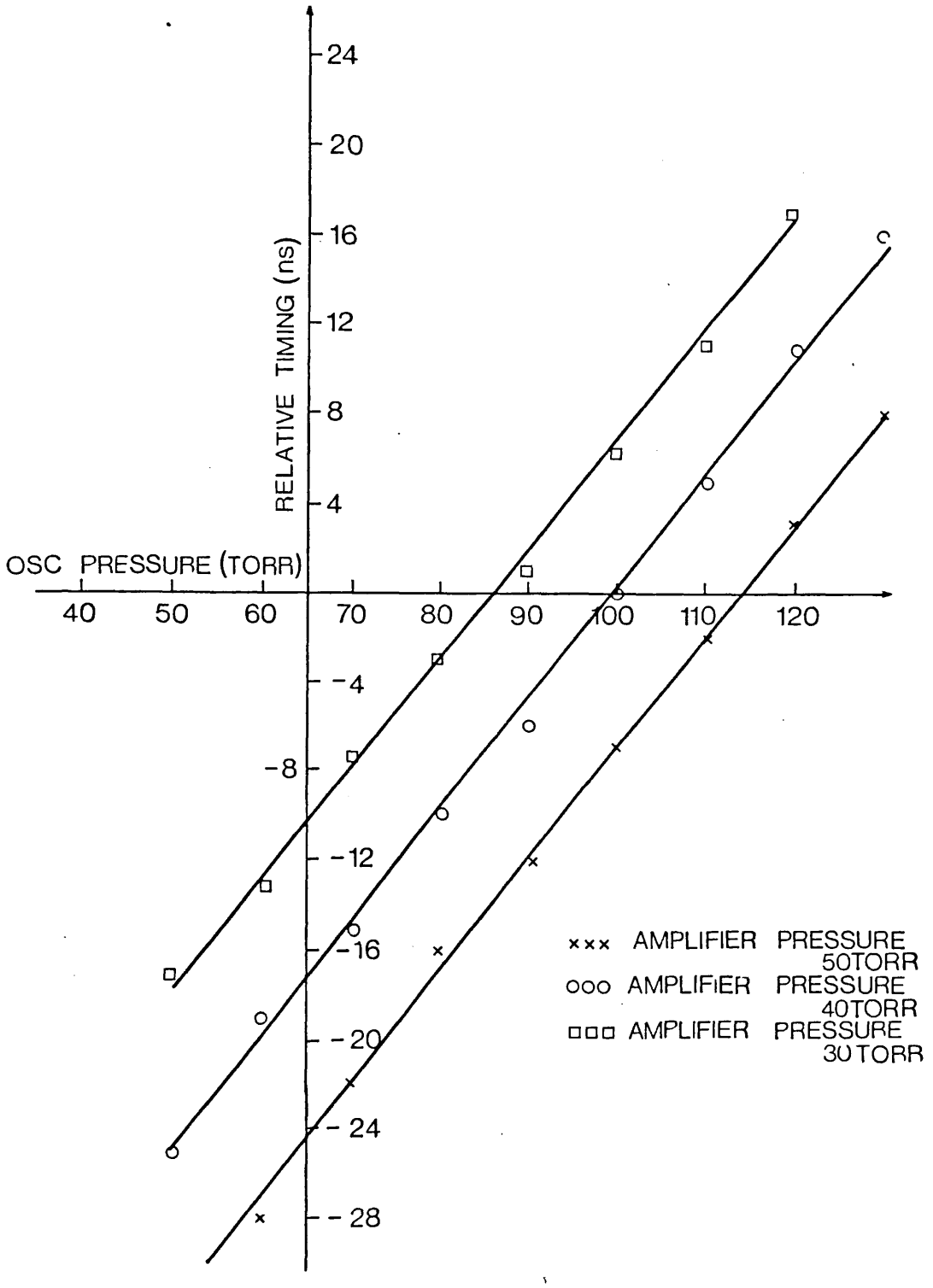

FIGURE 5.7 Relative timing of the oscillator output pulse as a function of oscillator pressure when using the 'new' grounding for the spark gap.
(V = 22.5kV, RR = 10Hz)

those in figure 5.6 indicating a faster voltage risetime in this case. The relative timing changes by about 5ns per 10 torr of pressure in the oscillator. Kagawa et al. (5.13) measured 3ns per 10 torr. The difference suggests a faster voltage risetime in this laser but they used a lower applied voltage (15.5kV) and had a wider electrode separation. The effect of the amplifier on the oscillator when the amplifier discharges first is less severe with this grounding.

The output of the oscillator (in position 2) was directed into the amplifier and the pressure in the oscillator was adjusted for maximum output (as a combined system) at various pressure settings of the amplifier. A plot of output pulse energy against amplifier pressure is shown in figure 5.8. Because the large area vacuum photodiode integrator combination was not functioning at this time the pulse energy had to be measured by the following less acurate method. A Molectron pyroelectric joulemeter (active area π mm^2) was positioned in the beam for maximum signal and the energy density profile was assumed to remain constant whilst the pressure was varied.

Figure 5.9 shows plots of the pulse energy as a function of pressure (ie. relative timing) for three different amplifier pressures. The curves became narrower at higher amplifier pressures because the gain increases with pressure (up to 50 torr) and the effects of amplified spontaneous emission (ASE) become more severe so that the timing of the oscillator pulse becomes more critical (ie. parasitic oscillations takes place).

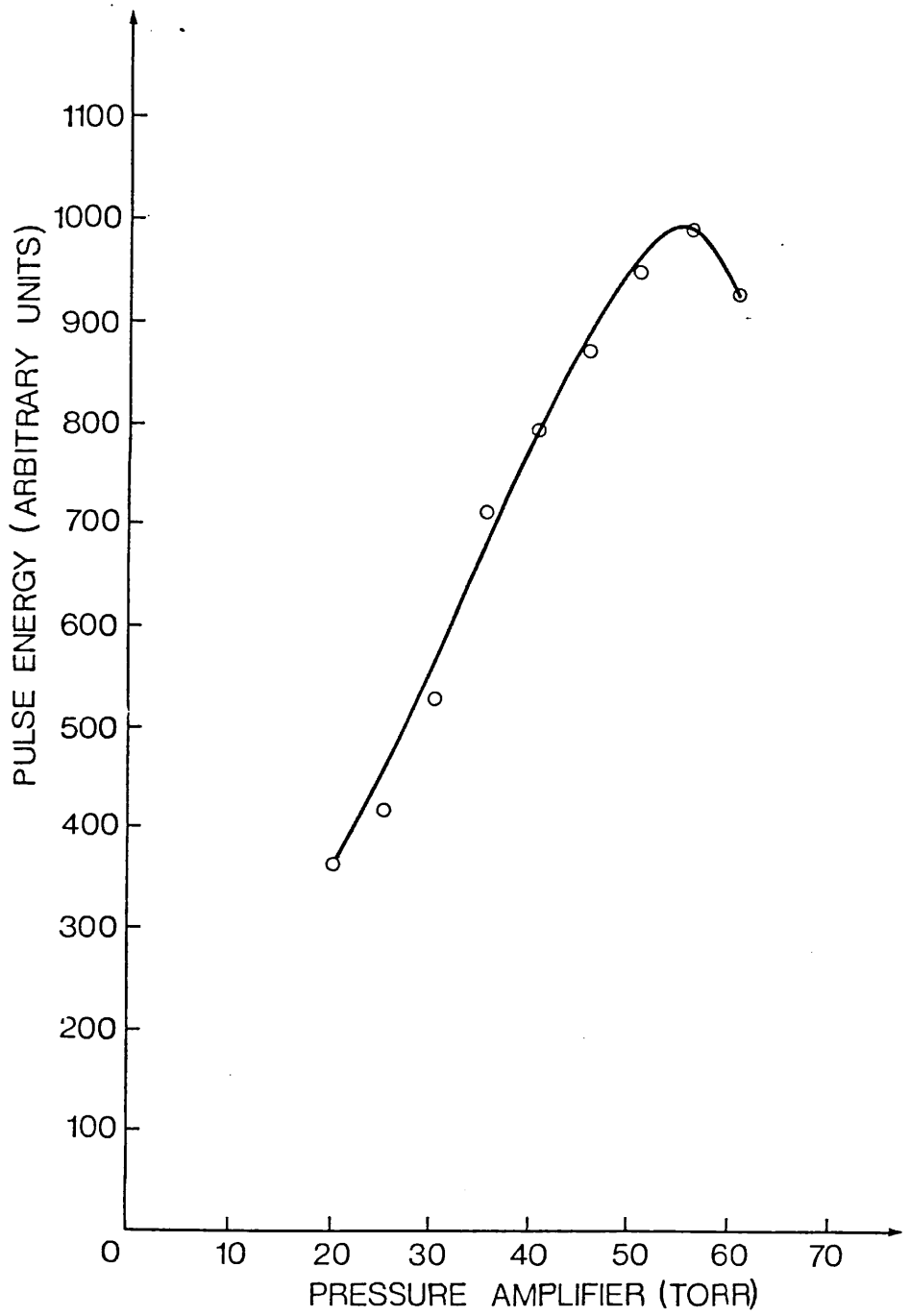

FIGURE 5.8 Variation of pulse energy of the MOPA system with the amplifier pressure.
(V = 22.5kV, RR = 10Hz).

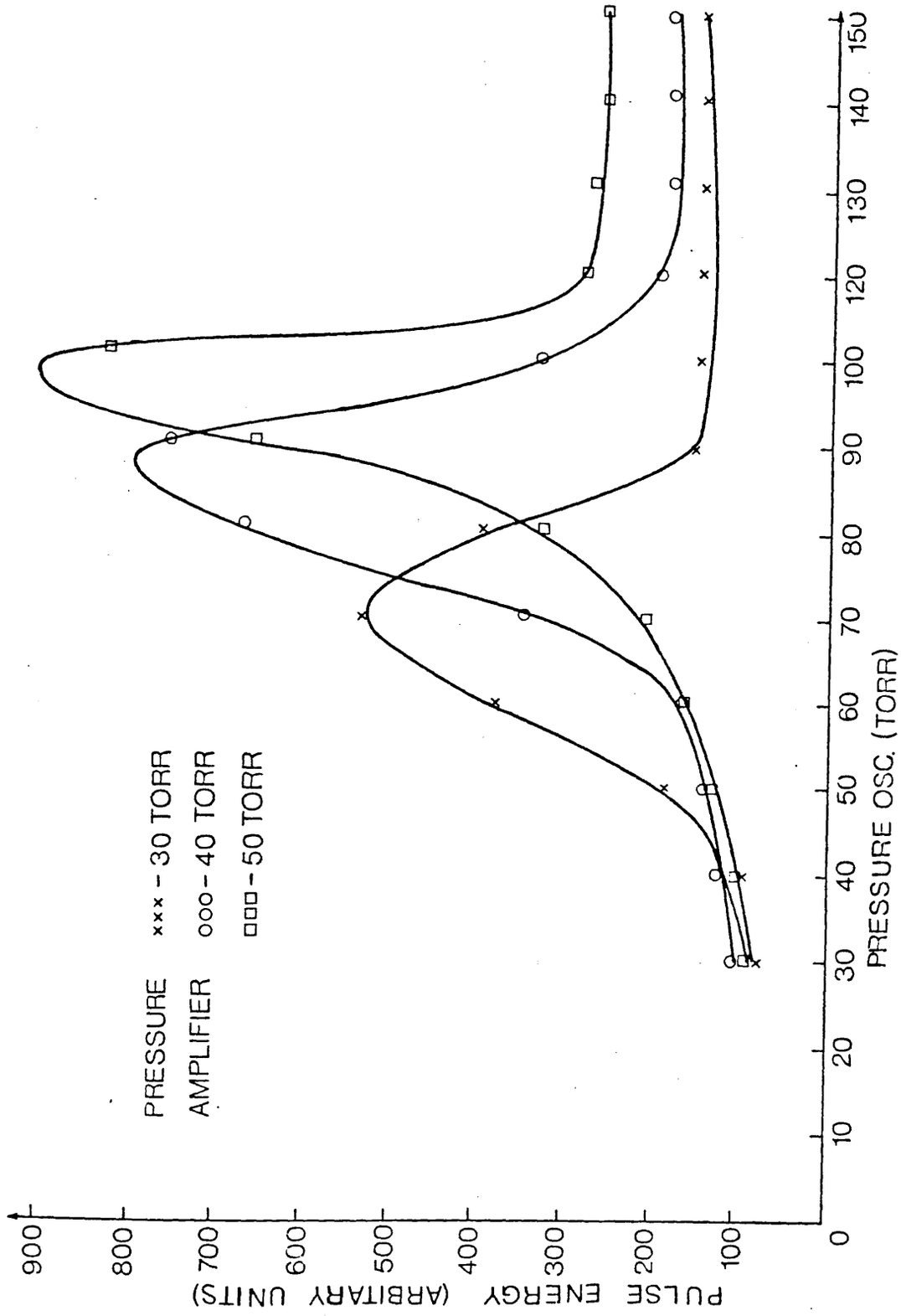

FIGURE 5.9 Variation of pulse energy of the MOPA system as a function of oscillator pressure.
(V = 20kV, RR = 10Hz).

Values just after the peak were difficult to measure because of a large amount of jitter, again caused by ASE (ie. the laser switching from being injection locked to not being so). Kagawa report a symmetric curve for a similar plot to 5.9 and they make no mention of the effects of ASE. This is because their amplifier has a very short active length (10cm).

Figure 5.10 (b) shows an output pulse from the oscillator amplifier system whilst figure 5.10 (a) shows the injected signal (heights are not relative). The pressure in the amplifier was 40 torr, in the oscillator 85 torr. The FWHM of the injected pulse is about 5ns whilst that of the amplified pulse is just over 6ns. The lengthening and different shape is probably due to the effect of ASE from the amplifier in the early part of the pulse. It was not possible to measure the gain of the amplifier because the injected pulse energy was too small to measure with the joulemeter. There is evidence to suggest that the amplifier is saturated in that the jitter of the injected signal is larger than that of the output signal.

The half angle beam divergence of the MOPA system was measured as previously and was found to be 1.3 mrad and 1.65 mrad in the vertical and horizontal planes respectively. A Glan-air polarizing prism was placed between the oscillator and amplifier to produce a polarized output. The polarization ratio of the output was measured by splitting the output with a quartz Rochon prism and comparing the maximum energy densities and this gave a ratio of about 30:1. The energy of the

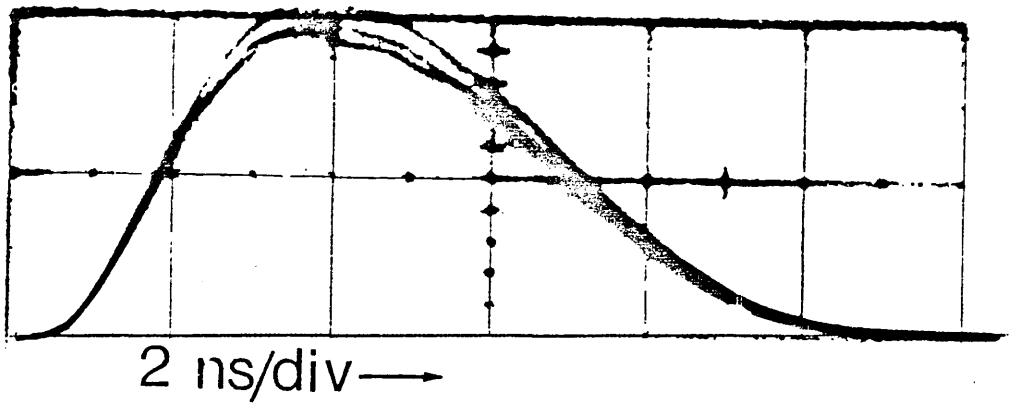

(a)

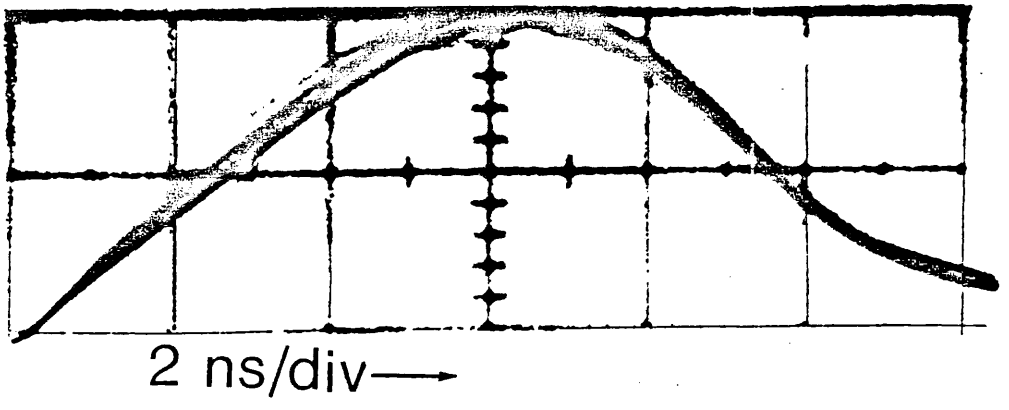

(b)

FIGURE 5.10 Injected (a) and output (b) pulse shapes of the MOPA system (V = 22.5kV, RR = 10Hz).

polarized output was estimated from the energy profile as previously and was found to be 2.1mJ. Operation of the amplifier as an oscillator (ie. with a rear mirror) under the same conditions gave a pulse energy of 2.3 mJ.

5.3 SUMMARY

The Mk II and Mk III lasers have been coupled together, synchronized and operated as an oscillator amplifier system and the output produced is highly polarized and of a similar energy to the Mk II operating singly. Hence a conventional low pressure TE N_2 laser has been converted to one that is suitable for pumping the two wavelength dye laser. The system is suitable for further development; in particular the use of beam control optics between the oscillator and amplifier in combination with the square discharge which can be produced in the amplifier should make it possible to produce an output with equal beam divergences.

CHAPTER VI

NITROGEN LASER PUMPED DYE LASERS

6.1 INTRODUCTION

Laser action in an organic liquid was first discovered by Sorokin and Lankard (6.1) and subsequently many dyes have been found to lase with a variety of excitation sources. The first demonstration of spectral narrowing and tuning was by Soffer and MacFarland (6.2). The efficiency of spectral narrowing is high because the dye laser is a homogeneously broadened laser which means that all excited molecules can radiate at the same wavelength. Hence the output power in a narrow bandwidth is comparable to that when operating with a broad bandwidth. The first tuned nitrogen laser pumped dye laser (NLPDL) reported was that of Myer et al. (6.3) and subsequently the NLPDL has been shown to operate over the large wavelength range of 350-730nm (Stokes et al. (6.4)). Because of its short wavelength the nitrogen laser is most useful as a pump for dyes in the near ultraviolet (Dunning & Stebbings (6.5), Maeda and Miyazoe (6.6)). Additionally the high peak powers generated can be utilized for second harmonic generation (Saikan (6.7)) extending the wavelength range down to 230nm.

6.2 PRINCIPLES OF DYE LASER OPERATION

Organic dyes usually have strong absorption bands in the ultraviolet or visible range of the spectrum. When excited with

light of the appropriate wavelength they display intense Stokes-shifted broadband fluorescence spectra, an example of which is shown in figure 6.1 (a). The broad band structure of absorption and fluorescence is due to the large number of atoms which contribute to the spectroscopic properties of a dye molecule, leading to electronic levels which are composed of a quasi-continuum of vibrational and rotational sublevels. An energy level diagram applicable to most dye molecules in liquid solution is shown in figure 6.1 (b) . The absorption of pump light from the electronic ground state S_0 to the first excited state S_1 is followed by a rapid thermalization in the excited vibronic manifold in S_1. This thermalization takes place within a few picoseconds whereas the radiative lifetime of the vibronic ground state of S_1 is typically a few nanoseconds. In addition pump light with shorter wavelengths can be absorbed with the molecule being excited to higher lying excited states (not shown in figure 6.1 (b)). These decay by non-radiative transitions to the lowest lying excited singlet state S_1, again in a few picoseconds. Several deexcitation processes can start from S_1, as shown in figure 6.1 (b); these can either be radiative (straight arrows) or non-radiative (wavy arrows). The excited molecule can return to S_0 by the emission of a wanted fluorescence photon, it can undergo a non-radiative transition to S_0 or it can populate the triplet system by intersystem crossing.

The radiative transition from S_1 to S_0 can terminate in one of the higher lying vibronic levels of the electronic ground state according to the requirements of the external resonator. The

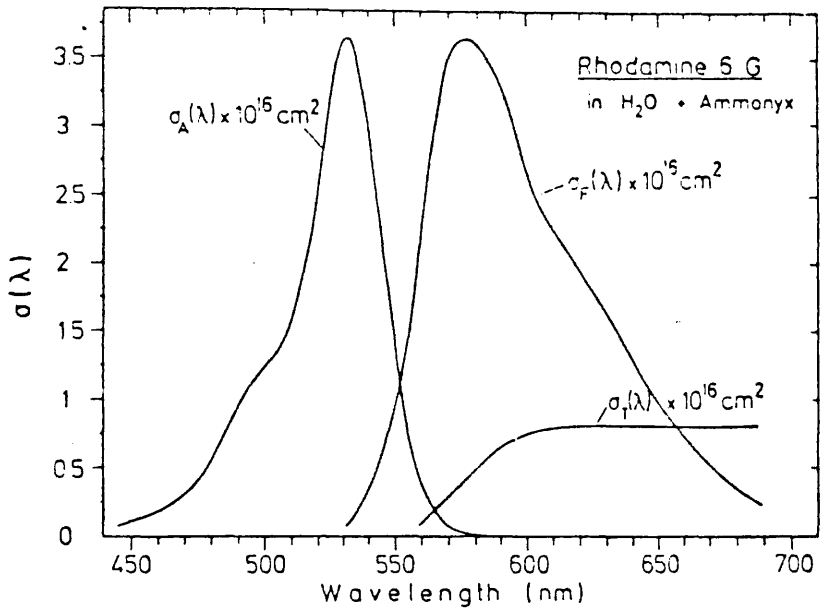

(a) Cross sections for absorption (σ_A), for fluorescence (σ_F) and for triplet absorption (σ_T) for rhodamine 6 G, dissolved in water with Ammonyx, a commercial surfactant, added.

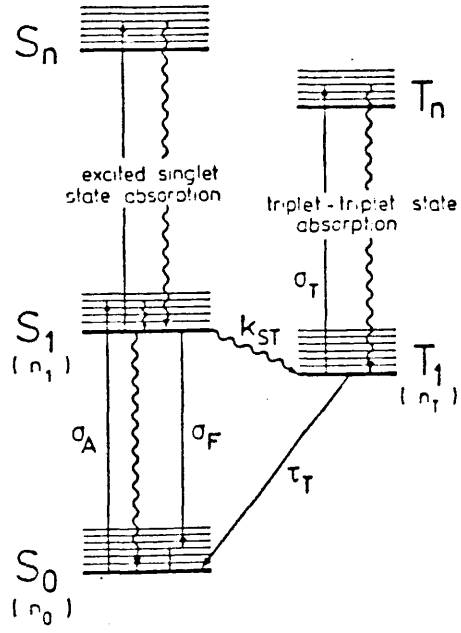

(b) Schematic energy level diagram for a typical dye molecule.

FIGURE 6.1 Various cross-sections for Rhodamine 6G (a) and schematic energy level diagram for a typical dye molecule (b).

pumping-deexcitation is then completed by another rapid thermalization to the temperature dependent vibronic distribution of the ground state S_o. The dye laser may be considered to be four level system because the terminal state of the laser transition is essentially empty and hence it is very efficient. However, there are losses associated with this laser. The gain coefficient of the dye laser medium at a wavelength λ (in the absence of external losses) is defined as (6.8)

$$g(\lambda) = \sigma_E(\lambda)n_1 - \sigma_A(\lambda)n_o - \sigma_F(\lambda)n_1 - \sigma_T(\lambda)n_T \qquad (6.1)$$

where n_o, n_1 and n_T are the molecular population densities (molecules/cm^3) in the states S_o, S_1 and T_1 respectively; σ_F, σ_A, σ_E and σ_T are respectively the stimulated emission cross-section, the $S_o \rightarrow S_1/S_n$ cross-section, S_1-S_n absorption cross-section and the triplet-triplet (T_1-T_n) absorption cross-section. The three absorption processes (given by the last three terms in (6.1)) which lead to a decrease in gain at a given wavelength, are ground state absorption, excited singlet state absorption and triplet-triplet absorption.

Ground state absorption at lasing wavelengths is due to the partial overlap of the fluorescence and absorption spectrum of the dye. This absorption arises from the molecular population in the higher vibrational-rotational levels of S_o. The effect of ground state absorption is to move the peak of the gain to slightly longer wavelengths and away from the fluoresence peak and is most noticeable for those dyes with small Stokes shifts (eg. Xanthene dyes). Although ground state absorption affects the spectral distribution of the gain the absorbed photons are

not lost to the lasing process because they repump the dye molecules and hence increase the inversion.

Excited state absorption (ESA) is the process whereby molecules in S_1 absorb pump or fluorescence photons and are excited to higher singlet states S_n. Rapid radiationless decay from S_n by a cascade of internal conversion and vibrational relaxation processes brings the molecule back to the lowest vibrational level of S_1. Therefore ESA does not in general cause an inversion loss unless molecular decomposition takes place from S_n. However it does lower the gain and if $\sigma_E < \sigma_F$ lasing is not possible. Also because the S_n-S_1 transition is radiationless it causes a heating of the dye. However in general ESA is only a problem in high power lasers and it does not greatly affect the output of NLPDL's.

Triplet state absorption occurs because some molecules cross from the singlet system to the triplet system. The transition T_1-S_o is spin forbidden and the triplet state lifetime τ_T is relatively long (10^{-7}-10^{-3}s range), depending on the environment of the dye. Hence any molecules which cross from S_1-T_1, become trapped, cannot take part in laser action and because of the relatively large value of σ_T at the lasing wavelengths become highly absorbing. Because of the short pulse width of nitrogen lasers problems with the triplet system do not arise. This is because the intersystem crossing rate K_{ST} from S_1 to T_1, has a value of about 2×10^{-7} s^{-1} so that for pumping lasers with pulse durations much less than $1/K_{ST}$ the triplet state effects become negligible. Hence the short pulsewidth, high peak power

and short wavelength make the nitrogen laser very suitable for pumping dye lasers.

6.3 NITROGEN LASER PUMPED DYE LASER CONFIGURATIONS

The first tuned nitrogen laser pumped dye lasers consisted simply of a dye cell with a grating in Littrow configuration on one side and an uncoated flat or wedge on the other side for output coupling. Because of the beam geometry of most nitrogen lasers a transverse pumping arrangement was usually used and the power density was increased by focusing with a suitable lens. A diffraction grating in Littrow configuration has an angular dispersion given by (6.9)

$$\frac{d\beta}{d\lambda} = \frac{2 \tan \beta}{\lambda} \qquad (6.2)$$

where β is the angle of diffraction (which equals the angle of incidence). If $\delta\theta$ is the divergence of the beam incident on the grating, then the single pass (passive) linewidth of a Littrow grating tuned resonator is (6.9)

$$\delta\lambda = \frac{\delta\theta}{d\beta/d\lambda} \qquad (6.3)$$

The usual way to reduce $\delta\lambda$ is to use a highly dispersive grating (a grating used at large angles of diffraction) and simultaneously reduce the beam divergence by expanding the beam incident on the grating. Beam expansion by a ratio M decreases the beam divergence $\delta\theta$ by the same factor M, so that

$$\delta\lambda = \frac{\delta\theta}{M} \frac{1}{d\beta/d\lambda} \qquad (6.4)$$

or equivalently, the angular dispersion of the beam expander-grating combination in autocollimation (ie. at the exit of the beam expander where the beam contracts to its original size) is M times the angular dispersion of the grating used alone,

$$\delta\lambda = \frac{\delta\theta}{M(d\beta/d\lambda)} \qquad (6.5)$$

This is true for all beam expander-dispersive element combinations used in autocollimation. The beam expander can itself be the main dispersive element, as discussed later.

One of the earliest designs used a telescope in reverse as the beam expander and is due to Hansch (6.10). This design is shown in figure 6.2 (a). Without an etalon Hansch produced an output with a linewidth of 3×10^{-3}nm at 600nm with an efficiency of about 10%. Inclusion of the etalon reduced the linewidth to less than 4×10^{-4}nm but the efficiency dropped to 1 or 2%. This design has proved very successful and has been used widely but it does have some major drawbacks. Because the beam is expanded in two dimensions the grating alignment is very critical and it must be precisely rotated to keep the grating rulings perpendicular to the laser axis. The telescope needs to be of high quality and achromatic making it expensive. The laser is particularly difficult to align and there is only a little polarization selection is the cavity without the addition of a crystal polarizer. Finally the cavity is long (typically 40cm) and the light does not have time to make many passes through the

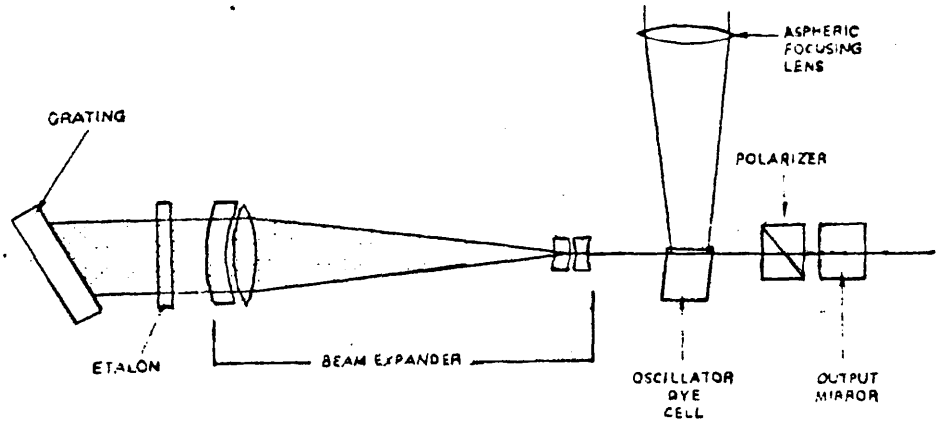

(a)

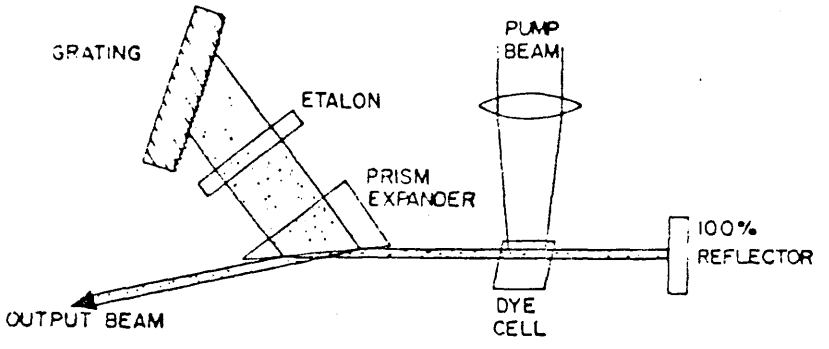

(b)

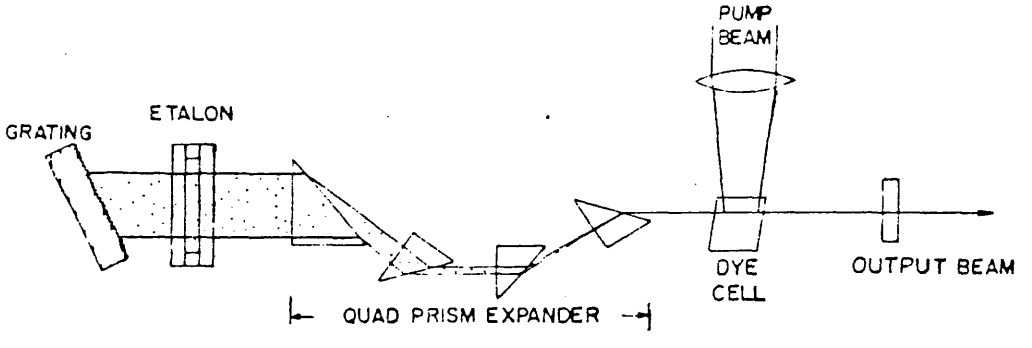

(c)

FIGURE 6.2 Some resonator designs of NLPDL's.

amplifying medium; this is particularly severe for NLPDL's which have pulsewidths of less than 10ns. For efficient nitrogen laser pumping of a dye laser the two way transit time of the dye laser must be much less than the nitrogen laser pulsewidth (Lawler et al. (6.11)). There is usually a trade off between linewidth and conversion efficiency because insertion of linewidth reducing elements always increases the length of the cavity. Also the long cavity causes problems because there is a long delay before the spectrally filtered light is returned to the dye cell for amplification, hence it is possible for superradiance to occur (saturation of the dye by unfiltered, amplified, spontaeous emission).

The first design proposed to circumvent these problems was by Stokes et al. (6.4) and used a prism with an incident angle of 40° as a beam expander. This design suffered from high losses from the reflection at the incident face on the prism and the low dispersion. These problems were overcome by Hanna et al. (6.12) who increased the incident angle on the prism to 89° (to provide high magnification) and replaced the uncoated output coupler with a total reflector. The output was then taken from the reflection from the incident face of the prism. The design is shown in figure 6.2 (b). Although this design considerably shortened the cavity another problem arose, that of a large superradiant background. This is because the total reflector feeds all of the on-axis dye fluorescence directly back into the dye cell for amplification and coupling out of the cavity off the prism. In addition the prisms are not achromatic and provide dispersion themselves. These problems were solved by Klauminzer

(6.13) who used an achromatic quadruple prism beam expander, his design is shown in figure 6.2 (c).

Littman and Metcalf (6.14) and Shoshan and Oppenheim (6.15) independently proposed the use of a grazing incidience grating both for beam expansion and angular dispersion. A beam incident on a grating at an angle of incidence α , approaching 90°, is diffracted at an angle β and expanded in the plane of incidence by the factor (6.16)

$$M = \frac{\cos\beta}{\cos\alpha} \qquad (6.6).$$

M is plotted in figure 6.3 for various angles of incidence for an 1800 lines/millimetre grating (blaze angle 26° 45') used in first order at 632.8 nanometres (from Wilson et al (6.17)). Also shown is the theoretical first order efficiency of the grating for light polarized with the electric vector perpendicular to the grating grooves, w_o is the incident beam width radius. Resonators using grazing incidence gratings are shown in figure 6.4 (a) and (b). The grazing incidence grating expander has a large angular dispersion and it can be used as the sole dispersive element for narrowband operation as in figure 6.4 (a) or it can be used in combination with a second grating mounted in the Littrow configuration for further spectral narrowing as shown in figure 6.4 (b). Tuning is achieved by rotating the mirror M_2 or the Littrow grating G_2. The angular dispersion of the mirror-grazing incidence grating combination (in autocollimation) is (6.8)

$$\frac{d\alpha}{d\lambda} = M\frac{2n_1}{d_1\cos\beta} = \frac{2n_1}{d_1\cos\alpha} \qquad (6.7)$$

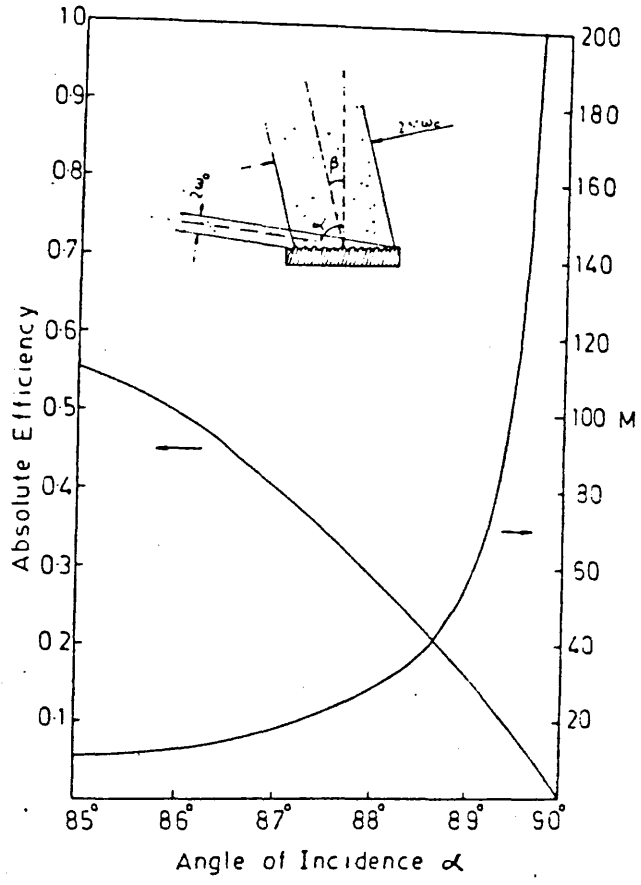

FIGURE 6.3 Beam magnification and theoretical first order efficiency of an 1800 lines/mm grating as a function of angle. (from Wilson et al. (6.17)).

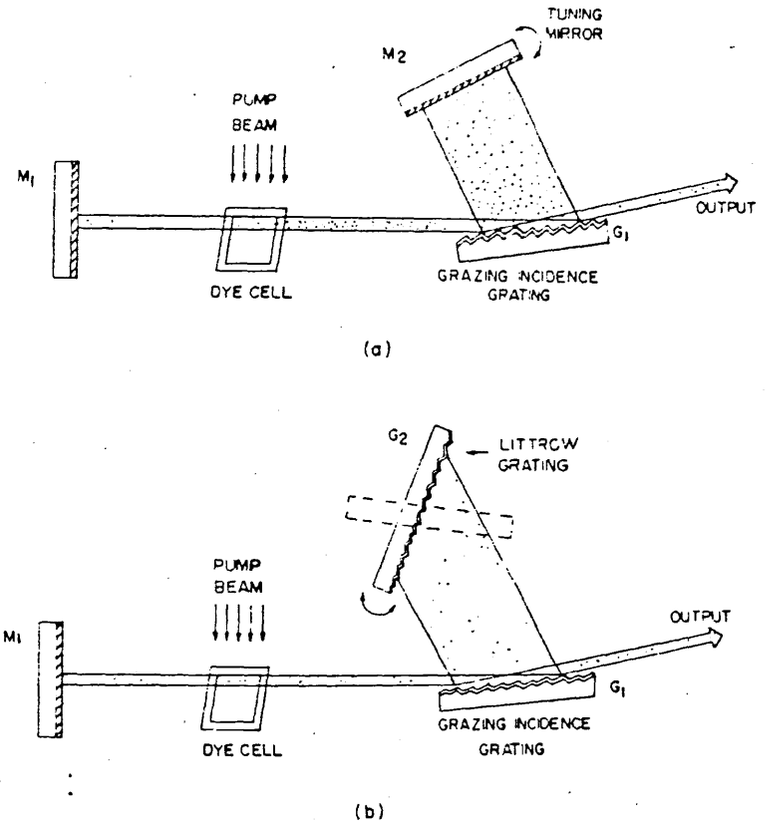

FIGURE 6.4 Schematic diagram of grazing incidence grating resonators using a grating-mirror combination (a) and using a grating-grating combination (b).

where n_1 and d_1, are the order of diffraction and groove spacing respectively for G_1. Hence according to equation 6.3 the single pass linewidth of the cavity is

$$\delta\lambda = \frac{d_1 \cos\alpha}{n_1} \delta\theta \qquad (6.8)$$

For the double grating combination the total angular dispersion (in autocollimation) is (6.2)

$$\frac{d\alpha}{d\lambda} = \frac{2n_1}{d_1 \cos\alpha} \pm M \frac{n_2}{d_2 \cos\beta_2} \qquad (6.9)$$

where the subscript 2 denotes the parameters of the Littrow grating G_2. The dispersions are additive when the Littrow grating is in the position indicated by the solid line in figure 6.4 (b).

The main advantages of grazing incidence grating resonators are that narrow linewidths are achieved without the use of a Fabry-Perot etalon and that the cavity is short. By using very short cavities and hence expanding the mode spacing single mode operation of this resonator design has been readily achieved (6.18-6.23).

For most efficient operation M_1 is a total reflector and the zero order reflection from the grating is used for output coupling. However with this configuration the amount of background amplified spontaneous emission (ASE) is quite large but can be reduced by insertion of a horizontal polarizer between M and the dye cell (6.22). Alternatively mirror M_1 can be replaced by a quartz wedge with the output coupling taken through this element and in this way the ASE background is

reduced substantially (6.24), but the conversion effciency of the pump energy is also reduced. As seen from figure 6.3 the single pass efficiency of gratings at large angles of incidence is quite small so an increase in efficiency can be achieved by using a prism(s) for pre-expansion (6.25 and 6.26).

The low cost, short cavity length, reduced linewidth and simplicity of alignment make the grazing incidence grating configuration useful for many applications requiring NLPDL's.

6.4 REVIEW OF TUNABLE TWO WAVELENGTH NITROGEN LASER PUMPED DYE LASERS

Tunable two wavelength lasers have many applications, eg. sum or difference frequency generation (6.27, 6.28), excited state spectroscopy, two photon spectroscopy and differential absorption (6.29, 6.30). Accordingly many of the cavity configurations described previously have been adapted for two wavelength operation. The simple configuration of a partially transmitting mirror, dye cell and Littrow grating has been operated simultaneously at two wavelengths by adding a second grating and aligning this so that the zero order reflection from the first grating is incident at the Littrow angle (6.31) or such that it is at the Littrow angle for a spatially separated beam (6.30, 6.32, 6.33). The spatial separation was achieved by using a simple beam splitter (6.32) and by using the reflected beam from a Glan laser prism (6.30, 6.33), the latter arrangement producing two wavelengths with mutually orthogonal polarizations.

The 'Hansch' type dye laser has also been adapted for two wavelength operation. This was achieved by separating the beam into two components and changing the angle of incidence of one of the beams on to the Littrow grating with respect to the other beam. Lotem and Lynch (6.34) (figure 6.5 (a)) did this by inserting a wedge between the beam expander and the diffraction grating. The power ratio can be varied by translating the wedge into or out of the beam but the wavelength separation is rather limited. A similar arrangement was described by Schmidt (6.35) except that the wedge intercepted the beam in a horizontal plane. Marx et al.(6.36) reported a different system in which half of the beam was intercepted by a fully reflecting mirror after the beam expander and was then redirected onto the diffraction grating by a second mirror (figure 6.5 (b)). This system is useful in that etalons can be inserted into both beams for further spectral narrowing. Winter et al.(6.37) obtained two wavelength operation by dividing the unexpanded beam with a Glan prism and then redirecting the reflected beam into the beam expander at a slightly different angle to that of the transmitted beam by means of second Glan laser prism (see figure 6.5 (c)).

Since the first report of a NLPDL using a prism beam expander (6.4) there have been a few descriptions of cavities converted for two wavelength operation (6.38, 6.39). Nair (6.38) added a second prism-grating combination which intercepted the reflected beam from the grazing incidence face of the first. Again etalons could be inserted into each beam for further spectral narrowing. Kong and Lee (6.39) used an auxillary beam splitter to separate

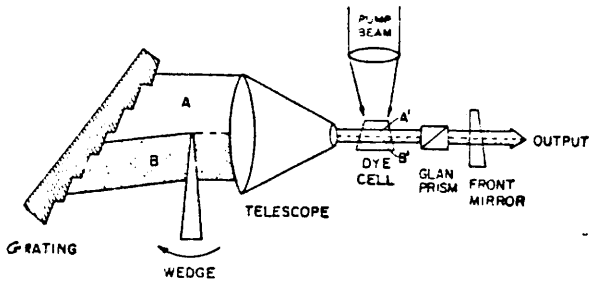

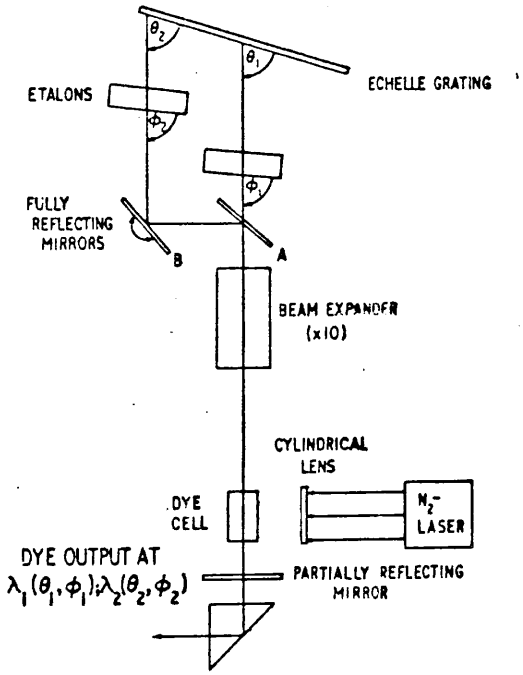

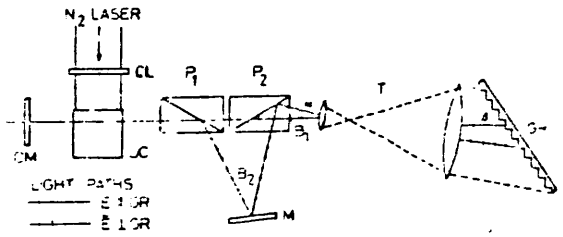

FIGURE 6.5 Schematic diagrams of two wavelength 'Hansch' type NLPDL's.

two beams and then used a prism-grating combination for each beam.

The grazing incidence grating design has proved very amenable to conversion for two wavelength operation. The first report was by Prior (6.40) who used two mirrors to reflect back different orders of diffraction from the grating (figure 6.6 (a)). Nair and Dasgupta (6.41) used a pair of grazing incidence gratings and mirrors in a similar manner to the prism system described by Nair (6.38) (figure 6.6 (b)). The element GP in the figure is a variable attentuator used for varying the power ratio. The most common way of achieving two wavelength operation of the grazing incidence grating laser is that shown in figure 6.6 (c) and was reported independently by three groups (6.42-6.44). In this system two tuning mirrors intercept different portions of the diffracted beam; the power ratio can be set at any level by varying the amount of light intercepted by each mirror.

In the reviewed and other (6.2, 6.45, 6.46) two wavelength NLPDL's there are two major drawbacks which both arise because there is only one excited region of dye. Firstly, because the dye laser is a homogeneously broadened system the lasers are subject to mode competition effects. This is well illustrated by some results published by Friesem et al. (6.31) and shown in figure 6.7. The power output at one wavelength is very dependent upon the wavelength setting of the other beam. Attempts have been made (6.34, 6.40, 6.42) to reduce the mode competition by probing distinct regions of the excited volume at each wavelength but the effects cannot be removed completely due to

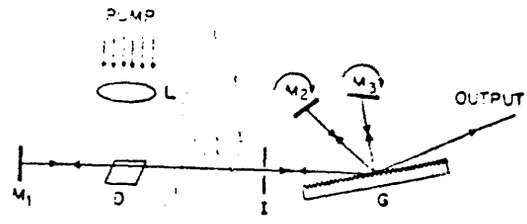

(a)

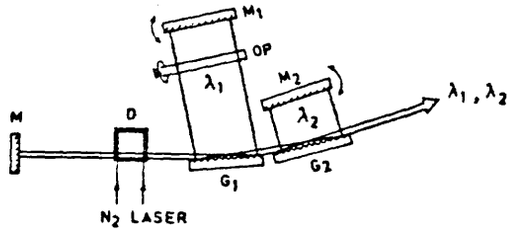

(b)

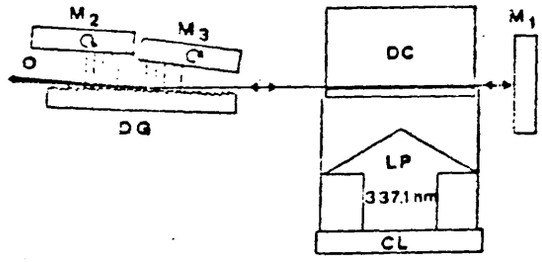

(c)

FIGURE 6.6 Schematic diagrams of two wavelength NLPDL's based on the grazing incidence resenator.

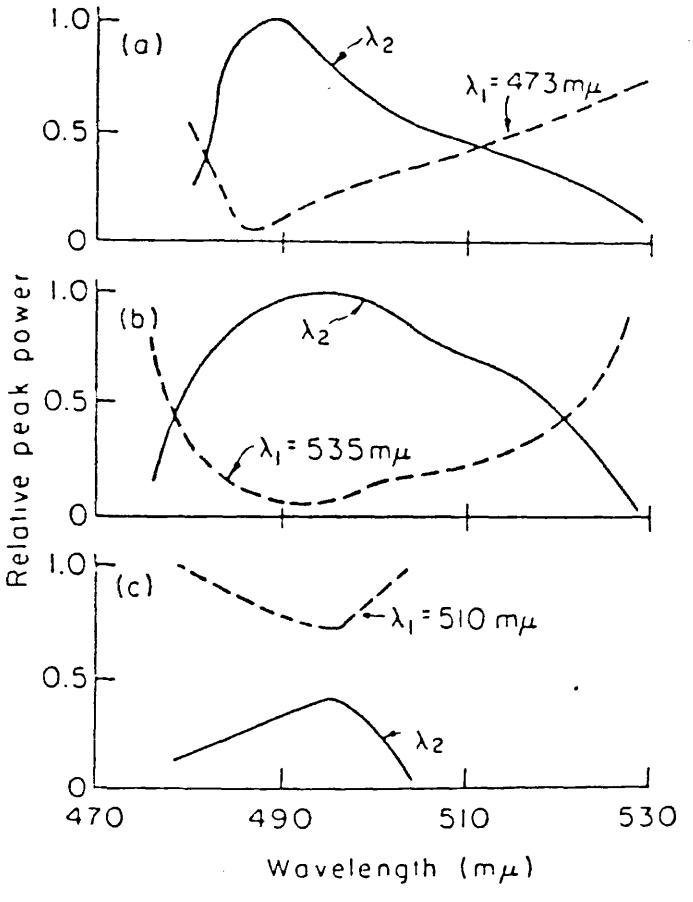

FIGURE 6.7 Gain competition effects in a two wavelength dye laser (From Friesem et al. (6.31)).

the effects of beam divergence. The second drawback is that the wavelength separation is restricted to the gain curve of the dye being used. Attempts have been made (6.43, 6.47) to extend the wavelength separation by using mixtures of dyes with some success but the number of compatible dyes and solvents is restricted and in most cases the overall pulse energy is severely reduced. In addition this technique requires critical adjustment of the dye concentrations (6.43). Another drawback of the described systems is that the polarization states of the two beams are fixed either parallel or perpendicular to each other and because the outputs are cospatial or more usually adjacent, extracavity polarizing elements can not be used for separate manipulation. Kong and Lee (6.39) were able to overcome this problem by rotating one of the their prism beam expander grating combinations about the optic axis. A further disadvantage is that in most cases the linewidths of the two beams are the same and cannot be separately varied.

6.5 CONCLUSION

The nitrogen laser pumped dye laser has been extensively studied and many cavity configurations described, culminating in the grazing incidence grating system. Most of the cavities have been adapted for two wavelength operation but they all suffer from two major drawbacks, namely mode competition and restricted wavelength separation. To overcome these drawbacks a novel pumping arrangement was conceived and a two wavelength laser based on the grazing incidence grating principle was designed and built.

CHAPTER VII

SIMULTANEOUS TWO WAVELENGTH DYE LASER

7.1 DESCRIPTION

This laser is the same as that described in reference 7.1. It utilizes the polarized output of the oscillator-amplifier nitrogen laser system described previously. The pumping arrangement used for two wavelength operation is shown in figure 7.1. The plain polarized pumping beam, PPB with its azimuth controlled by a half-wave plate, HWP, is divided by a birefringent beamsplitter, BBS, and focused by a lens, L, onto the dye cell, DC. With this arrangement two excited regions vertically separated by a few millimetres are produced in the dye. For operation in one dye the BBS is a quartz Rochon prism giving a fixed separation of about 4mm. For operation with two dyes the BBS is half of a calcite polarizing cube and the separation varies according to the position of the cube but was usually set at about 15mm. The focusing lens is not critical, for the results presented here it consisted of a combination of cylindrical quartz lenses with 22 and 30cm focal lengths for the vertical and horizontal planes respectively. This combination produces a line of about 15mm length in the dye cell which is a standard 20mm path length quartz fluorimeter cell. By rotating the half-wave plate the relative intensities of the two pumping beams can be accurately controlled, hence providing intensity control of the two dye laser output beams.

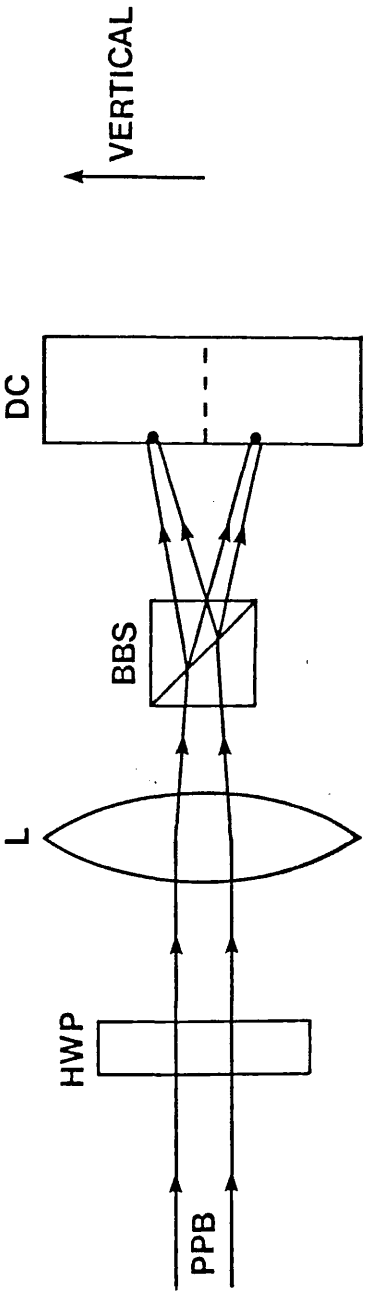

FIGURE 7.1 Schematic in a vertical plane of the pumping arrangement.

If this intensity control is not required the half-wave plate can be omitted and an unpolarized pumping beam used.

The dye laser cavity for two wavelength narrow linewidth operation is shown in figure 7.2. The resonator consists of a mirror, M_1, a diffraction grating, G, and two more mirrors, M_2 and M_3. The vertically displaced pumping beams, VDPB, which are incident into the dye cell, DC, produce a lower, LB, and upper, UB, output beam from the dye and after expansion by G these are intercepted by M_2 and M_3 respectively. Mirrors M_2 and M_3 are front aluminized glass flats and are 7cm wide, whilst M_1 is an uncoated glass flat 2.54cm in diameter. The dye cell is as described previously and is tilted at angle of 10° with respect to the optic axis so as to avoid reflecting spectrally unfiltered light from the cell walls back into the excited dye. When operating with a single dye a magnetic stirrer is used. The diffraction grating is oriented for grazing incidence operation (angle of incidence about 89°) and is a 2400 lines/mm holographic grating, 50mm wide and 25mm high. It produces one diffracted order for each incident beam. M_2 is mounted in a simple clamp whilst M_1, M_2 and G are held in adjustable kinematic mounts.

The linewidth of both beams can be increased by decreasing the angle of incidence on the grating, hence decreasing the expansion produced. To operate the two wavelengths with different linewidths the arrangement of figure 7.3 can be used. The mirror M_4 intercepts the upper beam and directs it via

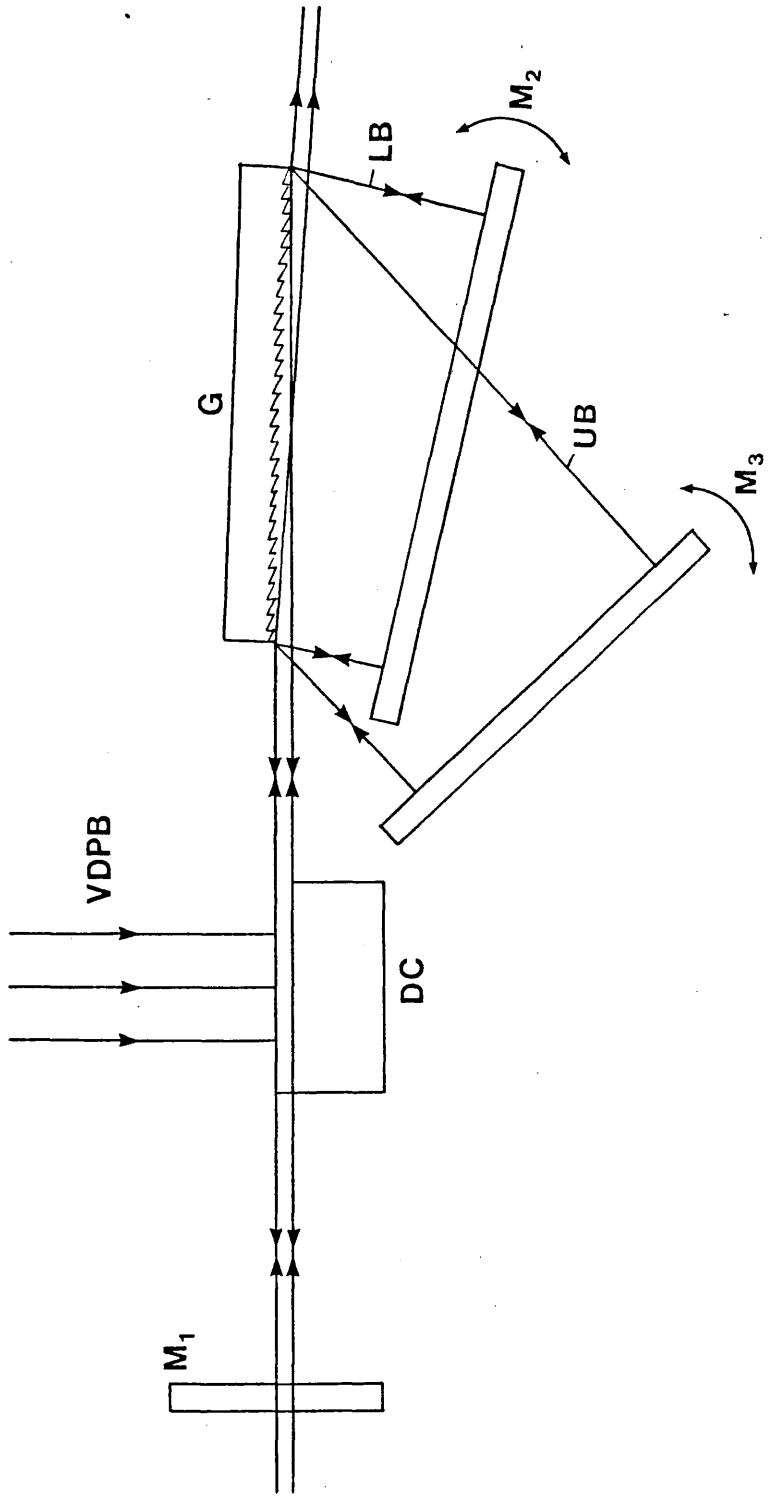

FIGURE 7.2 Schematic diagram in a horizontal plane of the two wavelength dye laser.

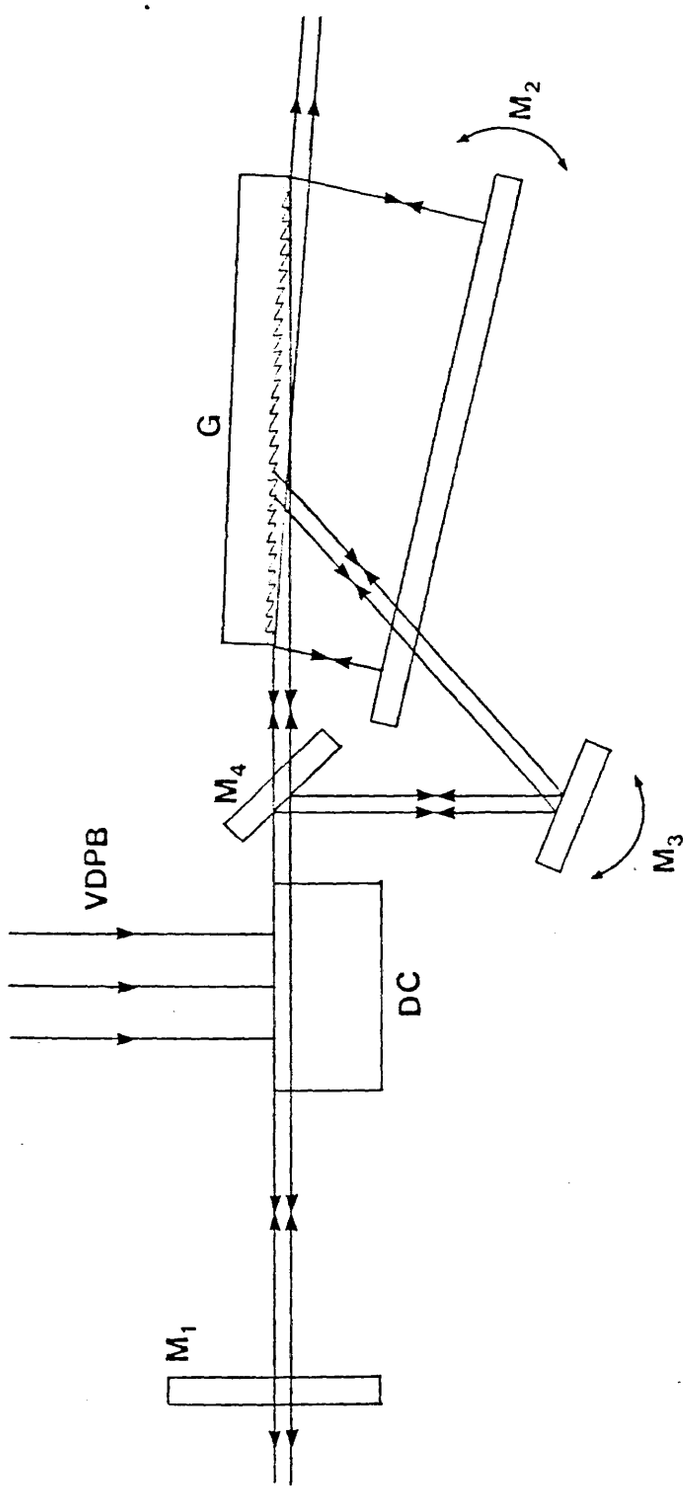

FIGURE 7.3 Schematic diagram in a horizontal plane of the two wavelength dye laser.

M_3 onto G at an angle controlled by rotation of M_3. In this case the grating is being used in the Littrow configuration and the upper beam will have a broader linewidth than the lower. To take this further M_3 can be rotated to form an untuned cavity with M_1 and M_4 and the upper beam then produces broadband emission.

7.2 OPERATION

The alignment of the cavity is straightforward. M_1 is aligned to produced two bright return spots and the dye cell is translated so that these spots are incident on the centre of G. The grating is then rotated so that the spots completely fill it. M_2 is then placed in position to intercept the lower diffracted beam and G is then adjusted in the vertical plane until lasing occurs. M_3 is then placed in position and adjusted in the vertical plane until lasing occurs in the upper beam. M_2 and M_3 are then rotated to produce the desired output wavelengths. There is no mode competition between the two beams because they use different active media and though there is only one dispersive element they are independently tunable. The output beams are linearly polarized in the horizontal plane and have a small divergence (3-4 milliradians). The energy of the beams was measured by alternately collecting all the radiation from each beam using a 20cm focal length glass lens and directing it onto the calibrated Molectron pyroelectric joulemeter. Using a single dye, 5×10^{-3} M R6G in ethanol, the output was measured at 25

μJ in each beam (unpolarized pump beam, energy about 1.2mJ). Without the birefringent beam splitter only a single wavelength is generated and with the same pump beam the output energy was 80μJ. The discrepancy is due to losses in the beam splitter and to the fact that the threshold energy has to be exceeded in two regions in the former case. Changing to the arrangement shown in figure 7.3 the energy in the lower beam (grazing incidence) was again about 25μJ whilst the energy in the upper beam (Littrow incidence) was 52μJ. By rotating the grating so that both beams were incident at the Littrow angle (M_4 removed) the energy in each beam was 60μJ with 140μJ recorded for single wavelength operation.

Using the polarized pump beam (energy about 0.8mJ) the effect of the half wave plate was examined and figure 7.4 shows a plot of the output energy of the two beams as a function of the angular setting of the half-wave plate. There is a slight asymmetry in the figure which is probably due to a combination of a higher threshold energy in the upper beam which has a slightly longer cavity length (15.5cm as opposed to 13.5cm) and a possible error in the zero setting of the half wave plate. The zero was found by noting the angles at which lasing action started in one beam, and then positioning the half wave plate at an angle midway between these two. The accuracy of setting and reading the angle of the half wave plate is about $\pm$ 0.5°. The points on the figure represent an average of readings taken whilst rotating the half-wave plate in opposite directions.

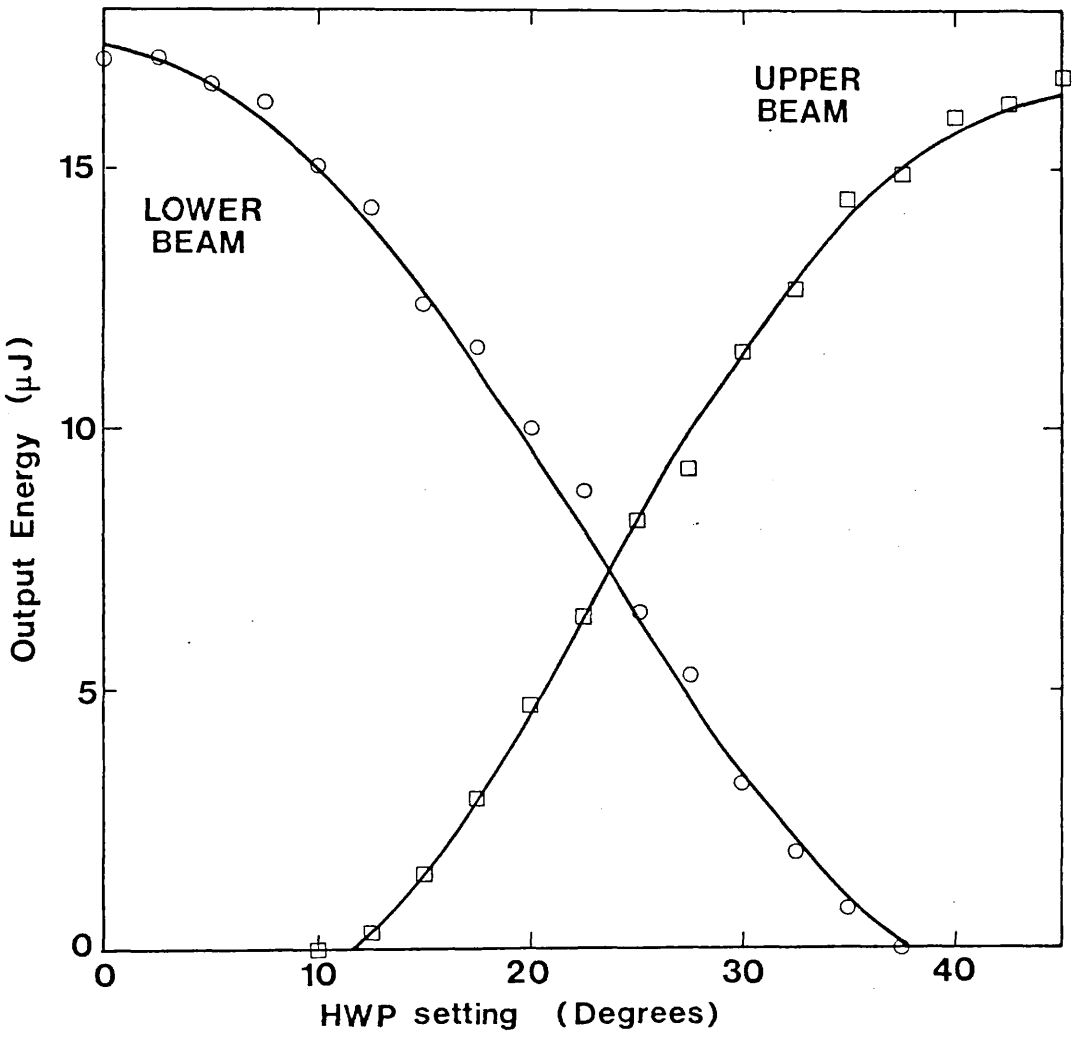

FIGURE 7.4 Variation of the output pulse energy in the upper and lower beam as a function of the angular setting of the half-wave plate.

For operation with two dyes the same dye cell was used with one dye floating on top of the other. This requires immiscible solvents; p-dioxane is suitable for the lower dye with alcohol for the upper. There is a tendency of the dyes to mix when pouring the upper one into the cell and also the dyes slowly diffuse into each other. This tendency to mix and the rate of diffusion can be greatly reduced by floating a piece of Mylar, which is a close fit to the dye cell, on top of the lower dye. Using this system it is possible to use a variety of dyes, eg. the scintillators for the lower and the Xanthenes for the upper. Using DPS and Rhodamine B a wavelength separation of more than 200nm was obtained. By utilizing a dual compartment dye cell any combination of dyes is possible.

The output pulse shape produced by this laser is shown in figure 7.5(a). The dye used in this case was Courmarin 460 10^{-2}M in ethanol. The FWHM is 6ns in regions of high gain (N_2 laser FWHM 8ns) and decreases in regions of lower gain.

Although in this particular figure much of the detail is lost in the 12 pulse superposition it is apparent that the output is partially self-modelocked. The time separation of the peaks is 1ns which is in good agreement with that expected from the cavity length (13.5cm). A similar but less noticeable effect was reported by Borgstrom (7.2) in a 'Hansch' type laser. It is not possible to ascertain the degree of modelocking due to risetime effects of the oscilloscope - photodiode combination. The degree of modelocking could be greatly reduced by

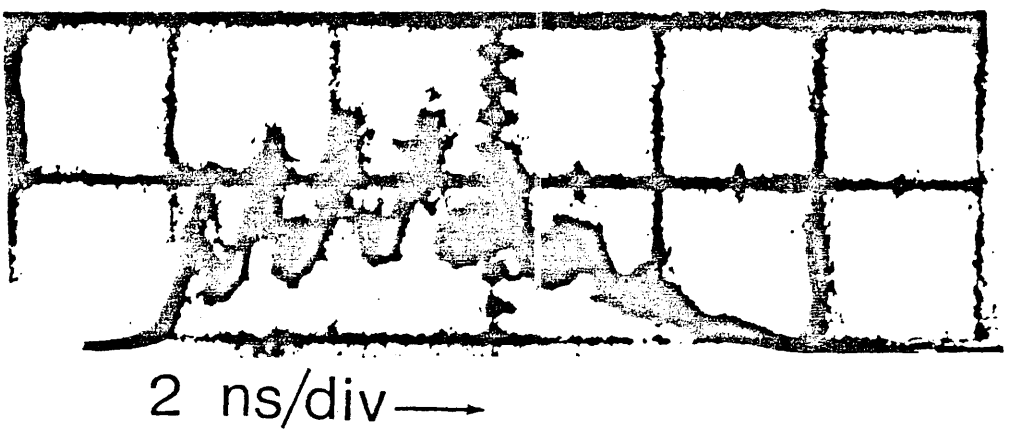

(a)

Angle of incidence 89°.

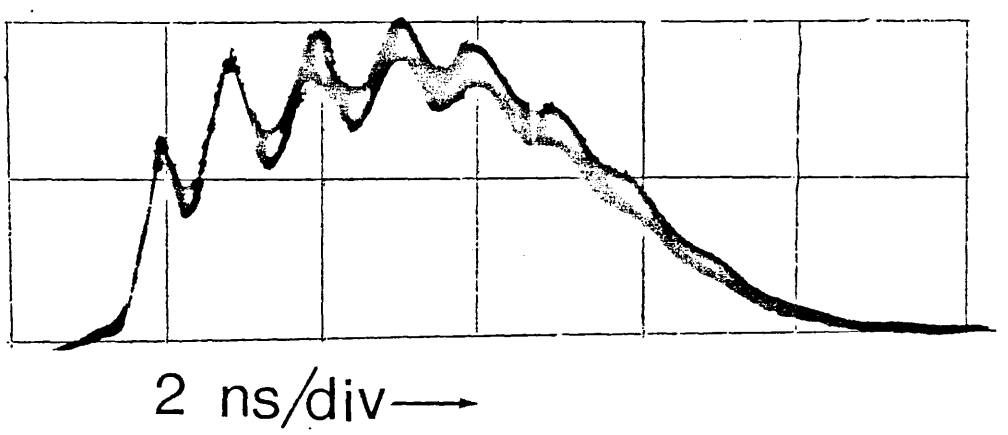

(b)

Angle of incidence approx. 70°.

FIGURE 7.5 Output pulse shapes of the grazing incidence grating dye laser.

decreasing the angle of incidence on the grating as shown by figure 7.5 (b) where the angle of incidence was 70^{o}. The modelocking is unaffected by the input power, repetition rate or the type of dye. It is certainly good confirmation that axial modes exist in the NLPDL as reported by Pease and Pearson (7.3).

7.3 SUMMARY

A novel design for a two wavelength nitrogen laser pumped dye laser has been presented. This laser has three major advantages over other similar lasers: firstly, there is no mode competition, secondly, the wavelength separation is unrestricted and thirdly, the linewidths of the two beams are independently variable. Although the output beams are separated by a few millimetres this is not a disadvantage because a focused crossover can easily be produced by using a concave mirror or an achromatic lens. Indeed in some cases the beam separation will be an advantage, eg. sum or difference frequency generation which utilise angle tuning. In addition the non-cospatial nature avoids non-linear interactions where they are not wanted. The slight beam separation will also allow the insertion of a half-wave plate into one of the beams so facilitating any relative polarization orientation.

APPENDIX I

Experimental Techniques.

The general experimental arrangement used throughout this work is shown in figure A1.1. The Woods glass was used to remove any IR output (cut off approx. 400nm) whilst the uncalibrated attenuator was used to ensure that the photodiode was never saturated. The anode of the photodiode was raised to a voltage of +2.5kV using a stabilized power supply. R_l and C were integral components of the photodiode. For pulsewidth measurements the biplanar vacuum photodiode was an ITL model mounted in an impedance matched housing. This was then connected directly to a Tektronix 519 oscilloscope which had the same 125 ohm impedance. For pulse energy and average power measurements the output of the photodiode was integrated using a capacitor and resistor (as shown in Figure A1.1). The values of these components were chosen to be 2 μF and 200 kΩ giving a time constant of 0.4 seconds. When the ITL photodiode was tested with this circuit it was found to be unuseable because the signal was swamped by the dark current. Hence an EMI biplanar vacuum photodiode was used instead and this had a dark current of a few nanoamps. The integrating capacitor and resistor were mounted directly onto the photocathode pin because this photodiode was not in an impedance matched housing. The voltmeter used for monitoring the output of the integrator was either a Dymar microvoltmeter with a mechanical meter or a Solartron digital voltmeter. The jitter produced by the lasers was usually about 5% and the reading was estimated to be in the middle of this range. The EMI photodiode had an active cathode diameter of 2 inches so that no focusing of the beam was necessary.

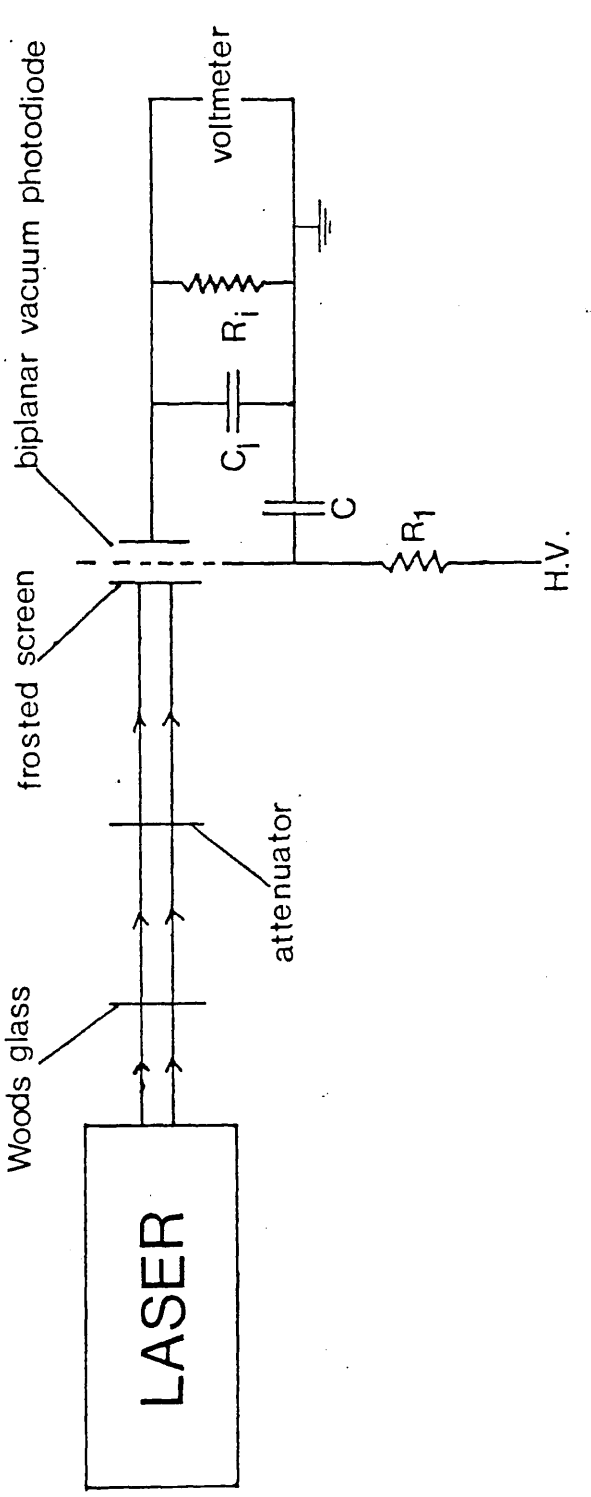

FIGURE AI.1 Experimental arrangement used for the measurement of pulse energy and average power of the nitrogen lasers.

The largest errors arose from the gauges monitoring the pressure of the lasers. These were 0-100 and 0-760 torr aneroid type gauges and for the 0-100 gauge the best resolution was $\pm$ 1 torr whilst for the 0-760 one it was $\pm$ 5 torr. In addition both gauges had zero offsets and they were assumed to remain constant at all pressures but the actual values could only be checked up to 30 torr using a mercury manometer. For all pressure measurements an average of two or four readings was taken with the pressure being alternately increased and then decreased. The applied voltage was measured using the meter on the high voltage power supply, which had a resolution of $\pm$ 0.5kV. The accuracy was checked using a Tektronix P6015 probe and an oscilloscope; it was found to be at least as good as the probe oscilloscope combination resolution ($\pm$ 0.5kV). The reptition rate was measured by observing the synchronization pulse provided by the trigger unit on an oscilloscope. This provided a variable resolution depending on the timebase of the scope and the actual repetition rate.

Finally for all measurements the lasers were run for a sufficient time to reach thermal equilibrium and it was ensured that the gas supply was at high level throughout the measurements.

The error bars shown on some graphs have been included to show the scatter of the points about the line. The size of the bars was calculated as the standard deviation of the difference between the actual points and the representative points on the line.

APPENDIX II

Photographs of Equipment.

P1 MkIII laser. This photograph shows an elevated side view of the MkIII laser when operated with a capacitor transfer circuit. The large capacitors in the foreground are the storage capacitors whilst the stack of smaller ones comprise the preionizing capacitor. The nearest electrode is adjustable and the screws securing this electrode to its mount can be seen in their grooves. Also visible is the sealing 'O' ring rubber and the inductively constructed resistor connected across the electrodes. Mirrors are mounted in the perspex holders at the ends of the laser.

P2 MkII laser. This photograph shows an elevated corner view of the MkII laser. The larger capacitors are the storage capacitors. The spark gap can be seen mounted centrally on the high voltage bar connecting the storage capacitors. The large amount of gas tubing is for both this laser and the MkIII laser when it is in position as an oscillator. The beam steering optics for the MOPA system would be fitted at the far end and the oscillator (in position 2) would be attached to the high voltage bar in the space in the perspex insulation shown in the foreground.

P3 Beam steering optics for the MOPA system.

P4 Overhead view of the two wavelength dye laser. The common output mirror is at the top left of the table and the grating at the

top right. The dye cell is located between them. The tuning mirrors can be seen below and slightly to the left of the grating. The large base protruding on the left contains the motor for the magnetic stirrer. The size of the table is 14 x 12cm^2.

P5 Elevated corner view of the two wavelength dye laser. The photograph clearly shows the tilted angle of the dye cell. The white disc is a step down pulley for the elastic band connecting the motor and the stirrer.

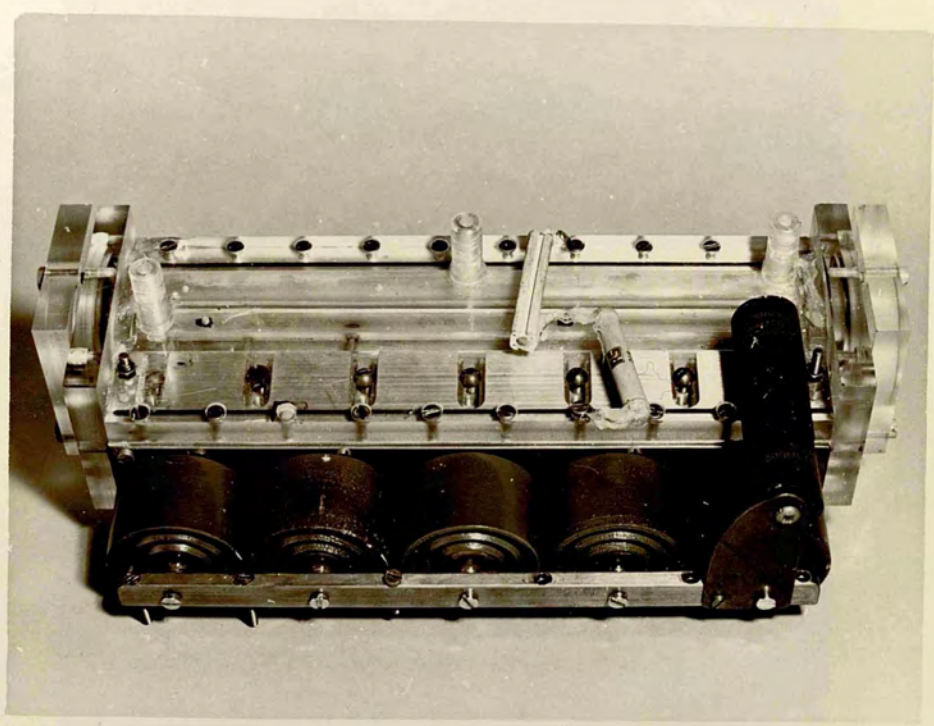

P1

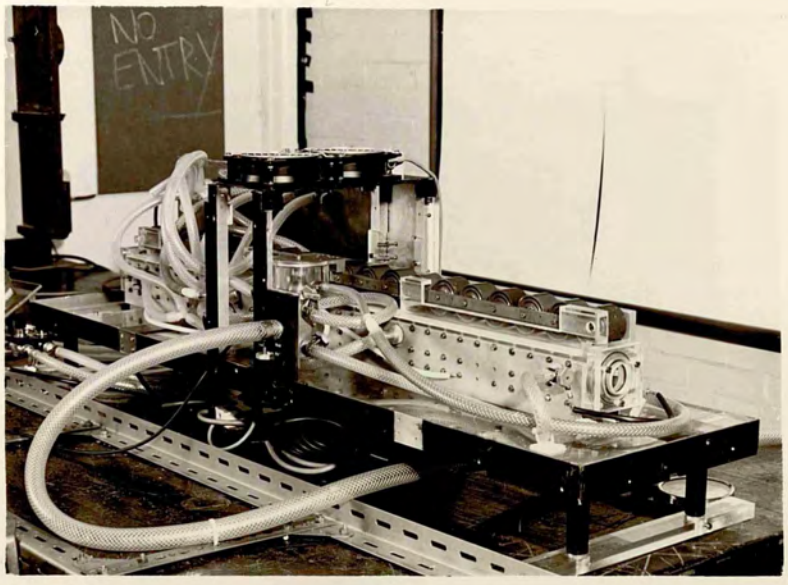

P_2

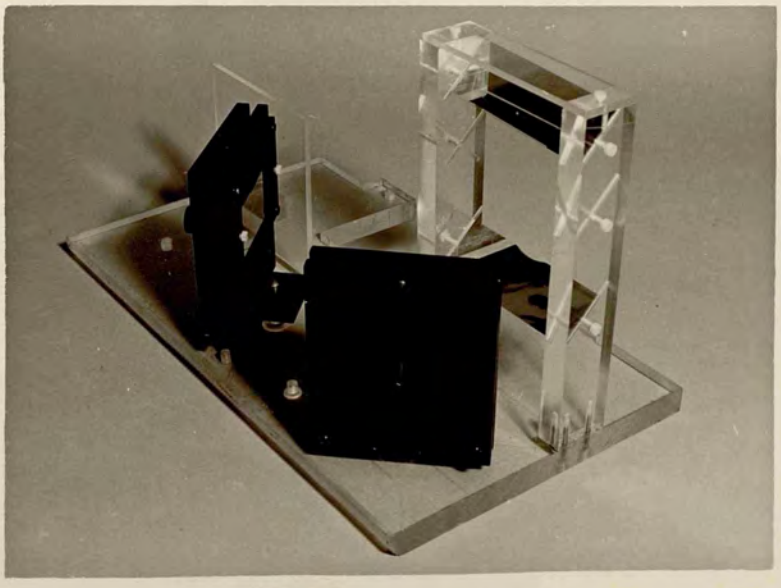

P_3

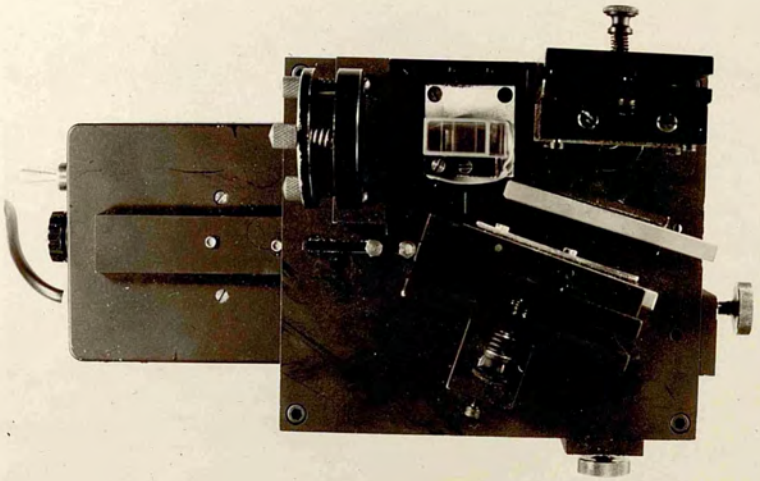

P_4

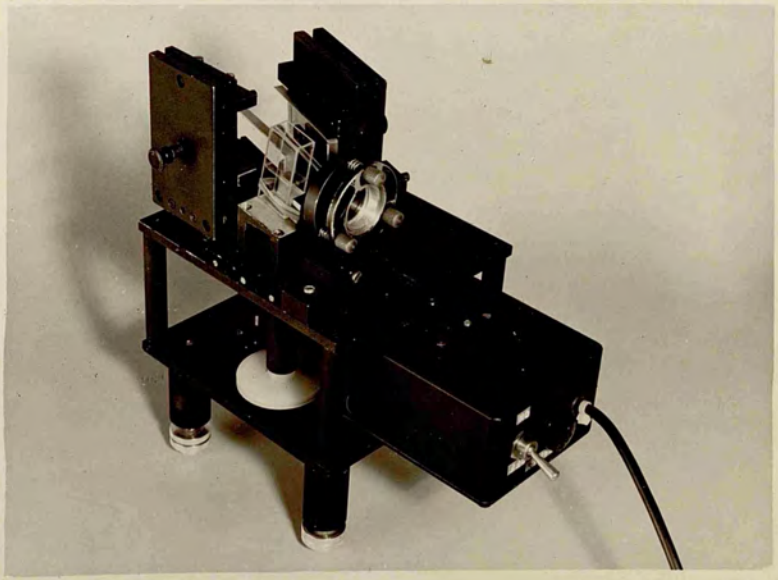

P_5

REFERENCES

CHAPTER I

1.1 J.H. Parks, D. Ramachandra Rao and A. Javan. Appl. Phys. Lett. 13, 142 (1963).

1.2 K.H. Wagner. Z. Naturforschung 19a, 716 (1974).

1.3 J.C. McCallum, W.R. Jarmain and R.W. Nicholls, York University CRESS Spectroscopic Rep. No 3 (1972).

1.4 D.C. Cartwright, Phys. Rev. A 2, 1331 (1970).

1.5 D.J. Burns, F.R. Simpson and J.W. McConkey. J. Phys. B 2, 52 (1969).

1.6 W.A. Fitzsimmons, L.W. Anderson, C.E. Riedhauser and J.M. Vrtilek. IEEE J. Quant. Electron. QE-12, 624 (1976).

1.7 A.W. Ali, A. C. Kolb and A.D. Anderson. Appl. Opt. 6, 2115 (1967).

1.8 E.T. Gerry. Appl. Phys. Lett. 7, 6 (1965).

1.9 A.W. Ali. Appl. Opt. 8, 993 (1969).

1.10 P. Richter, J.D. Kimel and G.C. Moulton. Appl. Opt. 15, 756 (1976).

1.11 P. Richter, J.D. Kimel and G.C. Moulton. Appl. Opt. 1-5, 1117 (1976).

1.12 H.G. Heard. Nature 200, 667 (1963).

1.13 O. Judd. IEEE. J. of Quant. Electron. Q.E.-12, 78 (1976).

1.14 L.A. Newman and J.A. DeTemple. J. of Appl. Phys. 47, 1912 (1976).

1.15 S.A. Borgstrom. Opt. Comm. 11, 105 (1974).

1.16 W.W. Wladimiroff and H.E.B. Andersson. J. Phys E. 10, 361 (1977).

1.17 D.A. Leonard. Appl. Phys. Lett. 7, 4 (1965).

1.18 I. Nagata and Y. Kimura. J. Phys. E 6, 1193 (1973).

1.19 C.P.Wang. Rev. Sci. Instrum. 47, 92 (1976).

1.20 A.J. Schwab and F.W. Hollinger. IEEE J. of Quant. Electron. QE-12, 183 (1976).

1.21 V.A.Bonch-Bruevich, Y.K.Dolgikh and A.A.Timokhin. Sov. J. Opt. Tech. 47 212 (1980).

1.22 J.D. Shipman. Appl. Phys. Lett. 10, 3 (1967).

1.23 D. Basting, F.P. Schafer and B. Steyer. Opto.Electron. 4, 43 (1972).

1.24 H.M. von Bergmann and V. Hasson. J. Phys. E. 9, 982 (1976).

1.25 S.A Borgstrom Optics Comm. 11, 105 (1974)

1.26 H. Salzmann and H. Strohwald. Opt. Comm. 12, 370 (1974).

1.27 M. Feldman, P. Lebow, F. Raab and H. Metcalf. Appl. Opt. 17, 774 (1978).

1.28 B.W. Woodward, V.J. Ehlers and W.C.Lineberger. Rev. Sci. Instrum. 44, 882 (1973).

1.29 M. Geller, D.E. Altman and T.A. Detemple. Appl. Opt. 7, 2232 (1968).

1.30 H.E.B. Andersson and S.A. Borgstrom. Opto. Electron. 225 (1974).

1.31 R. Cubeddu and S.M. Curry. IEEE J of Quant. Electron. QE-9, 499 (1973).

1.32 C.Iwasaki and T. Jitsuno. IEEE J.Quant. Electron. QE-18, 423 (1982).

1.33 J. Jethwa, E.E. Marinero and A. Muller. Rev. Sci. Instrum. 52, 989 (1981).

1.34 A.J. Palmer. Appl. Phys. Lett. 25, 138 (1974).

1.35 J.I. Levatter and S.C. Lin. J. Appl. Phys. 51, 210 (1980).

1.36 H.M. von Bergmann and V. Hasson. J. Phys. D 11, 2341 (1978).

1.37 A. Yariv. Quantum Electronics (Wiley, New York, (1967).

1.38 L. Allen and G.I. Peters. Phys. Rev. A 8, 2031 (1973).

1.39 T. Jitsuno. J. Phys. D. 13, 1405 (1980).

1.40 R. Targ. IEEE J. Quant. Electron. QE-8, 726 (1972).

1.41 A.V. Armichev, V.S. Aleinikov and T.B. Fogelson. Sov. J. Quant. Electron. 10, 592 (1980).

1.42 A.J. Schmidt. J. Phys E 10, 453 (1977).

1.43 J.G. Small and R. Ashari. Rev. Sci. Instrum. 43, 1205 (1972).

1.44 J.I. Levatter and S.C. Lin. Appl. Phys. Lett. 25, 703 (1974).

1.45 K.H. Krahn. J. Appl. Phys. 50, 6656 (1979).

1.46 K.H. Krahn. Appl. Phys. 21, 319 (1980).

1.47 R.C. Sze and P.B. Scott. J. Appl. Phys. 47, 5492 (1976).

1.48 J. Desquelles, M. Dufay and M.C. Poulizac. Phys. Lett. A. 35, 25 (1971).

1.49 V.N. Ischenko, V.N. Lisitsyn and V.N. Starinskii. Sov. J. of Quant. Electron. 5, 851 (1975).

1.50 G.J. Linford, E.R. Peressini, W.R. Sooy and M.L. Spaeth. Appl. Optics 13, 379 (1974).

1.51 H.M. von Bergmann. J. Phys. E 15, 807 (1982).

1.52 K.I. Zemiskov, A.A. Isaev, M.A. Kazaryan, G.G. Petrash and S.G. Rautian. Sov. J. Quant. Electron. 4, 474 (1974).

1.53 A.A. Isaev, M.A. Kazaryan, G.G. Petrash and S.G. Rautian. Sov. J. Quant. Electron. 4, 761 (1974).

1.54 A.A. Isaev, M.A. Kazaryan, G.G. Petrash, S.G. Rautian and A.M. Shalagin. Sov. J. Quant. Electron. 5, 607 (1975).

1.55 A.A. Isaev, M.A. Kazaryan, G.G. Petrash, S.G. Rautian and A.M. Shalagin. Sov. J. Quant. Electron. 7, 746 (1977).

1.56 A.E. Seigman . Laser Focus May 1971, 42.

1.57 Yu. A. Anan'ev. Sov. J. Quant. Electron. 5, 615 (1975).

1.58 C.S. Willett and D.M. Litynski. Appl. Phys. Lett 26, 118 (1975).

1.59 R.P. Akins and S.C. Lin. Appl. Phys. Lett. 28, 221 (1976)

1.60 S. Sumida, M. Obara and T. Fujioka. Appl. Phys. Lett. 34, 31 (1979).

1.61 F. Collier, G. Thiell and P. Cottin. Appl. Phys. Lett. 32, 739 (1978).

1.62 E. Armandillo and A.J. Kearsley. Appl. Phys. Lett. 41, 611 (1982).

CHAPTER III

3.1 V. Ischchenko, V.N. Lisitsyn and V.N. Starinsky. Opt. Tech. 41, 155 (1974).

3.2 Y. Yasuda, N. Sokabe and A. Murai. Japan. J. Appl. Phys. 19, 2197 (1980).

3.3 L. Allen, D.G.C. Jones and B.M. Sivaram. Phys. Lett. 25A, 280 (1967).

3.4 V.F. Taransenko and Y.I. Bychkov. Sov. Phys. Tech. Phys. 19, 693 (1974).

3.5 T.J. Gleason, C.S. Willett, R.M. Curnett and J.S. Kruger. Appl. Phys. Lett. 21, 276 (1972).

3.6 L.O. Hocker. IEEE J. Quant. Electron. QE-13, 548 (1977).

3.7 B. Godard and M. Vannier. Opt. Comm. 16, 37 (1976).

3.8 A. Fisher, J. Peacock and E.K.C. Lee. Rev. Sci. Instrum. 49, 395 (1978).

CHAPTER IV

4.1 E.E. Bergmann and N. Everhardt. IEEE J. Quant. Electron. QE-9, 853 (1973).

CHAPTER V

5.1 A. Schmidt, H. Salzmann and H.S. Trohwald. Appl. Opt. 14, 2250 (1975).

5.2 W. Nawrot and L. Pokora. Sov. J. Quant. Electron. 12, 960 (1982).

5.3 M. Hugenschmidt and K. Vollrath. Opt. Comm. 26, 415 (1978).

5.4 D.M. Rayner, P.A. Hackett and C. Willis. Rev. Sci. Instrum. 52, 1579 (1981).

5.5 G.C. Thomas, G. Chakrapani and C.M.L. Kerr. Appl. Phys. Lett. 30, 633 (1977).

5.6 A.H. Guenther and J.R. Bettis. J. Phys. D. 11, 1577 (1978).

5.7 F. Pinnekamp, G. Himmel and K. Bergstedt. Opt. Comm. 11, 225 (1974).

5.8 K. Schildbach and D. Basting. Rev. Sci. Instrum. 45, 1015 (1974).

5.9 I. Santa, S. Szatmari, B. Nemet and J. Hebling. Opt. Comm. 41, 59 (1982).

5.10 P.B. Stephenson and V.P. McDowell. Rev. Sci. Instrum. 45, 427 (1974).

5.11 R. Laval and S. Laval. J. Phys. E. 13 17 (1980).

5.12 M.H. Hugenschmidt and J. Wey. Opt. Comm. 29, 191 (1979).

5.13 K. Kagawa, H. Kobayashi and M. Ishikane. Japan. J. Appl. Phys. 18, 2187 (1979).

5.14 K. Kagawa, M. Tani, N. Shibata, R. Ueno and M. Ueda. J. Phys. E. 15, 1192 (1982).

5.15 S. Nakamura, H. Hara, K. Umezu and H. Takuma. Japan. J. Appl. Phys. 15 2491 (1976).

5.16 K. Harsch, H. Salzmann and H. Strohwald. Phys. Lett. 55A, 153 (1975).

5.17 R.G. Caro, M.C. Gower and C.E. Webb. J. Phys. D 15, 767 (1982).

CHAPTER VI

6.1 P.P. Sorokin and J.R. Lankard. IBM Journal 10, 162 (1966).

6.2 B.H. Soffer and B.B. Macfarland. Appl. Phys. Lett. 10, 266 (1967).

6.3 J.A. Myer, C.L. Johnson, E. Kierstead, R.D. Sharma and I. Itzkan. Appl. Phys. Lett. 16, 3 (1970).

6.4 E.D. Stokes, F.B. Dunning, R.F. Stebbings, G.K. Walters and R.D. Rundel. Opt. Comm. 5, 267 (1972).

6.5 F.B. Dunning and R.F. Stebbings. Opt. Comm. 11, 112 (1974).

6.6 M. Maeda and Y. Miyazoe. Japan. J. Appl. Phys. 13, 827 (1974).

6.7 S. Saikan. Opt. Comm. 18, 439 (1976).

6.8 L.G. Nair. Prog. in Quant. Electron. 7, (1982).

6.9 M. Born and E. Wolf. Principles of Optics. Pergamon, Oxford (1970).

6.10 T.W. Hansch. Appl. Opt. 11, 895 (1972).

6.11 J.E. Lawler, W.A. Fitzsimmons and L.W. Anderson. Appl. Opt. 15, 1083 (1976).

6.12 D.C. Hanna, P.A. Karkkainen and R. Wyatt. Opt. and Quant. Electron. 7, 115 (1975).

6.13 G. Klauminzer. IEEE J. Quant. Electron. QE-13, 92D (1977).

6.14 M.G. Littman and H.J. Metcalf. Appl. Opt. 17, 2224 (1978).

6.15 I. Shoshan, N.N. Danon and U.P. Oppenheim. J. Appl. Phys. 48, 4495 (1977).

6.16 I. Shoshan and U.P. Oppenheim. Opt. Comm. 25, 375 (1978).

6.17 I.J. Wilson, B. Brown and E.G. Loewen. Appl. Opt. 18, 426 (1979).

6.18 M.G. Littman. Opt. Lett. 3, 138 (1978).

6.19 V.V. Lebedev and V.M. Plyasulya. Opt. Spectrosc. 50, 408 (1981).

6.20 I.G. Koprinkov, K.V. Stamenov and K.A. Stankov. Opt. Comm. 42, 264 (1982).

6.21 S.G. Dinev, I.G. Koprinkov, K.V. Stamenov and K.A. Stankov. Appl. Phys. 22, 287 (1980).

6.22 M.K. Iles, A.P. D'Silva and V.A. Fassel. Opt. Comm. 35 133 (1980).

6.23 K. Liu and M.G. Littman. Opt. Lett. 6, 117 (1981).

6.24 S. Mory, A. Rosenfield, S. Polze and G. Korn. Opt. Comm. 36, 342 (1981).

6.25 F.J. Duarte and J.A. Piper. Appl. Opt. 20, 2113 (1981).

6.26 D.A. Greenhalgh and P.H. Sarkies. Appl. Opt. 21, 3234 (1982).

6.27 J. Bissinger and L. Grzywalz. Optica Applicata 11, 397 (1981).

6.28 K.H. Yang, J.R. Morris, P.L. Richards and Y.R. Shen. Appl. Phys. Lett. 23, 669 (1973).

6.29 H. Inomata and A.J. Carswell. Opt. Comm. 22, 278 (1977).

6.30 J.P. Sage and Y. Aubry. Opt. Comm. 42 428 (1982).

6.31 A.A. Friesem, U. Ganiel and G. Neumann. Appl. Phys. Lett. 23, 249 (1973).

6.32 C.Y. Wu and J.R. Lombardi Opt. Comm. 7, 233 (1973).

6.33 H.S. Pilloff. Appl. Phys. Lett. 21, 339 (1972).

6.34 H. Lotem and R.T. Lynch. Appl. Phys. Lett. 27, 344 (1975).

6.35 A.J. Schmidt. Opt. Comm. 14, 294 (1975).

6.36 B.R. Marx, G.Holloway and L. Allen. Opt. Comm. 18, 437 (1976).

6.37 E. Winter, G. Veith and A.J. Schmidt. Opt. Comm. 25, 87 (1978).

6.38 L.G. Nair. Appl. Phys. 20, 97 (1979).

6.39 H.J. Kong and S.S. Lee. IEEE J. Quant. Electron. QE-17, 439 (1981).

6.40 Y. Prior. Rev. Sci. Instrum. 50, 259 (1979).

6.41 L.G. Nair and K. Dasgupta. IEEE J. Quant. Electron. QE-16, 111 (1980).

6.42 S. Chandra and A. Compaan. Opt. Comm. 31, 73 (1979).

6.43 P. Burlamacchi and H.F.R. Sandoval. Opt. Comm. 31, 185 (1979).

6.44 S.G. Dinev, I.G. Koprinkov, K.V. Stamenov and K.A. Stankov. Opt. Comm. 32, 313 (1980).

6.45 F. Castano and M.N. Sanchez Ray. Anales de Fisca, 127 (1979).

6.46 M.N. Nenchev and Y.H. Meyer. Appl. Phys. 24, 7 (1981).

6.47 R.C. Hilborn and H.C. Brayman. J. Appl. Phys. 45, 4912 (1974).

6.48 A.W.H. Mau. Opt. Comm. 11, 356 (1974).

CHAPTER VII

7.1 S.W. Williams and D.W.O. Heddle. Opt. Comm. 45, 112 (1983).

7.2 S.A. Borgstrom. Physica Scripta 14, 92 (1976).

7.3 A.A. Pease and W.M. Pearson. Appl. Opt. 16, 57 (1977).

ACKNOWLEDGEMENTS

I would like to thank all those people who have assisted me throughout the course of my work and during the preparation of this thesis.

In particular I thank my supervisor Professor Doug Heddle for his support, encouragement and advice. Also I wish to thank the technical staff at RHC for their expert attention and undoubted friendship. I would particularly like to acknowledge the work of the late Tom Tedder who spent many hours constructing the lasers and who showed great patience in enduring the many modifications.

I also thank Gillian Campbell and Lesley Bryce for their speedy and superb production of the typescript and Sharron Watt for her help in the preparation of the drawings. In addition I thank Brian Tait for his expert photographic work. The critical reading of the manuscript by Dr John Colles is greatly appreciated.

Finally I would like to thank Vivienne Ryan for her support, both moral and financial, throughout the four years and I wish her well in the future.

R.H.C.
LIBRARY